FLUCTUATION SPECTRA OF MESOSCOPIC VIBRATIONAL SYSTEMS

By

Yaxing Zhang

A DISSERTATION

Submitted
to Michigan State University
in partial fulfillment of the requirements
for the degree of

Physics – Doctor of Philosophy

2016

ABSTRACT

FLUCTUATION SPECTRA OF MESOSCOPIC VIBRATIONAL SYSTEMS

By

Yaxing Zhang

We study the spectra of fluctuations in linear and nonlinear vibrational systems. Fluctuations play a major role in mesoscopic systems explored in nanomechanics, cavity and circuit quantum electrodynamics, and Josephson junction based systems to mention but a few. We find that important insights into the nature of the fluctuations can be gained by investigating the system dynamics in the presence of periodic driving. This is because the interplay of the driving and fluctuations leads to specific pronounced spectral features. Our predictions are corrobarated by measurements on a carbon nanotube resonator which show that the theory allows one both to reveal and to characterize frequency fluctuations in a vibrational system, as well as to determine the decay rate without ring-down measurements. Our results bear on the general area of decoherence of mesoscopic oscillators and also on the classical problems of resonance fluorescence and light scattering by oscillators.

An important and poorly understood mechanism of fluctuations in mesoscopic systems is the dispersive mode coupling. This coupling is inherent essentially to all mesoscopic systems. It comes from the nonlinear interaction between vibrational modes with non-resonating frequencies. We consider the power spectrum of one of these modes. Thermal fluctuations of the modes nonlinearly coupled to it lead to fluctuations of the mode frequency and thus to the broadening of its spectrum. However, the coupling-induced broadening is partly masked by the spectral broadening due to the mode decay. We show that the effect of the mode coupling can be identified and characterized using the change of the spectrum by resonant driving. The theoretical analysis is complicated by the fact that the dispersive-coupling induced fluctuations are non-Gaussian. We develop a path-integral method of averaging over the fluctuations and obtain the power spectrum in an explicit form. The shape of the spectrum depends on the interrelation between the coupling strength and the decay rates of the modes involved, providing a means of characterizing these modes even where

they cannot be directly accessed. The analysis is extended to the case of coupling to many modes which, because of the cumulative effect, can become effectively strong. We also find the power spectrum of a driven mode where the mode has internal nonlinearity. Unexpectedly, for a driven mode, the power spectra dominated by the intra- and inter-mode nonlinearities are qualitatively different. The analytical results are in excellent agreement with the numerical simulations.

Of significant interest for physics and biophysics are overdamped mesoscopic and microscopic systems. Inertial effects play no role in their dynamics. We show that where such systems are periodically driven, along with the conventional delta-peak at the driving frequency their power spectra display extra features. These can be peaks or dips with height quadratic in the driving amplitude, for weak driving. The peaks/dips are generally located at zero frequency and at the driving frequency. The shape and intensity of the spectra sensitively depend on the parameters of the system dynamics. To illustrate this sensitivity and the generality of the effect, we study three types of systems: an overdamped Brownian particle (e.g., an optically trapped particle), a two-state system that switches between the states at random, and a noisy threshold detector. The analytical results are in excellent agreement with numerical simulations.

Copyright by
YAXING ZHANG
2016

ACKNOWLEDGEMENTS

First of all, I would like to thank my advisor and teacher, Dr. Mark Dykman. I was lucky enough to meet Mark, who later taught me the fundamentals of doing science, and led me to discover and enjoy the beauty of physics world. In addition to the invaluable scientific knowledge that he has taught me, Mark always encourages me to go ahead and do the calculation when I was intimidated by the problem in the first place. Mark also taught me the importance of interpreting the mathematical results in a physical term and putting them in a physical picture. On the personal matters, Mark has always been very caring and considerate for which I greatly appreciate.

I would also like to thank my Thesis Committee members, Dr. Norman Birge, Scott Pratt, Carl Schmidt, and Steve Shaw, who have been enthusiastic about my work and helpful with their comments. Particularly, Norman has always been critical and raising questions during my presentations for which I greatly appreciate. Special thanks go to Scott who has been very supportive on academic and personal matters during my years at East Lansing. In fact, without encouragement from Scott, I probably would not start my adventure as a theorist. I would like to thank Carl, from whom I learned the basics of the quantum field theory and diagrammatic technique which I benefit from in my everyday research. As a close collaborator of Steve, I enjoyed and learned a lot on mechanical resonators and nonlinear dynamics which I will continue to work on in my future career.

Many thanks go to my colleagues and officemates at MSU, Dong Liu, Juan Atalaya, Pavel Pulunin, and Kirill Moskovtsev, with whom I enjoyed discussing physics and everything else. Special thanks go to Juan, who has been really patient and helpful in answering my questions in research.

I would also like to thank the staff at the Physics and Astronomy Department, who made my stay at MSU smooth and pleasant.

Last but not least, I would like to thank my family. I cannot imagine spending these five years

without my wife, Jun, by my side who is always patient, supportive, and caring towards me. I would like to thank my parents and parents-in-law who are also very patient to me and always teach me how to be a good person. I would also like to thank my daugher, Audrey, who teaches me being curious is important.

TABLE OF CONTENTS

LIST OF FIGURES

CHAPTER 1

INTRODUCTION

Mesoscopic vibrational systems (oscillators) have attracted much interest in recent years, including nanomechanical resonators [1], optomechanical systems [2], and superconducting cavity modes [3]. These systems are usually weakly coupled to the environment, therefore they have very small decay rate, much smaller than their vibration frequency. What accompanies the coupling to the environment is fluctuations. The mesoscopic nature of these systems is two-fold: on the one hand, due to their small size (typically of nano/micro scale), these systems usually experience comparatively large quantum and classical fluctuations. On the other hand, the systems can be individually accessed and manipulated, thus allowing to study their fluctuations without performing ensemble averaging. In a word, to study the dynamics of these systems, it is crucial to understand the fluctuations in the systems: how to measure them, where they come from and how they affect the system dynamics.

Another feature of mesoscopic vibrational systems is that they have relatively strong nonlinearity [4]. As is well known, frequency of a nonlinear oscillator depends on its amplitude. The effect of nonlinearity becomes already strong when the nonlinearity-induced frequency shift is comparable to the decay rate of oscillators. For oscillators with low decay rates this happens well before the conventional strongly nonlinear effects, such as dynamical chaos, for example, come into play. There are various mechanisms of nonlinearity. Some are intrinsic in the systems, and some come from nonlinear coupling to the external degrees of freedom. For nanomechanical resonators, the nonlinearity can come from the intrinsic phonon nonlinearity, or phonon-phonon scattering process. They are particularly important for resonators of small size, for example, a vibrating nanobeam. The nonlinearity can also come from nonlinear coupling to external electric field that is used to drive the resonator. For superconducting circuits, the dynamics of the employed Josephson junctions is intrinsically nonlinear.

A standard tool to characterize mesoscopic vibrational systems is spectroscopy. It can be transmission/reflection spectrum for a cavity mode, or the power spectrum of the displacement of mechanical resonators. Quite often, the spectrum is modeled as a Lorentzian whose width is thought to be given by the decay rate of the oscillators. However, there are other mechanisms of spectral broadening. One of them is fluctuations in the vibrational frequencies, that is, the system eigenfrequency is subject to a random perturbation in time. For a nanomechanical resonator, frequency fluctuations can result from attachment or detachment of molecules on the resonator, charge fluctuations in the substrate, or dispersive coupling between different vibrational modes, etc.. For a cavity mode, it can come from fluctuations in the dielectric constant. The nonlinearity in the systems also leads to spectral broadening via converting amplitude fluctuations of vibrations to frequency fluctuations. The convoluted effects of different spectral broadening mechanisms make the shape of spectral line complicated, and generally non-Lorentzian and asymmetric. In order to quantify different sources of fluctuations and nonlinearity in the system, it is important to be able to identify and characterize their effects on spectral broadening. This is the central topic of the thesis.

The effects of frequency noise on spectral broadening have been observed in different mesoscopic vibrational systems. To name a few, Sansa et al. [5] showed that frequency fluctuations play a crucial role in silicon nanoresonators based on a Allen variance analysis, yet the source of fluctuations largely remain unknown. Barnard et al. [6] showed that in carbon nanotube resonator, the frequency noise that comes from mode-mode coupling accounts for most of the observed spectral linewidth at room temperature; Miao et al. [7] observed the same effect in graphene resonator. In superconductivity cavity, the frequency noise/phase noise was measured via homodyne detection [8, 9], and was attributed to coupling between the cavity and two-level fluctuators in the cavity walls or the substrate.

To reveal and characterize frequency fluctuations remains a challenge. The previously mentioned Allen variance analysis gives informaiton about frequency noise in a narrow band, not the whole spectrum. Other methods such as homodyne detection, and direct observation of the spec-

tral line do not provide a direct probe of frequency noise, and are often mixed by other sources of fluctuations.

In this thesis, we propose a method to identify and characterize frequency-noise and nonlinearity - induced spectral broadening. The method is based on applying a near resonant driving to the oscillator, and analyzing the resulting change to the oscillator power spectrum because of the driving. More specifically, the oscillator power spectrum will display spectral peaks of certain shape and strength as a result of driving. As we will show, firstly, these peaks will not occur if there is no frequency noise. They are consequences of the interplay between frequency noise and the driving. Secondly, the characteristics of the peaks sensitively depend on the properties of frequency noise such as noise strength and spectrum, therefore allowing one to extract information about the underlying fluctuations or the nonlinearity mechanisms.

The idea behind the proposed method is analogous to shining electromagnetic wave onto an oscillating charge (a charged harmonic oscillator), and measure the luminescence spectrum of the charge. As a standard textbook result, a harmonic oscillator only scatters light elastically. Therefore, its luminescence spectrum will simply be a superposition of a δ-peak at the incident light frequency and the thermal spectrum due to thermal fluctuations of the oscillator [10]. However, if the oscillator frequency is randomly perturbed by the environment, the oscillating charge can scatter light inelastically for which the energy offset is provided by or dumped into the environment. As a result, the luminescence spectrum will show extra structure away from the frequency of incident light. Depending on the energy stored in the frequency noise (classically it relates to the correlation time of the noise) and the relaxation rate of the oscillating charge, one expects that the scattered light can be at frequencies different from the incident light frequency, and width of the spectral peaks reflects the bandwidth of the frequency noise.

To illustrate the method, we study in Chap. 2 the oscillator response to a near-resonant drive based on a phenomenological model of a harmonic oscillator with generic frequency fluctuations [11]. We formulate the problem in terms of oscillator susceptibility that fluctuates in time due to frequency noise. We show that indeed depending on the interrelation of the noise correlation time

and the oscillator relaxation time, the driving-induced power spectrum ("luminescence spectrum") has significantly different structure. We then show the experimental results on a carbon nanotube resonator obtained by our experimental collaborators, and apply the theory to quantitatively extract the properties of the observed frequency noise in the system.

An important source of frequency noise is nonlinear dispersive coupling between vibrational modes, as amplitude fluctuations of one mode lead to frequency fluctuations of the other mode. Dispersive mode coupling plays a central role in quantum non-demolition measurements, in particular in superconducting circuits [12, 13] and optomechanical systems [14]. However, revealing and characterizing the coupling-induced noise of the oscillator frequency becomes challenging in the presence of dissipation when the fine structure of the oscillator absorption spectrum cannot be resolved.

In Chap. 3, we focus on mode-coupling-induced frequency noise. We study a microscopic model of two nonlinearly coupled harmonic oscillator(or two modes), both of which are coupled to a thermal reservior. Because of the nonlinear coupling between the two oscillators, amplitude fluctuations of one oscillator become frequency fluctuations of the other. We find analytically using a path-integral technique the response of one of the oscillators to a near resonant driving, and the driving-induced power spectrum [15]. As in the generic case, this spectrum reflects the properties of the frequency noise, in particular, it depends sensitively on the interrelation between the coupling strength, and decay rates of the two oscillators. We then generalize the analysis from two coupled modes to many coupled modes.

The driving-induced spectral peaks of the power spectrum result from fluctuations in the system susceptibility. These peaks are sensitive tools to study system dynamics and fluctuations irrespective of the particular type of the system. With this in mind, in Chap. 4, we study the driving-induced power spectra of several types of systems different from a fluctuating oscillator, including an overdamped Brownian particle (e.g., an optically trapped particle), a two-state system that switches between the states at random, and a noisy threshold detector. In all studied cases we show that driving leads to the onset of spectral features near the driving frequency and the characteristic fre-

quencies of the systems [16]. The shape and intensity of these features are sensitive to the form of the system nonlinearity and the fluctuation mechanism.

In Chap. 5, we conclude by summarizing the major results of the thesis and discuss future directions.

CHAPTER 2

INTERPLAY OF DRIVING AND FREQUENCY NOISE IN THE SPECTRA OF VIBRATIONAL SYSTEMS

2.1 Introduction

The spectrum of response and the power spectrum of an oscillator is a textbook problem that goes back to Lorentz and Einstein [17, 18, 10]. It has attracted much attention recently in the context of nanomechanical systems. Here, the spectra are a major source of information about the classical and quantum dynamics [19, 20, 21, 22, 23, 24, 25, 26]. This is the case also for mesoscopic oscillators of different nature, such as superconducting cavity modes [8, 9, 27, 28] and optomechanical systems [2]. Mesoscopic oscillators experience comparatively large fluctuations. Along with dissipation, these fluctuations determine the shape of the vibrational spectra.

A well-understood and most frequently considered [10] source of fluctuations is thermal noise that comes from the coupling of an oscillator (vibrational system) to a thermal reservoir and is related to dissipation by the fluctuation-dissipation theorem. Dissipation leads to the broadening of the oscillator power spectrum and the spectrum of the response to external driving.

Spectral broadening can also come from fluctuations of the oscillator frequency, which play an important role in mesoscopic oscillators. For nanomechanical resonators, frequency fluctuations can be caused by tension and mass fluctuations, fluctuations of the charge in the substrate, or dispersive intermode coupling [22, 23, 24, 25, 26, 29, 30, 6, 7], whereas for electromagnetic cavity modes they can come from fluctuations of the effective dielectric constant [8, 9]. Identifying different broadening mechanisms is a delicate task that has been attracting much attention [24, 26, 8, 6, 31, 32].

In this chapter we study the combined effect of periodic driving and frequency fluctuations on the power spectra of nanomechanical vibrational systems. For a linear oscillator with no frequency

fluctuations, driving leads to a δ-like peak at the driving frequency ω_F [10, 19], because here the only effect of the driving is forced vibrations linearly superimposed on thermal motion. Frequency fluctuations make forced vibrations random. As we show, this qualitatively changes the spectrum leading to characteristic new spectral features. We observe these features in a carbon-nanotube resonator and use them to separate the energy relaxation rate from the overall broadening of the power spectrum in the absence of driving, as well as reveal and explore the narrow-band frequency noise.

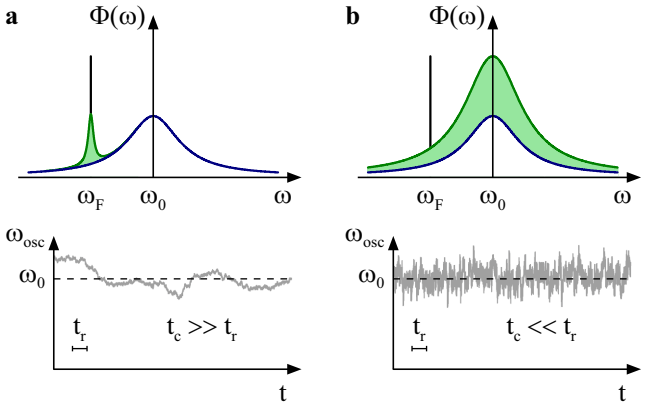

Figure 2.1 Top: sketches of the power spectra of a driven linear oscillator $\Phi(\omega)$. Panels (a) and (b) refer to large and small correlation time of the frequency noise t_c compared to the oscillator relaxation time t_r, respectively, i.e., to narrow- and broad-band frequency noise. The blue (lower) line shows the spectrum of thermal fluctuations in the absence of driving; it is centered at the oscillator eigenfrequency $\omega_0 = \langle \omega_{\rm osc}(t) \rangle$. In the presence of driving there is added a δ-peak at the driving frequency ω_F. The green areas show the spectral features from the interplay of the driving and fluctuations of $\omega_{\rm osc}(t)$. Bottom panels: $\omega_{\rm osc}(t)$ for $t_c \gg t_r$ (a) and $t_c \ll t_r$ (b).

For a linear oscillator, the spectral features resulting from the interplay of driving and frequency noise are sketched in Fig. 2.1. The two limiting cases shown in Fig. 2.1 correspond to the long and short correlation time of the frequency noise t_c compared to the oscillator relaxation (decay) time t_r. For $t_c \gg t_r$ (panel a) the oscillator frequency $\omega_{\rm osc}(t)$ slowly fluctuates about what can be called the eigenfrequency $\omega_0 = \langle \omega_{\rm osc}(t) \rangle$. One can then think of slow fluctuations of the oscillator susceptibility χ, which depends on the detuning of the driving frequency ω_F from $\omega_{\rm osc}(t)$. The associated slow fluctuations of the amplitude and phase of forced vibrations at frequency ω_F lead to a finite-width spectral peak centered at ω_F. This is a frequency-domain analog of the Einstein

light scattering due to spatial susceptibility fluctuations [33].

For $t_c \ll t_r$ (panel b), driving-induced random vibrations quickly lose the memory of the driving frequency. They become similar to thermal vibrations. However, their amplitude is determined by the driving, not the temperature. This leads to a spectral peak centered at the oscillator eigenfrequency ω_0, with the height quadratic in the driving amplitude.

In the quantum picture, one can think that, as a result of pumping by a driving field, the oscillator emits energy quanta. For the familiar example of an oscillating charge driven by an electromagnetic field these quanta can be photons, and one can speak of light scattering and fluorescence by an oscillator. A quantum is emitted over time t_r after the absorption event. For $t_c \ll t_r$ the frequency of the quantum is uncorrelated with the excitation frequency ω_F. This is a fluorescence-type process. The energy difference $\hbar(\omega_F - \omega_0)$ comes from the frequency noise. For $t_c \gg t_r$ emission occurs at frequencies close to ω_F. In the both cases the spectrum is qualitatively different from just a δ-like peak in the absence of frequency fluctuations [10].

2.2 Power spectrum of weakly driven systems

2.2.1 General expression

To describe the power spectrum of a nonlinear system one has to go beyond the approximation implied above, where only the linear susceptibility is fluctuating. If driving is described by the term $-qF(t)$ in the oscillator Hamiltonian, where q is the oscillator coordinate and $F(t) = F\cos\omega_F t$ is the driving force, to obtain terms $\propto F^2$ in the power spectrum one should keep terms $\propto F$ and $\propto F^2$ in the response,

$$q(t) \approx q_0(t) + \int_{-\infty}^{t} dt' \chi_1(t,t') F(t') + \iint_{-\infty}^{t} dt' dt'' \chi_2(t,t',t'') F(t') F(t''). \tag{2.1}$$

Here $q_0(t)$ is thermal displacement in the absence of driving. Equation (2.1) does not include averaging, χ_1 and χ_2 are the fluctuating linear and nonlinear susceptibilities. The standard linear

susceptibility is $\langle\chi_1(t,t')\rangle$, it is a function of $t-t'$. For a harmonic oscillator, which is the central topic of this chapter, $\chi_2 = 0$.

The conventionally measured oscillator power spectrum is

$$\Phi(\omega) = 2\mathrm{Re}\int_0^\infty dt e^{i\omega t}\langle\langle q(t+t')q(t')\rangle\rangle,$$

where $\langle\langle\cdot\rangle\rangle$ indicates statistical averaging and averaging with respect to t' over the driving period $2\pi/\omega_F$. For weak driving

$$\Phi(\omega) \approx \Phi_0(\omega) + \frac{\pi}{2}F^2|\chi(\omega_F)|^2\delta(\omega-\omega_F) + F^2\Phi_F(\omega). \tag{2.2}$$

This spectrum is sketched in Fig. 2.1. Function Φ_0 is the power spectrum in the absence of driving, a resonant peak associated with thermal vibrations of the oscillator. The δ-peak at the driving frequency in Eq. (2.2) and in Fig. 2.1 describes average forced oscillator vibrations, $\chi(\omega)$ is the Fourier transform of $\langle\chi_1(t,t')\rangle$ over $t-t'$.

Of primary interest to us is the term $\Phi_F(\omega)$, shown by the envelope of the green area in Fig. 2.1. It describes the interplay of frequency fluctuations and the driving. We consider it for ω close to ω_F assuming a high quality factor, $\omega_0 t_r \gg 1$, typical for mesoscopic systems, and resonant driving, $|\omega_F-\omega_0| \ll \omega_F$.

The explicit expression for the driving-induced term in the power spectrum of fluctuations of the oscillator reads

$$\Phi_F(\omega) = \frac{1}{2}\mathrm{Re}\int_0^\infty dt e^{i(\omega-\omega_F)t}\iint_{-\infty}^0 d\tau d\tau' e^{i\omega_F(\tau'-\tau)}$$
$$\times\langle\chi_1(t,t+\tau)\left[\chi_1(0,\tau') - \langle\chi_1(0,\tau')\rangle\right]\rangle + \Phi_F^{(2)}(\omega). \tag{2.3}$$

This expression follows from Eqs. (2.1) and (2.2). The first term gives the contribution of the fluctuations of the linear susceptibility. The second term gives the contribution from the nonlinear susceptibility,

$$\Phi_F^{(2)}(\omega) = \mathrm{Re}\int_0^\infty dt e^{i\omega t}\iint_{-\infty}^0 d\tau d\tau'\cos[\omega_F(\tau-\tau')]$$
$$\times\left[\langle\chi_2(t,t+\tau,t+\tau')q_0(0)\rangle + \langle q_0(t)\chi_2(0,\tau,\tau')\rangle\right]. \tag{2.4}$$

This term describes the correlation between fluctuations of the second-order susceptibility and thermal fluctuations in the absence of periodic driving. We emphasize that, for a resonantly modulated underdamped oscillator, it is pronounced at frequencies ω close to the driving frequency ω_F, not $2\omega_F$. Equation (2.4) describes, in particular, the contribution to the spectrum from the nonlinear susceptibility of a nonlinear oscillator. It is especially convenient in the case of weak nonlinearity, where the oscillator spectrum $\Phi_0(\omega)$ is broadened primarily by the decay rather than by frequency fluctuations due to the interplay of the nonlinearity and the amplitude fluctuations. In this case the term $\Phi_F^{(2)}$ gives the main contribution to Φ_F. The theory of a nonlinear oscillator will be discussed in Chap. 3.

2.2.2 Spectrum of a driven harmonic oscillator with fluctuating frequency

For a harmonic oscillator with fluctuating frequency, $\omega_{\rm osc}(t) = \omega_0 + \xi(t)$, where $\xi(t)$ is zero-mean noise. We assume that the noise is weak compared to ω_0 and that its correlation time $t_c \gg \omega_0^{-1}$. The noise then does not cause parametric excitation of the oscillator [34, 35].

The most simple model of the oscillator dynamics is described by equation

$$\ddot{q} + 2\Gamma\dot{q} + [\omega_0^2 + 2\omega_0\xi(t)]q = F\cos\omega_F t + f(t), \tag{2.5}$$

where $f(t)$ is thermal noise and $\Gamma = t_r^{-1}$ is the relaxation rate. Both $f(t)$ and the direct frequency noise $\xi(t)$ lead to fluctuations of the oscillator phase. Separating their contributions by measuring the commonly used Allan variance (cf. [19]) is complicated. However, these two types of noise have different physical origin, and our results show how they can be separated using the power spectrum; a different approach, which however may not be implemented with a standard spectrum analyzer, was proposed in [36].

The susceptibility of a linear underdamped oscillator with fluctuating frequency can be found in a standard way by changing from the fast oscillating variables $q, \dot{q}$ to slow complex oscillator amplitude $u(t) = [q(t) + (i\omega_F)^{-1}\dot{q}(t)]\exp(-i\omega_F t)/2$. From Eq. (2.5), the equation for $u(t)$ in the

rotating wave approximation reads

$$\dot{u} = -[\Gamma + i\delta\omega_F - i\xi(t)]u - i\frac{F}{4\omega_0} + f_u(t). \tag{2.6}$$

Here, $\delta\omega_F = \omega_F - \omega_0$ is the detuning of the driving frequency from the oscillator eigenfrequency; $f_u(t) = [f(t)/2i\omega_0]\exp(-i\omega_0 t)$. Equation (2.6) applies on the time scale that largely exceeds ω_0^{-1}. On this scale $f_u(t)$ is δ-correlated even where in the lab frame the oscillator dynamics is non-Markovian, cf [37]. Solving the linear equation (2.6), one immediately obtains the fluctuating linear susceptibility of a damped harmonic oscillator,

$$\chi_1(t,t') = \frac{i}{2\omega_0} e^{-(\Gamma+i\omega_0)(t-t') - i\int_{t'}^{t} dt''\xi(t'')} + \text{c.c.} \tag{2.7}$$

($\chi_2 = 0$). Equation (2.7) often applies even where the oscillator dynamics in the lab frame is non-Markovian. We disregard corrections $\sim |\delta\omega_F|/\omega_F$; in particular in Eq. (2.6) for convenience we replaced F/ω_F with F/ω_0; similarly, in the expression for f_u we replaced f/ω_F with f/ω_0.

We note that the noise $f_u(t)$ drops out from the moments $\langle u^n(t)\rangle$ [36]. This can be used to characterize the statistics of the frequency noise. Here we consider the change of the conventionally measured characteristic, the power spectrum, and the extra spectral features related to the interplay of the driving and frequency noise.

It is convenient to rewrite Eq. (2.3) for the spectrum $\Phi_F(\omega)$ near its maximum in the form that explicitly takes into account that, when the expression for the susceptibility is substituted into Eq. (2.3), the fast-oscillating terms in the integrands can be disregarded. This gives

$$\begin{aligned}
&\Phi_F(\omega) = (8\omega_0^2)^{-1}\,\mathrm{Re}\int_0^\infty dt \exp[i(\omega-\omega_F)t] \\
&\times \int_{-\infty}^{t} dt' \int_{-\infty}^{0} dt_1' \big\langle \chi_{\mathrm{sl}}(t,t')[\chi_{\mathrm{sl}}^*(0,t_1') - \langle\chi_{\mathrm{sl}}^*(0,t_1')\rangle]\big\rangle, \\
&\chi_{\mathrm{sl}}(t,t') = e^{-(\Gamma - i\delta\omega_F)(t-t')} \exp\left[-i\int_{t'}^{t} dt''\xi(t'')\right].
\end{aligned} \tag{2.8}$$

Here, function $\chi_{\mathrm{sl}}(t,t')$ gives the slowly varying factor in the fast-oscillating time-dependent oscillator susceptibility $\chi_1(t,t')$. Function $\langle\chi_{\mathrm{sl}}(0,t)\rangle \equiv \langle\chi_{\mathrm{sl}}(-t,0)\rangle$ gives the standard (average) sus-

ceptibility

$$\chi(\omega_F) = \int_0^\infty dt e^{i\omega_F t} \langle \chi_1(t,0) \rangle = \frac{i}{2\omega_0} \int_0^\infty dt \langle \chi_{\rm sl}(t,0) \rangle. \tag{2.9}$$

The mean forced displacement of the oscillator in the linear response theory is

$$\langle q(t) \rangle = \frac{1}{2} F e^{-i\omega_F t} \chi(\omega_F) + \text{c.c.}.$$

2.3 Oscillator power spectrum in the limiting cases

2.3.1 Weak frequency noise

Explicit expressions for $\Phi_F(\omega)$ can be obtained from Eq. (2.8) in the limiting cases. For weak frequency noise, one can expand $\chi_{\rm sl}$ in $\xi(t)$. To the leading order, the spectrum Φ_F is proportional to the noise power spectrum $\Xi(\Omega) = \int_{-\infty}^{\infty} dt \langle \xi(t)\xi(0) \rangle \exp(i\Omega t)$,

$$\Phi_F(\omega) \approx \frac{1}{16\omega_0^2[\Gamma^2 + (\omega_F - \omega_0)^2]} \frac{\Xi(\omega - \omega_F)}{\Gamma^2 + (\omega - \omega_0)^2}. \tag{2.10}$$

This expression provides a direct means for measuring the frequency noise spectrum. It already shows the peculiar features qualitatively discussed above. If $\Xi(\Omega)$ peaks at zero frequency and is narrow on the scale Γ (as for $1/f$-type noise, for example), $\Phi_F(\omega)$ has a peak at ω_F, cf. Fig. 2.1a. The shape of this peak coincides with that of $\Xi(\Omega)$. If, on the other hand, $\Xi(\Omega)$ is almost flat on the frequency scale $\Gamma, |\omega_F - \omega_0|$ (broad-band noise), $\Phi_F(\omega)$ has a Lorentzian peak at ω_0, cf. Fig. 2.1b.

2.3.2 Narrow-band frequency noise

To describe the effect of a narrow-band, but not necessarily weak frequency noise, one can replace $\xi(t'')$ in Eq. (2.8) with $\xi(t)$. Then it follows from Eq. (2.9) that the susceptibility reads

$$\chi(\omega_F) = \frac{i}{2\omega_0} \langle X(t) \rangle, \quad X(t) = [\Gamma - i\delta\omega_F + i\xi(t)]^{-1}. \tag{2.11}$$

whereas the expression for the driving-induced term in the power spectrum reads

$$\Phi_F(\omega) \approx \frac{1}{8\omega_0^2}\mathrm{Re}\int_0^\infty dt e^{i(\omega-\omega_F)t}\left\langle X(t)[X^*(0)-\langle X^*(0)\rangle]\right\rangle. \tag{2.12}$$

The quantity $iX(t)/2\omega_0$ corresponds to the "instantaneous" slowly fluctuating susceptibility. The narrow spectrum $\Phi_F(\omega)$ is determined by the spectrum and statistics of the frequency noise. These expressions can be used for numerical calculations if the statistics of the noise $\xi(t)$ is known. The simple relation (2.10) between $\Phi_F(\omega)$ and $\Xi(\omega)$ follows from this analysis for $\langle\xi^2\rangle \ll \Gamma^2+(\omega_F-\omega_0)^2$. Importantly, this condition can be achieved by tuning ω_F somewhat away from ω_0.

2.3.3 Broadband frequency noise

The case of flat $\Xi(\Omega)$, i.e., of $\xi(t)$ being δ-correlated on time scale t_r, can be analyzed for an arbitrary noise strength using the characteristic functional of a δ-correlated noise is

$$\mathscr{P}[k(t)] = \langle\exp[i\int dtk(t)\xi(t)]\rangle = \exp[-\int\mu(k(t))dt],$$

where function $\mu(k)$ is determined by the noise statistics.

As seen from Eq. (2.8), function $\langle\chi_{\mathrm{sl}}(t,t')\rangle$ is determined by $\mathscr{P}[k(t'')]$ with $k(t'')=-1$ if $t'<t''<t$ and $k(t)=0$ otherwise. For δ-correlated noise, where $\mathscr{P}[k(t)]=\exp[-\int dt\,\mu(k(t))]$, taking into account that $\mu(0)=(d\mu/dk)_{k=0}=0$ and $\mu(-k)=\mu^*(k)$, we obtain

$$\begin{aligned}\langle\chi_{\mathrm{sl}}(t,t')\rangle &= \exp\left[-\left(\Gamma-i\delta\omega_F+\mu^*(1)\right)(t-t')\right],\\ \chi(\omega_F) &= (i/2\omega_0)\left[\tilde{\Gamma}-i(\omega_F-\tilde{\omega}_0)\right]^{-1}\end{aligned} \tag{2.13}$$

with $\tilde{\Gamma}=\Gamma+\mathrm{Re}\,\mu(1)$ and $\tilde{\omega}_0=\omega_0-\mathrm{Im}\,\mu(1)$. Thus, frequency noise leads to the broadening of the conventional susceptibility $\mathrm{Re}\,\mu(1)$ and the effective shift of the oscillator eigenfrequency by $-\mathrm{Im}\,\mu(1)$. We note that the noise can be considered δ-correlated when its spectrum is flat not just on the scale $\gtrsim\Gamma$, but on the scale $\gtrsim\Gamma+\mathrm{Re}\;\mu(1)$, which itself depends on the noise intensity. At the same time, the noise spectrum is assumed to be much narrower than ω_0. As seen from Eq. (2.8) the noise components oscillating at frequencies much higher than $\Gamma+\mathrm{Re}\,\mu(1), |\delta\omega_F|$ are averaged

out; frequency noise with frequencies $\sim \omega_0$ was disregarded in Eq. (2.6). When writing Eq. (2.6) we also assumed that noise at frequencies close to $2\omega_0 \approx 2\omega_F$ is very weak and can be disregarded. If this were not the case, one would have to take into account the effects of nonlinear friction that come from the coupling to the source of the noise, cf. [37].

Averaging the term $\langle \chi_{\rm sl}(t,t')\chi^*_{\rm sl}(0,t'_1)\rangle$ in Eq. (2.8) comes to calculating

$$\left\langle \exp\left[-i\int_{t'}^{t} dt''\xi(t'') + i\int_{t'_1}^{0} dt''_1\xi(t''_1)\right]\right\rangle$$
$$\equiv \left\langle \exp\left[i\int_{-\infty}^{\infty} dt_2 k(t_2)\xi(t_2)\right]\right\rangle. \tag{2.14}$$

Here $t>0$ and $-\infty < t' \le t, -\infty < t'_1 \le 0$. Clearly, in this equation $k(t_2) = 0, \pm 1$. For $t'<0$ we have $k(t_2) = \mathrm{sgn}(t'-t'_1)$ if $\min(t',t'_1) < t_2 < \max(t_1,t'_1)$ and $k(t_2) = -1$ if $0 < t_2 < t$; for $t'>0$ we have $k(t_2)=1$, if $t'_1 < t_2 < 0$ and $k(t_2) = -1$, if $t' < t_2 < t$; otherwise $k(t_2) = 0$. For a δ-correlated noise the averaging using the explicit form of $\mathscr{P}[k(t)]$ and integration over t', t'_1, t gives

$$\Phi_F(\omega) = \frac{[\mathrm{Re}\,\mu(1)]/\Gamma}{8\omega_0^2[\tilde{\Gamma}^2 + (\omega_F - \tilde{\omega}_0)^2]} \frac{\tilde{\Gamma}}{\tilde{\Gamma}^2 + (\omega - \tilde{\omega}_0)^2}. \tag{2.15}$$

The spectrum (2.15) and the spectrum $\Phi_0(\omega)$ in the absence of periodic driving have the same shape given by the last factor in (2.15): a Lorentzian centered at the noise-renormalized oscillator eigenfrequency $\tilde{\omega}_0 = \omega_0 - \mathrm{Im}\,\mu(1)$ with halfwidth $\tilde{\Gamma} = \Gamma + \mathrm{Re}\,\mu(1)$. However, in contrast to $\Phi_0(\omega)$, the area of $F^2\Phi_F(\omega)$ is independent of the intensity ($\propto k_B T$) of the dissipation-related noise. Instead it is proportional to the frequency-noise characteristic $\mathrm{Re}\,\mu(1)$. Equation (2.15) suggests how to separate the noise-induced broadening of the oscillator spectrum from the decay-induced broadening, see below.

2.3.4 Gaussian frequency noise

For a stationary Gaussian noise the characteristic functional is expressed in terms of the noise correlator [38],

$$\mathscr{P}[k(t)] = \exp\left[-\frac{1}{2}\int dt\, dt'\, \langle \xi(t)\xi(t')\rangle k(t)k(t')\right].$$

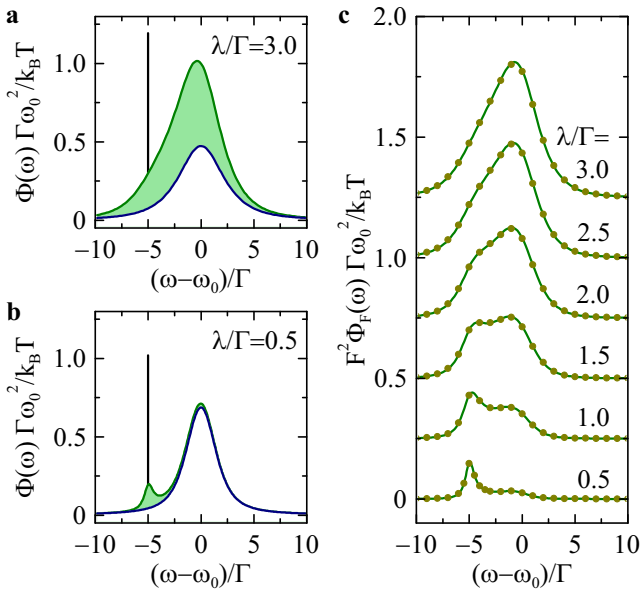

Figure 2.2 The power spectrum of the oscillator with a Gaussian frequency noise with the spectrum $\Xi(\Omega) = 2D\lambda^2/(\lambda^2+\Omega^2)$. The noise intensity is $D/\Gamma = 2$. Panels a and b: the full spectrum. The color coding is the same as in Fig. 2.1, $F^2/16\Gamma^2 = 20k_BT$. Panel c: the driving-induced term. The solid lines and dots show the analytic theory and simulations; the consecutive curves are shifted by 0.25 along the ordinate.

If the correlator $\langle \xi(t)\xi(t')\rangle$ or equivalently, the power spectrum $\Xi(\Omega)$, are known, using the values of $k(t)$ given below Eq. (2.14) one can perform the averaging in Eq. (2.8) and then perform integration over time to find the power spectrum Φ_F. The results are shown in Fig. 2.2 for the noise power spectrum with bandwidth λ, $\Xi(\Omega) = 2D\lambda^2/(\lambda^2+\Omega^2)$. They illustrate how the shape of $\Phi_F(\omega)$ changes from a peak at ω_F for a narrow-band noise ($\lambda \ll \Gamma$) to a peak at ω_0 for a broadband noise ($\lambda \gg \Gamma$). The overall area of the spectrum Φ_F nonmonotonically depends on the frequency noise intensity: it is linear in the noise intensity for weak noise, cf. Eq. (2.10), but for a large noise intensity it decreases, since the decoherence rate of the oscillator increases.

2.3.5 The weak-noise condition

In the limit of weak slow noise, $\langle \xi^2(t)\rangle \ll |\Gamma - i\delta\omega_F|^2$, Eq. (2.12) goes over into the result for such noise obtained above; note that in Eq. (2.10) one should replace $\omega - \omega_0$ with $\omega_F - \omega_0$ in the slow-noise limit, since function $\Xi(\Omega)$ is concentrated in the range of small $\Omega \ll \Gamma$. For the broad-

band noise, on the other hand, the weak-noise limit discussed above corresponds to $|\mu(1)| \ll \Gamma$. In this case the noise power spectrum is flat and $\Xi(\Omega) = (d^2\mu/dk^2)_{k=0} \sim |\mu(1)| \ll \Gamma$. Generally, the weak noise condition used to obtain Eq. (2.10) certainly holds for $\max \Xi(\Omega) \ll \Gamma$. It is important that, for slow noise, the condition is less stringent and can be met by increasing the detuning $|\delta\omega_F|$, allowing one to read the slow-noise power spectrum directly off the oscillator power spectrum.

2.3.6 Susceptibility with weakly fluctuating frequency

Both the standard susceptibility $\chi(\omega)$ and the power spectrum in the absence of driving $\Phi_0(\omega)$ are affected by frequency noise. In the considered case they are related by the fluctuation-dissipation relation, $\Phi_0(\omega) = (2k_BT/\omega)\mathrm{Im}\ \chi(\omega)$. For a non-white frequency noise the spectrum $\Phi_0(\omega)$ becomes non-Lorentzian.

The explicit expressions for the susceptibility in the limiting cases of fast and slow frequency noise were given above, Eqs. (2.13) and (2.11). A simple explicit expression for $\chi(\omega)$ follows from Eqs. (2.8) and (2.9) also in the case of weak noise. Here, the susceptibility becomes

$$\chi(\omega) \approx \frac{i}{2\omega_0(\Gamma - i\delta\omega)}\left[1 - \int \frac{d\Omega}{2\pi(\Gamma - i\delta\omega)}\frac{\Xi(\Omega)}{\Gamma - i\delta\omega - i\Omega}\right], \tag{2.16}$$

where $\Xi(\Omega)$ is the frequency noise power spectrum and $\delta\omega = \omega - \omega_0$. Importantly, the noise-induced correction just slightly distorts the susceptibility. For example, a sharp low-frequency peak of $\Xi(\Omega)$ does not lead to a narrow peak in $\chi(\omega)$ and, respectively, in the power spectrum $\Phi_0(\omega)$. This should be contrasted with the narrow peak in $\Phi_F(\omega)$, which emerges in this case.

2.4 The area of the driving-induced spectral peak

We now consider the area S_F of the driving induced spectral peak for ω close to ω_0, ω_F; note that this peak may have several maxima, as seen from Fig. 2.2. We define the area as an integral over positive frequencies, $S_F = \int_0^\infty d\omega\, \Phi_F(\omega)$. Keeping in mind that $\Phi_F(\omega)$ is small for large

$|\omega - \omega_F| \sim \omega_F$ [in fact, Eq. (2.8) does not apply for such ω], we obtain

$$S_F = \frac{\pi}{8\omega_0^2} \iint_{-\infty}^{0} dt\, dt' \langle \chi_{\rm sl}(0,t)\chi_{\rm sl}^*(0,t')\rangle - \frac{\pi}{8\omega_0^2} \left| \int_{-\infty}^{0} dt\, \langle \chi_{\rm sl}(0,t)\rangle \right|^2 . \tag{2.17}$$

This expression describes the dependence of the area of the driving-induced spectrum on the parameters and statistics of the frequency noise.

From Eq. (2.17), the area S_F becomes zero in the absence of frequency noise, since $\langle \chi_{\rm sl}(t,t')\rangle = \chi_{\rm sl}(t,t')$ in this case. The area S_F linearly increases with the frequency noise intensity for weak noise, as seen from Eq. (2.10).

An explicit expression for S_F can be obtained for white frequency noise. From Eq. (2.15),

$$S_F = \frac{\pi}{8\Gamma\omega_0^2} \frac{\mathrm{Re}\,\mu(1)}{|\Gamma + i(\omega_F - \omega_0) + \mu(1)|^2}. \tag{2.18}$$

From Eq. (2.18), S_F linearly increases with the characteristic noise strength Re $\mu(1)$ where it is small, but once the noise becomes strong, S_F decreases with increasing $|\mu(1)|$, with $S_F \propto$ Re $\mu(1)/|\mu(1)|^2$ for $|\mu(1)| \gg \Gamma, |\omega_F - \omega_0|$.

For weak narrow-band frequency noise, from Eq. (2.10) one obtains S_F in terms of the noise variance $\langle \xi^2(t)\rangle$ as

$$S_F = \frac{\pi}{8\omega_0^2} \frac{\langle \xi^2(t)\rangle}{[\Gamma^2 + (\omega_F - \omega_0)^2]^2}.$$

An explicit expression for S_F can be obtained also for a strong Gaussian noise. We will assume that the noise correlator $\langle \xi(t)\xi(0)\rangle$ is not fast oscillating and, respectively, the noise spectrum $\Xi(\Omega)$ does not have narrow peaks or dips. For the noise variance $\langle \xi^2(t)\rangle$ much larger than $\Gamma^2, \delta\omega_F^2$, and the squared reciprocal noise correlation time t_c^{-2}, from Eq. (2.17)

$$S_F \approx \frac{\pi^2}{8\Gamma\omega_0^2} [2\pi \langle \xi^2(t)\rangle]^{-1/2}. \tag{2.19}$$

The variation of S_F with the varying frequency-noise intensity and bandwidth is shown in Fig. 2.3, which refers to the exponentially correlated Gaussian noise. As seen from this figure, S_F displays a maximum as a function of the noise intensity D. The dependence on the noise bandwidth λ is more complicated; S_F can have two maxima as a function of λ for sufficiently strong noise intensity.

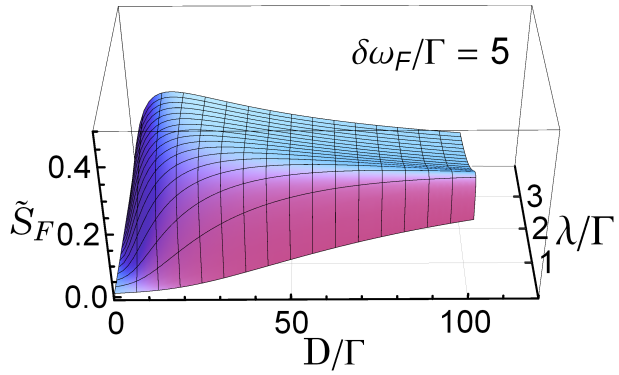

Figure 2.3 The scaled area $\tilde{S}_F = 8\Gamma^2\omega_0^2 S_F$ of the driving-induced peak in the oscillator power spectrum as a function of the frequency noise parameters. The data refer to Gaussian frequency noise with the power spectrum $\Xi(\Omega) = 2D\lambda^2/(\lambda^2+\Omega^2)$.

2.4.1 Scaling of the driving-induced power spectrum

A convenient scaling factor for the distribution $\Phi_F(\omega)$ and for the area S_F is provided by the area S_δ of the δ-peak in the oscillator power spectrum at the driving frequency. As seen from Eq. 2.2, $S_\delta = (\pi/2)|\chi(\omega_F)|^2$. If $\chi(\omega_F)$ is known from the measured power spectrum in the absence of driving with the invoked fluctuation-dissipation theorem, scaling by S_δ allows one to avoid the actual measurement of the force F, which requires knowledge of the coupling to the driving field.

The expression for S_δ simplifies if the frequency noise can be thought of as a sum of a weak narrow-band noise $\xi_{\rm nb}(t)$ and a broad-band (δ-correlated in slow time) noise $\xi_{\rm bb}(t)$, which is not weak, generally, and is statistically independent from the narrrow-band noise. In this case, combining Eqs. (2.13) and (2.11) and expanding to the leading order in the weak narrow-band noise, we obtain,

$$S_\delta \approx \frac{\pi}{8\omega_0^2}[\tilde{\Gamma}^2+(\omega_F-\tilde{\omega}_0)^2]^{-1} \times\left[1-\frac{\tilde{\Gamma}^2-(\omega_F-\tilde{\omega}_0)^2}{\pi[\tilde{\Gamma}^2+(\omega_F-\tilde{\omega}_0)^2]^2}\int d\omega\,\Xi_{\rm nb}(\omega)\right]. \tag{2.20}$$

Here, $\Xi_{\rm nb}(\omega)$ is the power spectrum of the narrow-band noise; the variance of the narrow-band noise is $\langle\xi_{\rm nb}^2(t)\rangle = (2\pi)^{-1}\int d\omega\,\Xi_{\rm nb}(\omega)$.

For not weak narrowband frequency noise, one has generally,

$$S_\delta = \frac{\pi}{8\omega_0^2}|\langle[\tilde{\Gamma} + i(\omega_F - \tilde{\omega}_0 - \xi_{\rm nb}(t))]^{-1}\rangle_{\rm nb}|^2 \tag{2.21}$$

where $\langle..\rangle_{\rm nb}$ indicates averaging over the narrow-band frequency noise.

The correction that contains $\Xi_{\rm nb}$ can be directly read off the area of the narrow peak $\Phi_F^{(\rm nb)}(\omega)$ in the spectrum $\Phi_F(\omega)$, which is due to the narrow-band noise. For weak narrow-band noise, this peak is described by Eq. (2.10) if one replaces in this equation Γ with $\tilde{\Gamma}$, ω_0 with $\tilde{\omega}_0$, and $\Xi(\omega)$ with $\Xi_{\rm nb}(\omega)$. This can be seen from Eq. (2.8). Indeed, in the expression for $\chi_{\rm sl}(t,t')$ in Eq. (2.8) one can write $\int_{t'}^{t} dt''\xi_{\rm nb}(t'') \approx \xi_{\rm nb}(t)(t-t')$. To find $\Phi_F^{(\rm nb)}(\omega)$, one should integrate over the range of t given by the reciprocal bandwidth of the narrow-band noise. Since it largely exceeds $1/\Gamma$, the contributions of the broad-band noise to $\chi_{\rm sl}(t,t')$ and $\chi_{\rm sl}(0,t_1')$ are statistically independent. Therefore the averaging over the broad-band noise in these susceptibilities can be done independently. If this averaging is denoted by $\langle\cdot\rangle_{\rm bb}$,

$$\langle\chi_{\rm sl}(t,t')\chi_{\rm sl}^*(0,t_1')\rangle_{\rm bb} \approx \langle\chi_{\rm sl}(t,t')\rangle_{\rm bb}\langle\chi_{\rm sl}^*(0,t_1')\rangle_{\rm bb}$$

for $\Gamma t \gg 1$. Here

$$\langle\chi_{\rm sl}(t,t')\rangle_{\rm bb} \approx e^{-\left[\tilde{\Gamma} - i\left(\omega_F - \tilde{\omega}_0 - \xi_{\rm nb}(t)\right)\right](t-t')}.$$

Since function $\Xi_{\rm nb}(\omega)$ quickly falls off with increasing $|\omega|$, in the denominator of Eq. (2.10) one can replace ω with ω_F. One then sees that, to the leading order in the narrow-band noise strength, the ratio of the area $S_{\rm nb}$ of the narrow peak $\Phi_F^{(\rm nb)}(\omega)$ to the area of the δ-peak in the spectrum is

$$\frac{S_{\rm nb}}{S_\delta} \approx \frac{1}{2\pi}\frac{1}{\tilde{\Gamma}^2 + (\omega_F - \tilde{\omega}_0)^2}\int d\omega\,\Xi_{\rm nb}(\omega). \tag{2.22}$$

For not weak narrow-band noise, it follows from Eq. (2.17) that,

$$S_{\rm nb} = \frac{\pi}{8\omega_0^2}\langle[\tilde{\Gamma}^2 + (\omega_F - \tilde{\omega}_0 - \xi_{\rm nb}(t))^2]^{-1}\rangle_{\rm nb} - S_\delta \tag{2.23}$$

where S_δ is given by Eq. (2.21).

Equations (2.20) and (2.22) can be used to scale the area of the broader peak of $\Phi_F(\omega)$ by S_δ with account taken of the effect of the narrow-band frequency noise. Along with the onset of a narrow peak in Φ_F, this noise leads to the change of the shape and area of the broad peak. To find the area of the broad peak $\Phi_F^{(\mathrm{bb})}(\omega)$, one need to integrate over the range of time t given by $1/\tilde{\Gamma}$ in Eq. (2.8). During this period of time, the narrow band frequency noise stays almost constant, that is, $\xi_{\mathrm{nb}}(t) \approx \xi_{\mathrm{nb}}(0)$. Then the one can simply replace $\delta\omega_F$ with $\delta\omega_F - \xi_{\mathrm{nb}}(t)$ in Eq. (2.8) for $\chi_{\mathrm{sl}}(t,t')$. The result is particularly simple in the considered case here where the broad-band frequency noise is δ-correlated in slow time and the broad peak of $\Phi_F(\omega)$ is described by Eq. (2.15). One just has to replace in this equations $\tilde{\omega}_0$ with $\tilde{\omega}_0 + \xi_{\mathrm{nb}}(t)$, then averaging the expression over the distribution of $\xi_{\mathrm{nb}}(t)$. To the second order in the $\xi_{\mathrm{nb}}(t)$, the area of the broader peak is given by,

$$S_{\mathrm{bb}} \approx \frac{\pi}{8\omega_0^2} \frac{\mathrm{Re}\,\mu(1)/\Gamma}{[\tilde{\Gamma} + (\omega_F - \tilde{\omega}_0)]^2} \times \left[1 - \frac{\tilde{\Gamma}^2 - 3(\omega_F - \tilde{\omega}_0)^2)}{2\pi[\tilde{\Gamma}^2 + (\omega_F - \tilde{\omega}_0)^2]^2} \int d\omega\, \Xi_{\mathrm{nb}}(\omega)\right]. \tag{2.24}$$

For not weak narrowband noise, one has

$$S_{\mathrm{bb}} = \frac{\pi}{8\Gamma\omega_0^2} \langle \frac{\mathrm{Re}\,\mu(1)}{|\Gamma + i(\omega_F - \omega_0 - \xi_{\mathrm{nb}}(t)) + \mu(1)|^2} \rangle_{\mathrm{nb}}. \tag{2.25}$$

One immediately sees from Eq. (2.23) and Eq. (2.25) that,

$$\tilde{\Gamma}/\Gamma = 1 + S_{\mathrm{bb}}/(S_{\mathrm{nb}} + S_\delta). \tag{2.26}$$

When the narrow-band frequency noise is weak, the width of the broad peak is determined by primarily the broadband noise, that is, it is close to a Lorentzian with halfwdith $\tilde{\Gamma}$. One can then use the above equation to extract the spectral broadening due to broadband frequency noise.

2.5 Experiments on carbon nanotube vibrational system

To corroborate the theory, Moser et al. [11] measured the spectrum of a modulated carbon nanotube resonator. The device consists of a carbon nanotube contacted by source and drain electrodes and

suspended over a gate electrode, see Fig. 2.4. The vibrational mode under study is a flexural mode as indicated in the lower panel of the Fig. 2.4. Details of the fabrication and the geometry of the device can be found in Ref. [39]. The measurement was performed at $T = 1.2$K. For such T and weak driving, low-lying flexural modes of the resonator are well described by harmonic oscillators. The driving was applied as an ac voltage δV_g on the gate electrode, and the power spectrum of the mechanical vibrations was probed by measuring the noise in the current flowing through the nanotube.

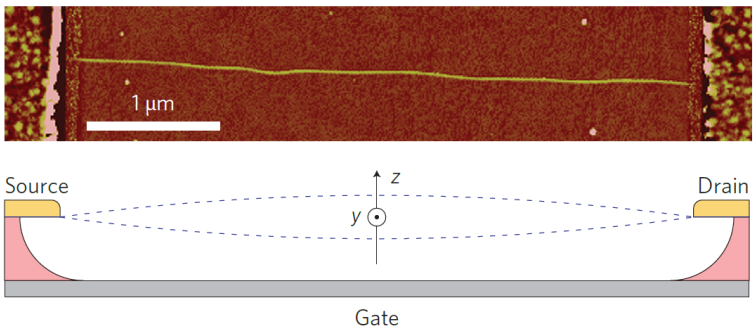

Figure 2.4 AFM image of a 4-μm-long nanotube before removing the silicon oxide (top) and schematic of the device (bottom).

Fig. 2.5 compares the power spectra of the nanotube vibrations obtained with and without the oscillating force. The spectrum without modulation (blue trace) is close to a Lorentzian, as expected for thermal vibrations. The spectrum with modulation (green trace) displays a narrow peak centered at the modulation frequency and a much broader peak of the same shape as the spectrum without modulation. The areas of the both modulation-induced parts of the spectrum scale as δV_g^2 (Fig. 2.5b, c), in agreement with Eq. (2). The separation between the parts is subject to some uncertainty because of the measurement noise in Fig. 2.5a. The resulting uncertainty in the slopes in Fig. 2.5b, c is $\lesssim 10\%$. The change of the spectrum is not a heating effect associated with the modulation, since we estimate temperature increases as $\lesssim 10^{-8}$ K. The spectral feature at ω_F is not related to the phase noise of the source used for the modulation; indeed, the phase noise of our source ≈ 10 Hz away from ω_F could only account for ≈ 0.01 % of the measured power spectrum.

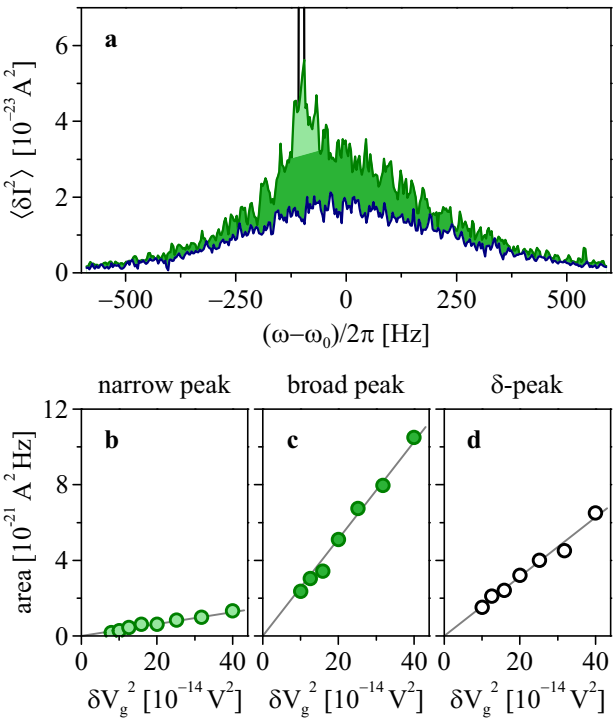

Figure 2.5 (a) The power spectrum of the fluctuating current $\delta I(t)$ through a driven carbon nanotube. The measurement bandwidth is 4.7 Hz. The eigenfrequency of the studied flexural mode is 6.3 MHz. The driving frequency is 100 Hz below the resonance frequency. The blue line refers to the power spectrum without driving; the green area shows the driving-induced spectral change. This change is separated into the broad peak (darker green), narrow peak (lighter green), and a delta-spike at the modulation frequency. This spike lies within 3 bins, within our experimental resolution, and is represented by the black vertical lines. The separation of the broad and narrow peaks is done by the straight line that interpolates the broad peak. Shown in the lower panels is the dependence of the lighter green area (b), the darker green area (c), and the area under the δ-peak (d) on the squared amplitude of the modulating gate voltage; as expected from the theory, it is close to linear.

The driving-induced spectral change provides a simple means for estimating the intrinsic relaxation rate of the resonator Γ from our experimental data. This can be done using the areas $F^2 S_{\rm nb}$ and $F^2 S_{\rm bb}$ of the narrow and broad peaks in Fig. 2.5, respectively. Comparing them to the area under the driving-induced δ-peak $F^2 S_\delta$, we eliminate F and obtain from Eq. (2.26)

$$\tilde{\Gamma}/\Gamma \approx 1 + (S_{\rm bb}/S_\delta)\,[1 - (S_{\rm nb}/S_\delta)]\,; \tag{2.27}$$

we used $S_{\rm nb} \ll S_\delta$. With $\tilde{\Gamma}/(2\pi) \simeq 230$ Hz read out from the collected spectra (such as the one in Fig. 2.5a), along with $S_{\rm bb}/S_\delta$ and $S_{\rm nb}/S_\delta$ measured from Figs. 2.5b-d, we obtain $\tilde{\Gamma}/\Gamma \simeq 2.1$, which

gives $\Gamma/(2\pi) \simeq 110$ Hz. Therefore, the broad-band fluctuations of the resonant frequency account for $\gtrsim 50\%$ of the measured mechanical linewidth. Because of the noise in the measurement in Fig. 2.5a, the uncertainty in Γ is $\lesssim 10\%$.

The narrow-band frequency noise can also be characterized from the measurements. Since the narrow-band frequency noise in the nanotube is comparatively weak, one can interpret the results using the weak-noise expression for the spectrum Eq. (2.10). Then the shape of the resonator spectrum gives the shape of the noise power spectrum. Figure 2.6 shows the narrowband frequency noise spectrum obtained by subtracting the broad part of the resonator spectrum from whole spectrum as shown in Fig. 2.5a. The spectrum is of $1/f^{\alpha}$ type. The data indicate that α is close to 1/2. Obtaining the power spectra Φ_F for several values of $\omega_F - \omega_0$ should allow separating the low-frequency part of the frequency noise spectrum $\Xi(\omega)$ even where it is not weaker than the broad-band part, and reading it directly off the data on the power spectrum using Eq. (2.10).

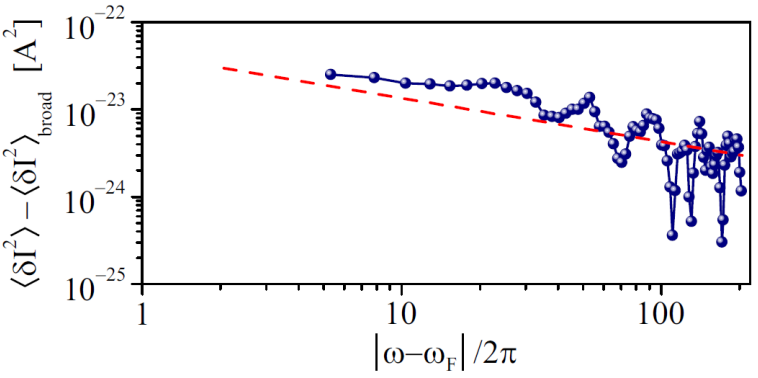

Figure 2.6 Narrow band frequency noise spectrum. It is obtained by fitting the broad part $\langle \delta I^2 \rangle_{broad}(\omega)$ of the experimental spectrum in Fig. 2.5a to a Lorentzian, and then by subtracting this fit from the experimental spectrum. The red line is a fit to $1/f^{1/2}$, where $f = |\omega - \omega_F|/2\pi$.

2.6 Conclusion

The above results show that the interplay of driving and frequency noise qualitatively changes oscillator spectra compared to the spectra with no frequency fluctuations [10]. The change sensitively depends on the frequency noise intensity and power spectrum. The possibility to separate

contributions from different parts of the frequency-noise spectrum is of significant interest, as they may come from physically different sources, like two-level fluctuators and dispersive coupling to other modes, to mention but a few.

The results suggest a way of discriminating between two major factors of the broadening of the oscillator spectra: decay (energy relaxation), frequency fluctuations induced directly by the noise that modulates the eigenfrequency. For linear oscillators, our simple procedure yields the decay rate without the need of an actual ring-down measurement that is often difficult to implement, in particular for nanotube mechanical resonators.

The analysis of driven linear oscillators with a fluctuating frequency immediately extends to the quantum regime, which is attracting much interest in nano- and optomechanics [2, 40, 41, 42, 43, 32]. For nonlinear oscillators, the nonequidistance of the energy levels can bring in new features compared to the classical limit.

CHAPTER 3

SPECTRAL EFFECTS OF DISPERSIVE MODE COUPLING IN MESOSCOPIC SYSTEMS

3.1 Introduction

Mesoscopic vibrational systems typically have several nonlinearly coupled modes. These can be flexural, torsional, or acoustic modes in the case of nanomechanical resonators[6, 44, 45, 46, 47, 48, 49, 7], photon and phonon modes in optomechanics[50, 51, 2, 52, 53, 54], or modes of microwave cavities in circuit quantum electrodynamical systems[13]. Often different modes have significantly different frequencies, so that the interaction between them is primarily dispersive. A major effect of such interaction is that the frequency of one mode depends on the amplitude of the other mode. The related shift of the mode frequency provides a means of characterizing the coupling strength where both modes can be accessed, cf. Refs. [45, 55, 49, 56] and can be used for quantum nondemolition measurements of the oscillator Fock states.[57, 58]

In many mesoscopic systems only one or a few modes can be directly accessed and controlled. The presence of dispersive coupling to other modes and the strength of this coupling have to be inferred from the data on the accessible modes. To the best of our knowledge, there have been no generally accepted means of doing this.

An important consequence of dispersive coupling is that amplitude fluctuations of one mode lead to frequency fluctuations of the other mode [37]. The amplitude fluctuations come from the coupling to a thermal reservoir, but they can also be of nonthermal origin. The mode-coupling induced frequency fluctuations broaden the spectrum of the response to an external force and the power spectrum. Such broadening has been suggested as a major broadening mechanism for flexural modes in carbon nanotubes [6], graphene sheets[7], doubly clamped beams[55, 49] as well as microcantilevers.[56]

Separating the mode-coupling induced fluctuations from other spectral broadening mechanisms is nontrivial, see Ref. [5] for a recent review of the broadening mechanisms. The most familiar broadening mechanism is vibration decay due to energy dissipation. Another mechanism of interest for the present chapter is internal vibration nonlinearity. Because of such nonlinearity, the frequency of a vibrational mode depends on the mode amplitude and thermal fluctuations of the amplitude lead to frequency fluctuations. This is reminiscent of the mode-coupling effect, yet the nonlinearity is different. We show below how the two nonlinearity mechanisms can be clearly distinguished.

In this chapter, we propose a means for identifying and characterizing the mode-coupling induced frequency fluctuations. The approach is based on studying the change of the power spectrum of the considered mode, which is due to an additionally applied periodic driving. The approach does not require access to other modes, in contrast to Refs. [45, 55, 49, 56], for example. It relies on the fact that, quite generally, frequency fluctuations lead to the features in the power spectrum of a periodically driven mode, which do not occur without such fluctuations, see Chap. 2. If one thinks of the driven mode as a charged oscillator in a stationary radiation field, these features correspond to fluorescence and quasi-elastic light scattering. The absence of these effects in the case of a periodically driven linear oscillator with constant frequency is a textbook result.[17, 18, 10]

The analysis of the power spectra of driven modes with fluctuating frequency in Chap. 2 was phenomenological. The results were obtained in several limiting cases and in the case of Gaussian fluctuations. The dispersive mode coupling studied here leads to strongly non-Gaussian frequency fluctuations. The simplest type of such coupling corresponds to the coupling energy $\propto q^2 q_d^2$, where q is the coordinate of the considered driven mode and q_d is the coordinate of the mode to which it is dispersively coupled and which we call the d-mode. Where the modes are far from resonance, the frequency change of the considered mode is proportional to the period-average value of q_d^2, i.e., to the squared amplitude of $q_d(t)$. Even where $q_d(t)$ is Gaussian, as in the case of thermal displacement of a linear mode,[18] the squared displacement $q_d^2(t)$ is not.

The features of the spectra related to the dispersive-coupling induced frequency fluctuations

depend on the interrelation between three parameters. These are the typical magnitude of the frequency fluctuations $\Delta\omega$, their reciprocal correlation time Γ_d, and the decay rate of the considered mode Γ. We assume that all these parameters are small compared to the mode eigenfrequencies and their difference.

In the absence of driving, the power spectrum and the linear response spectrum of the considered mode have the form of a convolution of the spectrum calculated without dispersive coupling and a function that depends on the parameter $\alpha_d = \Delta\omega/\Gamma_d$. [59] We call α_d the motional narrowing parameter to draw the similarity (although somewhat indirect) with the motional narrowing effect in nuclear magnetic resonance (NMR).[60, 61] For $\alpha_d \ll 1$ the correlation time of the frequency fluctuations is comparatively small. Then the fluctuations are averaged out and their effect is small, as in the case of fast decay of correlations in NMR. On the other hand, for $\alpha_d \gg 1$, the spectrum can be thought of as a superposition of partial spectra, each for a given value of the amplitude of $q_d(t)$. The weight of the partial spectrum is determined by the probability distribution of this amplitude.

In the presence of driving, the situation is different. The first distinction is that, without the dispersive coupling, there is no driving-induced part of the power spectrum at all, except for the trivial δ-peak at the driving frequency. Based on the previous results in Chap. 2, we expect that the driving-induced part of the spectrum will strongly depend on the interrelation between the rates Γ and Γ_d. It is clear that it will also strongly depend on α_d, but this dependence is not known in advance.

The formulation below is in the classical terms. However, as we explain, the results fully apply also to the case where the considered driven mode is quantum, i.e., its energy level spacing is comparable or exceeds the temperature. At the same time, it is essential that the d-mode is classical. The case of the deeply quantum regime of the d-mode is in a way simpler. In this case, the power spectrum of the considered mode without driving can have a pronounced fine structure, with different lines corresponding to different occupation numbers of the d-mode.[37] This is similar to the spectrum of a two-level system dispersively coupled to a quantum vibrational

mode[62, 63], where the fine structure has been seen in the experiment.[12]

3.1.1 The structure of the chapter

An important part of the chapter is the averaging over the fluctuations of the d-mode. This is an interesting theoretical problem, with direct relevance to the experiment. It involves an explicit calculation of the appropriate path integral. The calculation is presented in Secs. 3.4 and 3.5. These sections as well as Sec. 3.3.1 can be skipped if one is interested primarily in the predictions for the experiment. Below in Sec. 3.2 we give a general expression for the power spectrum of a mode driven by an external field, which applies where the field is comparatively weak, so that the internal nonlinearity of the mode remains small. The effect of the field is most pronounced where it is close to resonance. In Sec. 3.3 we derive equations of motion for weakly damped dispersively coupled modes in the rotating wave approximation. Section 3.6 provides the explicit analytical expressions for the driving-induced part of the power spectrum in the limiting cases, which refer to the fast or slow relaxation of the d-mode compared to the relaxation of the driven mode and also to the large or small frequency shift due to the dispersive coupling compared to the relaxation rate of the d-mode. This section also presents results of numerical calculations of the spectra, which are compared with the results of simulations. The last part of the section describes the dependence of the area of the driving-induced peak on the dispersive coupling parameters. Section 3.7 extends the results to dispersive coupling to several modes. In particular, we consider the cumulative effect of dispersive coupling to many, but not too many modes, which may become strong even where the coupling to each of the modes is weak. Section 3.8 describes the driving-induced part of the power spectrum for a nonlinear oscillator, where the fluctuations of the oscillator frequency are due not to dispersive coupling but to the internal nonlinearity. The last section provides a summary of the results. The transfer-matrix method used to perform the averaging over the dispersive-coupling induced fluctuations and an outline of an alternative derivation of the major result are given in the appendices.

3.2 Driving-induced part of the power spectrum

Frequency fluctuations render the mode response to driving random. Generally, the response is nonlinear in the driving strength. Respectively, even for sinusoidal driving, the mode power spectrum $\Phi(\omega)$ is a complicated function of the driving amplitude F and frequency ω_F. The conventional way of measuring the power spectrum of a driven system with coordinate q corresponds to the definition

$$\Phi(\omega) = 2\mathrm{Re} \int_0^\infty dt e^{i\omega t} \langle\langle q(t+t')q(t')\rangle\rangle,$$

where $\langle\langle\cdot\rangle\rangle$ indicates statistical averaging and averaging with respect to t' over the driving period $2\pi/\omega_F$ (sometimes the power spectrum is also defined as $\Phi(\omega)/2\pi$). If the driving is weak, one can keep in $\Phi(\omega)$ only the terms quadratic in F,

$$\Phi(\omega) \approx \Phi_0(\omega) + \frac{\pi}{2} F^2 |\chi(\omega_F)|^2 \delta(\omega - \omega_F) + F^2 \Phi_F(\omega). \tag{3.1}$$

Here, Φ_0 is the power spectrum in the absence of driving. For the considered underdamped mode, it is a resonant peak at the mode eigenfrequency ω_0, which is due to thermal vibrations; the width of the peak is small compared to ω_0. Function $\chi(\omega)$ is the mode susceptibility, $\Phi_0(\omega) = (2k_BT/\omega_0)\mathrm{Im}\ \chi(\omega)$ in the classical limit. The term $\propto |\chi(\omega_F)|^2$ describes the contribution of stationary forced vibrations at frequency ω_F.

Of utmost interest to us is the last term in Eq. (3.1), $\Phi_F(\omega)$. For a linear oscillator with non-fluctuating frequency, this term is equal to zero. Indeed, the motion of such oscillator is a superposition of thermal vibrations and forced vibrations at frequency ω_F, which are uncoupled. Frequency fluctuations affect both thermal vibrations, leading to spectral broadening, and forced vibrations. The latter effect is particularly easy to understand in the case of slow frequency fluctuations. Here, one can think of the amplitude and phase of forced vibrations as being determined by the detuning of the instantaneous mode frequency from the driving frequency. Therefore they fluctuate in time, which leads to the onset of a “pedestal" of the δ-peak at $\omega = \omega_F$ in Eq. (3.1). Some other limiting cases have been considered earlier in Chap. 2.

3.3 Equations of motion for the slow variables

We will consider the power spectrum $\Phi(\omega)$ in the case where the mode of interest is dispersively coupled to another mode (mode d). The modes are weakly coupled to a thermal reservoir, so that their decay rates are small. The mode of interest is driven by a periodic field $F\cos\omega_F t$. The Hamiltonian of the system is

$$H = H_0 + H_b + H_i, \qquad H_0 = \frac{1}{2}(p^2 + \omega_0^2 q^2) + \frac{1}{4}\gamma q^4$$
$$+ \frac{1}{2}(p_d^2 + \omega_d^2 q_d^2) + \frac{3}{4}\gamma_d q^2 q_d^2 - qF\cos\omega_F t. \tag{3.2}$$

Here, p and p_d are the momenta of the considered mode and the d-mode, respectively, ω_0 and ω_d are the mode eigenfrequencies, γ is the parameter of the intrinsic nonlinearity of the considered mode, and γ_d is the dispersive coupling parameter. We do not incorporate the intrinsic nonlinearity of the d-mode, as it will not affect the results if it is small, see below.

The term H_b is the Hamiltonian of the thermal bath (each mode can have its own bath, but we assume that in this case the baths have the same temperature), whereas H_i describes the modes-to-bath coupling. We assume the coupling to be linear in the modes coordinates, $H_i = qh + q_d h_d$, where h and h_d are functions of the dynamical variables of the bath. Such coupling is the dominant mechanism of relaxation for small mode displacements and velocities. For H_i of this form, the decay rate of the considered mode is[64, 65]

$$\Gamma \equiv \Gamma(\omega_0) = \hbar^{-2}\mathrm{Re}\int_0^\infty dt\langle[h^{(0)}(t), h^{(0)}(0)]\rangle e^{i\omega_0 t}, \tag{3.3}$$

where $h^{(0)}$ is function h calculated in the neglect of the mode-bath coupling. The expression for the decay rate Γ_d of the d-mode is similar to Eq. (3.3), with $h^{(0)}$ replaced with $h_d^{(0)}$ and ω_0 replaced with ω_d. Parameters Γ, Γ_d correspond to friction coefficients in the phenomenological description of the mode dynamics

$$\ddot{q} + \partial_q H_0 = -2\Gamma\dot{q} - h^{(0)}(t). \tag{3.4}$$

The analysis below refers to slowly varying amplitudes and phases of the modes and applies even where the above phenomenological description does not apply.[64, 65, 37]

In what follows we assume that the modes are underdamped, the nonlinearity is weak, and the driving frequency is close to resonance,

$$\Gamma, \Gamma_d, \frac{|\gamma|\langle q^2\rangle}{\omega_0}, \frac{|\gamma_d|\langle q_d^2\rangle}{\omega_0}, |\omega_0 - \omega_F| \ll \omega_0, \omega_d, |\omega_0 - \omega_d|. \tag{3.5}$$

The condition on γ, γ_d means that the change of the mode frequencies due to the nonlinearity is small compared to the eigenfrequency. However, it does not mean that the effect of the nonlinearity is small, as the frequency change has to be compared with the frequency uncertainty due to the decay Γ, Γ_d. We assume that the nonlinear change of the d-mode frequency, which comes from the dispersive coupling and the internal nonlinearity of the d-mode, is also small compared to ω_d.

3.3.1 Stochastic equations for slow variables

Where conditions (3.5) apply, the motion of the underdamped modes presents almost sinusoidal vibrations with slowly varying amplitudes and phases. It can be described by the standard method of averaging, which is similar to the rotating wave approximation in quantum optics. To this end, we change to complex variables

$$u(t) = \frac{1}{2}[q(t) + (i\omega_F)^{-1}\dot{q}(t)]\exp(-i\omega_F t) \tag{3.6}$$

and similarly $u_d(t) = \frac{1}{2}[q_d(t) + (i\omega_d)^{-1}\dot{q}_d(t)]\exp(-i\omega_d t)$. Disregarding fast oscillating terms in the equation for $u(t)$, we obtain

$$\begin{aligned} \dot{u} &= -[\Gamma + i\delta\omega_F - i\xi(t)]u - i\frac{F}{4\omega_0} + f(t), \\ \delta\omega_F &= \omega_F - \omega_0, \quad \xi(t) = \frac{3\gamma}{2\omega_0}|u(t)|^2 + \frac{3\gamma_d}{2\omega_0}|u_d(t)|^2, \end{aligned} \tag{3.7}$$

where $f(t) = -(2i\omega_0)^{-1}h^{(0)}(t)\exp(-i\omega_F t)$. Similarly, the equation for $u_d(t)$ reads

$$\dot{u}_d = -\left[\Gamma_d - i\frac{3\gamma_d}{2\omega_d}|u(t)|^2)\right]u_d + f_d(t), \tag{3.8}$$

with $f_d(t) = -(2i\omega_d)^{-1}h_d^{(0)}(t)\exp(-i\omega_d t)$.

Functions f, f_d describe the forces on the modes from the thermal bath. The forces are random, and one can always choose $\langle f \rangle = \langle f_d \rangle = 0$. Asymptotically, they are delta-correlated Gaussian noises,

$$\langle f(t) f^*(t') \rangle = (\Gamma k_B T/\omega_0^2)\delta(t-t'),$$
$$\langle f_d(t) f_d^*(t') \rangle = (\Gamma_d k_B T/\omega_d^2)\delta(t-t'); \tag{3.9}$$

all other correlators vanish. The δ-functions here are δ-functions in "slow" time compared to $\omega_0^{-1}, \omega_d^{-1}$, and the correlation time of the thermal bath. The stochastic differential equations (3.7) and (3.8) are understood in the Stratonovich sense: $\langle u(t) f^*(t) \rangle = \Gamma k_B T/2\omega_0^2, \langle u_d(t) f_d^*(t) \rangle = \Gamma_d k_B T/2\omega_d^2$. These equations were obtained and their range of applicability established for a harmonic oscillator coupled to a bath,[64, 65] but they also hold for a weakly anharmonic oscillator.[37]

As seen from the definition of the complex amplitude $u(t)$, function $\xi(t)$ in Eq. (3.7) describes a change of the frequency of the considered mode due to the intrinsic nonlinearity and the dispersive coupling. Because of the noise terms f, f_d, the frequency becomes a random function of time. The related frequency noise is of primary interest for this chapter.

3.4 The driving-induced spectrum $\Phi_F(\omega)$ for dispersive coupling

In this and the two following sections we will study the spectrum $\Phi_F(\omega)$ in the case where the internal nonlinearity of the mode can be disregarded, i.e., one can set $\gamma = 0$. In this case frequency fluctuations $\xi(t) \propto |u_d(t)|^2$ in Eq. (3.7) are due only to the dispersive nonlinear mode coupling. An important feature of this coupling is that it does not affect the frequency noise $\xi(t)$ itself, as essentially was noticed earlier.[59] In other words, fluctuations of $|u_d(t)|^2$ are the same as if the d-mode were just a linear oscillator uncoupled from the considered mode.

The simplest way to see this is to change in the equation of motion (3.8) from $u_d(t)$ to $\tilde{u}_d(t) = K(t)u_d(t)$ with $K(t) = \exp[-3i(\gamma_d/2\omega_d)\int^t dt' |u(t')|^2]$. The Langevin equation for $\tilde{u}_d$ is $\dot{\tilde{u}}_d = -\Gamma_d \tilde{u}_d + \tilde{f}_d(t)$ with $\tilde{f}_d(t) = K(t) f_d(t)$. From Eq. (3.9), the noise $\tilde{f}_d(t)$ has the same correlation

functions as $f_d(t)$. Therefore the term $\propto \gamma_d$ drops out of the equation for $\tilde{u}_d$. Since $|u_d|^2 = |\tilde{u}_d|^2$, the term $\propto \gamma_d$ does not affect $|u_d(t)|^2$ either [even though it does affect $u_d(t)$].

It is convenient to write $\xi(t)$ in terms of the scaled real and imaginary part of

$$\tilde{u}_d = (2\omega_0/3|\gamma_d|)^{1/2}(Q_d + iP_d).$$

Functions Q_d, P_d are the scaled quadratures of a damped harmonic oscillator. They are described by the independent exponentially correlated Gaussian noises (the Ornstein-Uhlenbeck noises)[66]. Using the Langevin equation for $\tilde{u}_d$, we obtain

$$\begin{aligned}
&\langle Q_d(t)Q_d(0)\rangle = \langle P_d(t)P_d(0)\rangle = \alpha_d\Gamma_d \exp(-\Gamma_d|t|),\\
&\alpha_d = 3|\gamma_d|k_BT/8\omega_0\omega_d^2\Gamma_d,\\
&\xi(t) = [Q_d^2(t) + P_d^2(t)]\mathrm{sgn}\gamma_d.
\end{aligned} \tag{3.10}$$

The frequency noise of the driven mode $\xi(t)$ is non-Gaussian. Parameter α_d characterizes the ratio of the standard deviation of the noise, which is equal to the noise mean value $\langle\xi(t)\rangle = 3\gamma_d k_BT/4\omega_0\omega_d^2$, to its correlation rate Γ_d.

Since $\xi(t)$ is independent of $u(t)$, the Langevin equation for $u(t)$ (3.7) is linear. Its solution reads

$$\begin{aligned}
&u(t) = \int_{-\infty}^{t} dt' \chi_{\mathrm{sl}}^*(t,t')[(-iF/4\omega_0) + f(t')],\\
&\chi_{\mathrm{sl}}(t,t') = e^{-(\Gamma - i\delta\omega_F)(t-t')} \exp\left[-i\int_{t'}^{t} dt''\xi(t'')\right].
\end{aligned} \tag{3.11}$$

Function $\chi_{\mathrm{sl}}(t,t')$ describes the response of the considered driven mode to a resonant perturbation. The coefficient at F averaged over realizations of $\xi(t)$ gives the resonant susceptibility of the mode,

$$\chi(\omega_F) = \frac{i}{2\omega_0}\int_0^\infty dt\langle\chi_{\mathrm{sl}}(t,0)\rangle. \tag{3.12}$$

It determines the δ-peak in the power spectrum (3.1). From Eq. (3.11), the term $\Phi_F(\omega)$ in Eq. (3.1)

for the power spectrum has the form

$$\Phi_F(\omega) = (8\omega_0^2)^{-1}\Re\int_0^\infty dt\exp[i(\omega-\omega_F)t]$$
$$\times\left[\int_{-\infty}^{t}dt'\int_{-\infty}^{0}dt_1'\langle\chi_{\rm sl}(t,t')\chi_{\rm sl}^*(0,t_1')\rangle - 4\omega_0^2|\chi(\omega_F)|^2\right] \tag{3.13}$$

(in the integral over t it is implied that Im $\omega\to+0$).

The term $\propto f(t')$ in Eq. (3.11) determines the power spectrum of the mode $\Phi_0(\omega)$ near its maximum, $|\omega-\omega_0|\ll\omega_0$, in the absence of driving. Thus, Eqs. (3.11) - (3.13) give a general expression for the power spectrum of an underdamped mode with fluctuating frequency in the absence of internal nonlinearity.

3.5 Averaging over the frequency noise for dispersive coupling

To find the driving-induced part of the power spectrum $F^2\Phi_F(\omega)$, one has to perform averaging over fluctuations of $\xi(t)$ in Eq. (3.13). This calculation is the central theoretical part of the chapter. In what follows we outline the critical steps that are involved.

The integrand in the expression for $\Phi_F(\omega)$ can be written as

$$\langle\chi_{\rm sl}(t,t')\chi_{\rm sl}^*(0,t_1')\rangle = e^{-(\Gamma-i\delta\omega_F)(t-t')+(\Gamma+i\delta\omega_F)t_1'}$$
$$\times G^2(t,t',t_1'),\quad G^2(t,t',t_1') = \langle e^{-i\phi_\xi(t,t')+i\phi_\xi(0,t_1')}\rangle,$$
$$\phi_\xi(t,t') = \int_{t'}^{t}dt''\xi(t''). \tag{3.14}$$

Here, $\phi_\xi(t,t')$ is the increment of the phase of the oscillator over the time interval (t',t) due to the frequency noise $\xi(t)$. Function G describes the result of the averaging over the noise.

Expression (3.14) can be slightly simplified using the relation (3.10) between $\xi(t)$ and the quadratures Q_d and P_d. These quadratures are statistically independent, and therefore averaging over them can be done independently, so that

$$G(t,t',t_1') = \left\langle\exp\left[i\int_{t_0}^{t}dt''k(t'')Q_d^2(t'')\right]\right\rangle, \tag{3.15}$$

where $t_0 = \min(t', t_1')$ and in the interval $t_0 < t'' < t$ function $k(t'')$ is equal to $0, \pm 1$,

$$k(t'') = \begin{cases} -\mathrm{sgn}\gamma_d, & \tau \le t'' \le t; \quad \tau = \max(t', 0) \\ 0, & \tau' < t'' < \tau; \quad \tau' = \max\left[\min(0, t'), t_1'\right] \\ \mathrm{sgn}(t' - t_1')\mathrm{sgn}\gamma_d, & t_0 = \min(t', t_1') \le t'' \le \tau'. \end{cases} \tag{3.16}$$

The averaging in Eq. (3.15) can be conveniently done using the path-integral technique. A theory of the power spectrum based on this technique was previously developed for the case where there is no driving.[59] The approach[59] can be extended to the present problem, as discussed in the Sec. 3.5.5. However, the calculation is cumbersome. Here we use a different method, which is based on the technique [67] for calculating determinants in path integrals.

In terms of a path integral, the mean value of a functional $L[Q_d(t)]$ of $Q_d(t)$ can be written as $\int \mathscr{D}Q_d(t) L[Q_d(t)] \mathscr{P}[Q_d(t)]$. For the considered exponentially correlated noise $Q_d(t)$, the probability density functional is (cf. Ref. [38])

$$\mathscr{P}[Q_d(t)] = \exp\left[-(4\alpha_d \Gamma_d^2)^{-1} \int dt (\dot{Q}_d + \Gamma_d Q_d)^2\right].$$

To find $G(t, t', t_1')$ we need to perform averaging over the values of $Q_d(t'')$ in the interval (t_0, t). In a standard way, we discretize the time as $t_n = t_0 + n\varepsilon, n = 0, \ldots, N$, where $\varepsilon = (t - t_0)/N$ and $N \gg 1$. The path integral is then reduced to integrating over the values of $Q_n \equiv Q_d(t_n)/(4\alpha_d \Gamma_d^2 \varepsilon)^{1/2}$ with $1 \le n \le N$ followed by averaging over $Q_0 \equiv Q_d(t_0)/(4\alpha_d \Gamma_d^2 \varepsilon)^{1/2}$ with the Boltzmann weighting factor $\exp[-2\varepsilon \Gamma_d Q_0^2]$.

In the mid-point discretization, in the integrals over time one uses $\dot{Q}_d(t) \to [Q_d(t) - Q_d(t - \varepsilon)]/\varepsilon$ and $f\big(Q_d(t)\big) \to [f\big(Q_d(t)\big) + f\big(Q_d(t - \varepsilon)\big)]/2$ for an arbitrary $f(Q_d)$.[68] Then the exponent in $\mathscr{P}[Q_d(t)]$ becomes

$$-(4\alpha_d \Gamma_d^2)^{-1} \int dt (\dot{Q}_d + \Gamma_d Q_d)^2 \to -\sum_{n=1}^{N} \Big[(Q_n - Q_{n-1})^2 + \varepsilon^2 \Gamma_d^2 Q_n^2\Big] - \varepsilon \Gamma_d (Q_N^2 - Q_0^2). \tag{3.17}$$

The integral over t'' in Eq. (3.15) is similarly discretized and goes over into $4\alpha_d\Gamma_d^2\varepsilon^2\sum_n k_n Q_n^2$ with $k_n \equiv k(t_n)$. Then the expression for function G becomes

$$G(t,t',t_1') = I[k]/I[0], \qquad I[k] = \int dQ_0 e^{-Q_0^2(1+\varepsilon\Gamma_d)} \int \prod_{n=1}^{N} dQ_n \exp\left[-\mathbf{Q}^\dagger \hat{\Lambda}[k]\mathbf{Q} + 2Q_0Q_1\right]. \tag{3.18}$$

Here, $\mathbf{Q}$ is a vector with components $Q_1,\ldots,Q_N$. From Eq. (3.17), the diagonal matrix elements of $\hat{\Lambda}[k]$ are $\Lambda_{nn}[k] = 2+\varepsilon^2\Gamma_d^2(1-4i\alpha_d k_n)$ for $1 \le n \le N-1$, $\Lambda_{NN}[k] = 1+\varepsilon^2\Gamma_d^2(1-4i\alpha_d k_N)+\varepsilon\Gamma_d$. The only non-zero off-diagonal matrix elements of $\hat{\Lambda}$ are $\Lambda_{n\,n\pm1}[k] = -1$.

3.5.1 Finding the determinant

The integrals in Eq. (3.18) are Gaussian. Therefore the calculation of G requires finding the determinants of the matrices $\hat{\Lambda}[k]$ and $\hat{\Lambda}[0]$. This can be done following the approach [67]. We consider the determinant $D_n \equiv D_n[k]$ of the square submatrix of $\hat{\Lambda}[k]$, which is located at the lower right corner and has rank $N-n+1$. For example, D_1 is the determinant of the whole matrix $\hat{\Lambda}$, whereas D_N is the matrix element Λ_{NN}. The result of integration over $Q_1,\ldots,Q_N$ in Eq. (3.18) for $I[k]$, besides the Q_0-dependent factor discussed below, is $\pi^{N/2}/\sqrt{D_1[k]}$.

It is straightforward to see that D_n satisfies the recurrence relation

$$D_n = [2+\varepsilon^2\Gamma_d^2(1-4i\alpha_d k_n)]D_{n+1} - D_{n+2}, \quad 1 \le n \le N-2. \tag{3.19}$$

In the limit $\varepsilon \to 0$, $D_n[k]$ goes over into $D(t_n;k)$ and Eq. (3.19) reduces to a differential equation for $D(t'') \equiv D(t'';k)$,

$$\ddot{D}(t'') - \Gamma_d^2[1-4i\alpha_d k(t'')]D(t'') = 0 \tag{3.20}$$

The obvious boundary conditions for function D are $D(t) = \lim_{\varepsilon\to0} D_N = 1$ and $\dot{D}(t) = \lim_{\varepsilon\to0}(D_N - D_{N-1})/\varepsilon = -\Gamma_d$. The quantity of interest is $D_1[k] \approx D(t_0;k)$; we will also need $\dot{D}(t_0;k)$, see below.

Integrating the linear in Q_1 term in the exponent in Eq. (3.18) gives the factor $\exp[Q_0^2(\hat{\Lambda}^{-1})_{11}]$. It follows from the above analysis that $(\hat{\Lambda}^{-1})_{11} = D(t_0+2\varepsilon)/D(t_0+\varepsilon) \approx 1+\varepsilon\dot{D}(t_0)/D(t_0)$. Then the result of integration over Q_0 in Eq. (3.18) is the factor $\{\pi/\varepsilon[\Gamma_d - \dot{D}(t_0;k)/D(t_0;k)]\}^{1/2}$ in $I[k]$.

For $k = 0$, we have from Eq. (3.20) $D(t'';0) = \exp[\Gamma_d(t-t'')]$. With this, the expression (3.18) for function G becomes

$$G(t,t',t_1') = \left\{2\Gamma_d e^{\Gamma_d(t-t_0)}/[\Gamma_d D(t_0;k) - \dot{D}(t_0;k)]\right\}^{1/2} \tag{3.21}$$

This expression is the central result of the section. It reduces the problem of calculating the driving-induced part of the power spectrum to solving an ordinary differential equation (3.20).

3.5.2 The average susceptibility

We start the discussion of the applications of the general result (3.21) with the analysis of the factor $\langle\chi_{\rm sl}(t,0)\rangle$, which gives the average mode susceptibility, Eq. (3.12). Function $\langle\chi_{\rm sl}(t,0)\rangle$ is given by $\langle\exp[-i\int_0^t dt''\xi(t'')]\rangle$, which in turn is given by Eq. (3.14) with G of the form of Eq. (3.15) in which $t' = t_1' = 0$ and $k(t'') = -\mathrm{sgn}\gamma_d$. Solving Eq. (3.20) with $k(t'') = \text{const}$ is straightforward, as is also finding then $G(t,0,0)$ from Eq. (3.21). The result reads

$$\begin{aligned}
&\langle\chi_{\rm sl}(t,0)\rangle = \exp\left[-(\Gamma - i\delta\omega_F)t\right]\tilde{\chi}(t), \qquad \tilde{\chi}(t) = e^{\Gamma_d t} \\
&\times\left[\cosh a_d t + (\Gamma_d/a_d)(1+2i\alpha_d\mathrm{sgn}\gamma_d)\sinh a_d t\right]^{-1}, \\
&a_d = \Gamma_d(1+4i\alpha_d\mathrm{sgn}\gamma_d)^{1/2}.
\end{aligned} \tag{3.22}$$

Equation (3.22) expresses the average susceptibility in elementary functions. It agrees with the result[59] for the correlation function of the mode dispersively coupled to a fluctuating mode.

3.5.3 The average of the product of the susceptibilities

Solving the full Eq. (3.20) with discontinuous $k(t'')$ is more complicated. It can be done by finding function $D(t'')$ piecewise where $k(t'') = \text{const}$ as a sum of "incident" and "reflected" waves and then matching the solutions. The corresponding method reminds the transfer matrix method. It is

described in Sec. 3.5.4. The result reads

$$[G(t,t',t_1')]^{-2} = [\tilde{\chi}(\tau_1)\tilde{\chi}'(\tau_3)]^{-1} - \frac{(\Gamma_d^2 - a_d^2)(\Gamma_d^2 - a_d'^2)}{4\Gamma_d^2 a_d a_d'}$$
$$\times \sinh(a_d\tau_1)\sinh(a_d'\tau_3)\exp[-\Gamma_d(2\tau_2+\tau_1+\tau_3)] \tag{3.23}$$

where $\tau_1 = t-\tau, \tau_2 = \tau-\tau', \tau_3 = \tau'-t_0$; parameters t_0, τ, and τ' are expressed in terms of t,t',t_1' in Eq. (3.16), and $\tilde{\chi}(t)$ is given by Eq. (3.22). Function $\tilde{\chi}'(t) = \tilde{\chi}(t)$ and $a_d' = a_d$ for $t' < t_1'$, whereas $\tilde{\chi}'(t) = \tilde{\chi}^*(t)$ and $a_d' = a_d^*$ for $t' > t_1'$.

This expression is unexpectedly simple. We use it below for analytical calculations, in particular for calculating the driving-induced part of the power spectrum in the limiting cases.

3.5.4 The transfer-matrix type construction

The central part of the calculation of the driving-induced power spectrum is the averaging over the frequency noise due to dispersive coupling. Equations (3.14) and (3.21) reduce this averaging to solving an ordinary differential equation (3.20) with the coefficient that varies with time stepwise. The solution can be simplified by taking advantage of this specific time dependence.

From Eq. (3.16), the interval (t_0,t) in Eq. (3.20) is separated into three regions $m = 1,2,3$ within which the time-dependent coefficient $k(t'') = \bar{k}_m$ is constant. The boundaries between the regions τ and τ' and the values of $\bar{k}_m$ are specified in Eq. (3.16). We enumerate the regions in the order of decreasing time, that is, the region $\tau < t'' < t$ corresponds to $m = 1$, etc. In each region

$$D(t'';k) = M_{11}(t''-t_0;m)A_m + M_{12}(t''-t_0;m)B_m. \tag{3.24}$$

Here, M_{ij} are the matrix elements of the matrix

$$\hat{M}(t'';m) = \begin{pmatrix} \cosh a_m t'' & \sinh a_m t'' \\ a_m \sinh a_m t'' & a_m \cosh a_m t'' \end{pmatrix},$$
$$a_m \equiv a(\bar{k}_m) = \Gamma_d(1-4i\alpha_d\bar{k}_m)^{1/2} \tag{3.25}$$

We note that, from Eq. (3.16), $a_1 = \Gamma_d(1+4i\alpha_d \mathrm{sgn}\gamma_d)^{1/2}$, whereas $a_2 = \Gamma_d$; a_3 is equal to either a_1 or a_1^* depending on whether $t' < t_1'$ or $t' > t_1'$ in the argument of the G-function in (3.21).

The values of A_1, B_1 in Eq. (3.24) are determined by the conditions $D(t;k) = 1, \dot{D}(t;k) = -\Gamma_d$. The values of A_m, B_m for $m = 2,3$ are found from the continuity of $D(t'';k), \dot{D}(t'';k)$ at the boundaries $t'' = \tau, \tau'$.

Function $G(t,t',t_1')$ in Eq. (3.21) is determined by $D(t_0;k) = A_3$ and $\dot{D}(t_0;k) = a_3 B_3$. From Eqs. (3.24) and (3.25) we have

$$\begin{pmatrix} A_3 \\ B_3 \end{pmatrix} = \hat{M}^{-1}(\tau' - t_0;3)\hat{M}(\tau' - t_0;2)\hat{M}^{-1}(\tau - t_0;2)$$

$$\times \hat{M}(\tau - t_0;1)\hat{M}^{-1}(t - t_0;1) \begin{pmatrix} 1 \\ -\Gamma_d \end{pmatrix}, \tag{3.26}$$

This simple relation combined with Eq. (3.21) give the integrand in the expression for the power spectrum $\Phi_F(\omega)$ in a simple form, which is convenient for numerical integration. The expression (3.26) can be evaluated in the explicit form. The result is given in Sec. 3.5.3. It is advantageous when one looks for the asymptotic expressions for the spectrum $\Phi_F(\omega)$.

3.5.5 Alternative path-integral approach to averaging over frequency noise

Here we provide an alternative approach to evaluating function $G(t,t',t_1')$, which is defined by Eq. (3.15) and describes the outcome of averaging over the frequency noise. The method is related, albeit fairly remotely, to the method developed for calculating the power spectrum of a nonlinear oscillator in the absence of driving.[59, 37] We start with writing the probability density functional of the Gaussian process $Q_d(t)$ on the whole time axes, $-\infty < t < \infty$, in terms of the correlation function $A(t_2,t_3) = \langle Q_d(t_2)Q_d(t_3)\rangle$ and its inverse $A^{-1}(t_2,t_3)$,

$$\mathscr{P}[Q_d(t)] = \exp\left[-\frac{1}{2}\int\int dt_1 dt_2 Q_d(t_1)A^{-1}(t_1,t_2)Q_d(t_2)\right],$$

$$\int dt_2 A^{-1}(t_1,t_2)A(t_2,t_3) = \delta(t_1 - t_3), \tag{3.27}$$

cf. Ref. [38]).

From Eq. (3.15), function G and its derivative $\partial G/\partial t$ can be written as

$$G(t,t',t_1') = \frac{\int \mathscr{D}[Q_d]\tilde{\mathscr{P}}[Q_d]}{\int \mathscr{D}[Q_d]\mathscr{P}[Q_d]},$$
$$\frac{\partial G}{\partial t} = -i\mathrm{sgn}(\gamma_d)\frac{\int \mathscr{D}[Q_d]Q_d^2(t)\tilde{\mathscr{P}}[Q_d]}{\int \mathscr{D}[Q_d]\mathscr{P}[Q_d]}, \tag{3.28}$$

where functional $\tilde{\mathscr{P}}$ has the form

$$\tilde{\mathscr{P}}[Q_d] = \exp\left[-\frac{1}{2}\int\int dt_1 dt_2 Q_d(t_1)\tilde{A}^{-1}(t_1,t_2)Q_d(t_2)\right],$$
$$\tilde{A}^{-1}(t_1,t_2) = A^{-1}(t_1,t_2) - 2ik(t_2)\delta(t_1-t_2). \tag{3.29}$$

Here $k(t_2)$ is a stepwise function, which is equal to 0 or ± 1 in the time interval (t_0,t), where $t_0 \equiv \min(t',t_1')$ is defined in Eq. (3.16). This definition has to be extended in the present formulation, $k(t_2) = 0$ for $t_2 > t$ and $t_2 < t_0$.

A key observation is that functional $\tilde{\mathscr{P}}[Q_d]$ is also Gaussian. One can introduce an operator $\tilde{A}(t,t_1)$ reciprocal to $\tilde{A}^{-1}$,

$$\int dt_1 \tilde{A}(t,t_1)\tilde{A}^{-1}(t_1,t_2) = \delta(t-t_2). \tag{3.30}$$

In terms of this operator,

$$\tilde{A}(t,t) = \frac{\int \mathscr{D}[Q_d]Q_d^2(t)\tilde{\mathscr{P}}[Q_d]}{\int \mathscr{D}[Q_d]\tilde{\mathscr{P}}[Q_d]}. \tag{3.31}$$

Multiplying equation (3.29) for $\tilde{A}^{-1}$ by $A(t_2,t_3)\tilde{A}(t_1,t)$ and integrating with respect to t_1,t_2, we obtain an integral equation for $\tilde{A}(t,t_3)$,

$$\tilde{A}(t,t_3) - 2i\int k(t_1)\tilde{A}(t,t_1)A(t_1,t_3)dt_1 = A(t,t_3). \tag{3.32}$$

This equation can be reduced to a differential equation by differentiating twice with respect to t_3,

$$\frac{\partial^2\tilde{A}(t,t_3)}{\partial t_3^2} - \Gamma_d^2[1-4i\alpha_d k(t_3)]\tilde{A}(t,t_3) = -2\alpha_d\Gamma_d^2\delta(t_3-t). \tag{3.33}$$

Interestingly, Eq. (3.33) has the same structure as the differential equation for the "time-dependent" determinant found in the other method, see Eq. (3.20). Thus it can be solved in a similar fashion as

in Sec. (3.5.4). The boundary conditions are $\tilde{A}(t,\pm\infty)=0$. It follows from the decay of correlations of $Q_d(t)$. At the values of t_3 where $k(t_3)$ changes stepwise, see Eq. (3.16), $\tilde{A}$ and $\partial\tilde{A}/\partial t_3$ remain continuous, except $t_3=t$, where $\partial\tilde{A}/\partial t_3$ changes by $2\alpha_d\Gamma_d^2$,as seen from Eq. (3.33).

We can now write Eq. (3.29) for function $G(t,t',t_1')$, in terms of function $\tilde{A}$,

$$\partial_t G(t,t',t_1') = -i\mathrm{sgn}(\gamma_d)\tilde{A}(t,t)G. \tag{3.34}$$

The boundary condition for this equation is $G(t,t,0)=1$. From the explicit expression for G we also have

$$\begin{aligned}\partial_{t'} G(t,t',t_1') &= i\mathrm{sgn}(\gamma_d)\tilde{A}(t',t')G(t,t',t_1'),\\ \partial_{t_1'} G(t,t',t_1') &= -i\mathrm{sgn}(\gamma_d)\tilde{A}(t_1',t_1')G(t,t',t_1').\end{aligned} \tag{3.35}$$

The solution of these equations reads

$$G(t,t',t_1') = \exp\left\{-i\mathrm{sgn}(\gamma_d)\left[\int_{t'}^{t}\tilde{A}(t'',t'')dt'' - \int_{t_1'}^{0}\tilde{A}(t'',t'')dt''\right]\right\}. \tag{3.36}$$

We have checked that the expression for function G that follows from Eqs. (3.33) and (3.36) coincides with the result obtained using the transfer matrix method.

3.6 Discussion of results

In this section we use the above results to discuss the form of the driving-induced part $F^2\Phi_F(\omega)$ of the power spectrum in the case of dispersive coupling. We give explicit expressions for the spectrum in the limiting cases. We also present the results of the numerical calculations of the spectrum based on the general expressions (3.13), (3.14), and (3.23). These results are compared with the simulations. The simulations were performed in a standard way by integrating the stochastic equations of motion (3.7) - (3.9) using the Heun scheme [69].

As we show, the shape and the magnitude of $\Phi_F(\omega)$ sensitively depend on two factors. One is the interrelation between the magnitude of frequency fluctuations $\Delta\omega$ and their bandwidth $2\Gamma_d$,

the motional-narrowing parameter α_d defined in Eq. (3.10). The other is the interrelation between Γ_d and the width of the mode spectrum in the absence of driving $\Phi_0(\omega)$.

The width of the mode spectrum is not given just by the mode decay rate Γ. It is affected by the frequency noise and depends on α_d. This is seen from Eqs. (3.12) and (3.22) for the susceptibility Im $\chi(\omega)$, cf. Ref. [59]. The halfwidth of the peak of Im $\chi(\omega)$ varies with the frequency noise strength $\alpha_d\Gamma_d$ from $\Gamma+2\alpha_d^2\Gamma_d$, for $\alpha_d \ll 1$, to $\sim \Gamma+2\alpha_d\Gamma_d$ for $\alpha_d \gg 1$ (the peak of Im $\chi(\omega)$ is profoundly non-Lorentzian for $\alpha_d \gg 1$ and $\alpha_d\Gamma_d \gtrsim \Gamma$).

An important outcome of the analysis in the previous sections is that the spectrum $\Phi_F(\omega)$ allows one to measure both the strength and the correlation time of the frequency noise due to dispersive coupling. In the first place, it allows one to directly identify the very presence of this noise. We emphasize that the full driving-induced term in the power spectrum $F^2\Phi_F(\omega)$ can be seen even where thermal fluctuations of the driven mode are weak and the peak in the power spectrum $\Phi_0(\omega)$ is too small to be resolved.

3.6.1 The spectrum $\Phi_F(\omega)$ in the limiting cases

3.6.1.1 Weak frequency noise

The general expression for the spectrum simplifies in the limiting cases where the frequency noise is weak or its bandwidth is large or small compared to the width of the driven mode spectrum $\Phi_0(\omega)$. In the case of dispersive coupling, the limit of weak frequency noise is realized where $\alpha_d\Gamma_d \ll \Gamma$. A general expression for $\Phi_F(\omega)$ for weak frequency noise was obtained earlier Eq. (2.10). It relates $\Phi_F(\omega)$ to the power spectrum of the frequency noise $\xi(t)$. From Eq. (3.10), in the present case we have $\langle\xi(t)\rangle = 2\langle Q_d^2(t)\rangle \operatorname{sgn}\gamma_d = 2\alpha_d\Gamma_d \operatorname{sgn}\gamma_d$, whereas the correlation function of the noise deviation from the average $\delta\xi(t) = \xi(t) - \langle\xi(t)\rangle$ is $4\alpha_d^2\Gamma_d^2\exp(-2\Gamma_d|t|)$. Then,

extending the results (2.10) to noise with non-zero average, we obtain

$$\Phi_F(\omega) = (\alpha_d^2\Gamma_d^3/\omega_0^2)[(\omega_F-\tilde{\omega}_0)^2+\Gamma^2]^{-1} \times \{[(\omega-\omega_F)^2+4\Gamma_d^2][(\omega-\tilde{\omega}_0)^2+\Gamma^2]\}^{-1}, \quad (3.37)$$

where $\tilde{\omega}_0 = \omega_0 + \langle\xi(t)\rangle = \omega_0 + 2\alpha_d\Gamma_d \mathrm{sgn}\gamma_d$. This expression can be also directly obtained from Eq. (3.23) in the corresponding limit.

From Eq. (3.37), for weak dispersive-coupling induced noise, the intensity of the spectrum $\Phi_F(\omega)$ is proportional to the square of the coupling parameter. If the detuning of the driving field frequency from the eigenfrequency of the driven oscillator largely exceeds the half widths of the power spectra of the both oscillators in the absence of driving, $|\omega_F - \tilde{\omega}_0| \gg \Gamma, \Gamma_d$, the power spectrum $\Phi_F(\omega)$ has two distinct peaks. One is located at the oscillator frequency $\tilde{\omega}_0$ and has halfwidth Γ. The other is located at the driving frequency ω_F and has halfwidth $2\Gamma_d$. We note that the noise variance $4\alpha_d^2\Gamma_d^2$ is independent of Γ_d. For constant $\alpha_d^2\Gamma_d^2$, the areas of the peaks at $\tilde{\omega}_0$ and ω_F are $\propto \Gamma_d/\Gamma\delta\omega_F^4$ and $\delta\omega_F^{-4}$, respectively (the ratio Γ_d/Γ affects only the area of the peak at ω_0). As $|\delta\omega_F|$ decreases, the peaks start overlapping. For small $|\delta\omega_F|$ they cannot be resolved. This behavior is general and occurs also where the frequency noise is not weak, as we show below.

3.6.1.2 Broad-band frequency noise

We now consider the case of the broad-band frequency noise, where the decay rate of the d-mode Γ_d largely exceeds the width of the driven mode spectrum. This condition requires that the motional-narrowing parameter be small, $\alpha_d \ll 1$. At the same time, the contribution of the frequency noise to the spectrum width of the considered mode does not have to be small compared to its decay rate, i.e., the ratio $\alpha_d^2\Gamma_d/\Gamma$ can be arbitrary. In other words, the broadening of the spectrum of the considered mode can still largely come from the dispersive coupling.

To describe the most pronounced peak in the spectrum $\Phi_F(\omega)$ for large Γ_d and small α_d, one can solve Eq. (3.20) in the WKB approximation, $D(t'') \approx \exp\{-\Gamma_d\int_t^{t''} dt_2[1-4i\alpha_d k(t_2)]^{1/2}\}$. Combined with Eq. (3.21), this solution immediately gives the averaging factor G in Eq. (3.14)

and thus the spectrum Φ_F. Alternatively, one can use the explicit expression (3.23) for function G. Only the first term has to be kept in this expression for $\alpha_d \ll 1$ and $\Gamma \ll \Gamma_d$. Integration over time in Eq. (3.13) gives

$$\Phi_F(\omega) \approx \frac{2\alpha_d^2\Gamma_d/\Gamma}{4\omega_0[\tilde{\Gamma}^2 + (\omega_F - \tilde{\omega}_0)^2]}\text{Im}\,\chi(\omega),$$
$$\chi(\omega) = (i/2\omega_0)[\tilde{\Gamma} - i(\omega - \tilde{\omega}_0)]^{-1}. \tag{3.38}$$

Parameters $\tilde{\Gamma}$ and $\tilde{\omega}_0$ are the halfwidth of the spectrum and the eigenfrequency of the driven mode renormalized due to the dispersive coupling, $\tilde{\Gamma} = \Gamma + 2\alpha_d^2\Gamma_d$ and $\tilde{\omega}_0$ is the same as in Eq. (3.37).

Equation (3.38) shows that, for a broad-band frequency noise, the spectrum $\Phi_F(\omega)$ has the same shape as the spectrum in the absence of driving, $\Phi_F(\omega) \propto \Phi_0(\omega) \propto \text{Im}\,\chi(\omega)$. However, from the spectrum $\Phi_0(\omega)$, which is Lorentzian in this case, one cannot tell whether the spectrum halfwidth $\tilde{\Gamma}$ is due to decay or to frequency fluctuations. In contrast, $\Phi_F \propto \alpha_d^2$ is proportional to the variance of the frequency noise and has a characteristic temperature dependence ($\alpha_d^2 \propto T^2$ if Γ_d is T-independent). It enables identifying the frequency noise contribution to the spectral broadening, as it was earlier demonstrated for a δ-correlated frequency noise, see Chap. 2.

Along with the comparatively narrow peak (3.38), for $\alpha_d^2\Gamma_d \gtrsim \Gamma$ the spectrum $\Phi_F(\omega)$ has a broad background near ω_0, with the typical frequency scale Γ_d. To describe it one has to take into account corrections $\propto \alpha_d^2$ to the leading-order term in function G (3.23). For large $|\delta\omega_F| \gg \tilde{\Gamma}$, the spectrum also has a peak near ω_F with width $\sim 2\Gamma_d$.

3.6.1.3 Narrow-band frequency noise

The spectrum $\Phi_F(\omega)$ has a characteristic shape also in the opposite limit where the bandwidth of the frequency noise $2\Gamma_d$ is small compared to the width of the spectrum in the absence of driving $\Phi_0(\omega)$. In this case $\Phi_F(\omega)$ displays a characteristic peak at the driving frequency ω_F, as can be already inferred from the weak-noise expression (3.37). In the overall spectrum $\Phi(\omega)$ it looks like a pedestal of the δ-peak at ω_F. The typical halfwidth of the pedestal is given by Γ_d. This allows one to read off the decay rate of the d-mode from the spectrum $\Phi_F(\omega)$ without accessing

the d-mode directly. To resolve the pedestal for large α_d, where $\alpha_d\Gamma_d \gtrsim \Gamma$ so that the width of the spectrum $\Phi_0(\omega)$ is primarily determined by the dispersive coupling, we need a comparatively large detuning of the driving frequency from the maximum of $\Phi_0(\omega)$.

The simplest way to find $\Phi_F(\omega)$ near ω_F for small Γ_d is based on Eq. (3.23). One first notices from Eq. (3.13) that the major contribution to $\Phi_F(\omega)$ in this case comes from the time range $t \sim \Gamma_d^{-1}$, whereas $t-t', |t_1'| \lesssim |\Gamma - i\delta\omega_F|^{-1}$. Therefore in Eq. (3.23) one is interested in the limit of large t but comparatively small $t-t', |t_1'|$. In the limit $t \to \infty$ but for fixed $t-t'$, function $G^{-2}(t,t',t_1') \to 1/\tilde{\chi}(t-t')\tilde{\chi}^*(-t_1')$ with $\tilde{\chi}(t)$ given by Eq. (3.22). The remaining term in G^{-2} is $\propto \exp(-2\Gamma_d t)$. One can then write the integrand in the expression (3.13) for $\Phi_F(\omega)$ as a series in $\exp(-2\Gamma_d t)$. The next simplification comes from the fact that $|a_d(t-t')|, |a_d t_1'| \ll 1$ for $|\Gamma - i\delta\omega_F|/|a_d| \gg 1$. Therefore one can expand $\tilde{\chi}(t-t') \approx [1 + 2i\alpha_d\Gamma_d(t-t')\mathrm{sgn}\gamma_d]^{-1}$ and similarly for $\tilde{\chi}^*(-t_1')$. Ultimately, the result of integration over the times t, t', t_1' reads

$$\Phi_F(\omega) = \sum_{n=1}^{\infty} \left| \frac{1}{n!}\alpha_d^n \frac{\partial^n}{\partial \alpha_d^n}\chi(\omega_F) \right|^2 \frac{n\Gamma_d}{(\omega-\omega_F)^2 + (2n\Gamma_d)^2}. \tag{3.39}$$

This expression describes the spectral peak at small $|\omega - \omega_F|$ in terms of the derivatives of the susceptibility $\chi(\omega)$ calculated as a function of the motional-narrowing parameter α_d. The width of the spectral peak (3.39) is given by the bandwidth of the frequency noise $2\Gamma_d$. The peak is generally non-Lorentzian.

3.6.2 Evolution of $\Phi_F(\omega)$ with the varying bandwidth and strength of the frequency noise

To visualize the dependence of the spectrum $\Phi_F(\omega)$ on the parameters of the system, we now present the results of numerical evaluation of the general expressions (3.13), (3.14), and (3.23). Fig. 3.1 shows the evolution of the driving-induced power spectrum $\Phi_F(\omega)$ with the varying ratio of the decay rates Γ_d/Γ, i.e., the varying ratio of the bandwidth of the frequency noise and the decay rate of the driven mode. We use as a scaling factor the susceptibility χ_0 of the driven mode in the absence of dispersive coupling,

$$\chi_0(\omega_F) = i[2\omega_0(\Gamma - i\delta\omega_F)]^{-1}. \tag{3.40}$$

In Fig. 3.1 (a), the frequency noise bandwidth is much larger than the width of the spectrum $\Phi_0(\omega)$ in the absence of driving. The spectrum $\Phi_F(\omega)$ is close to a Lorentzian centered near the shifted eigenfrequency of the driven mode, see Eq. (3.38); for small α_d the shift should be $2\alpha_d\Gamma_d$, whereas the halfwidth should be close to $\Gamma + 2\alpha_d^2\Gamma_d$,[59] which agrees with the numerics. In Fig. 3.1 (d), on the other hand, the noise bandwidth is small. The spectrum $\Phi_F(\omega)$ is a narrow peak near the driving frequency ω_F, see Eq. (3.39), with halfwidth $\approx \Gamma_d$. In Figs. 3.1 (b) and (c) the frequency noise bandwidth is comparable to the width of the spectrum $\Phi_0(\omega)$. In this case the spectrum $\Phi_F(\omega)$ displays two partly overlapping peaks. The overlapping can be reduced by tuning the driving frequency ω_F further away from the resonance, see below.

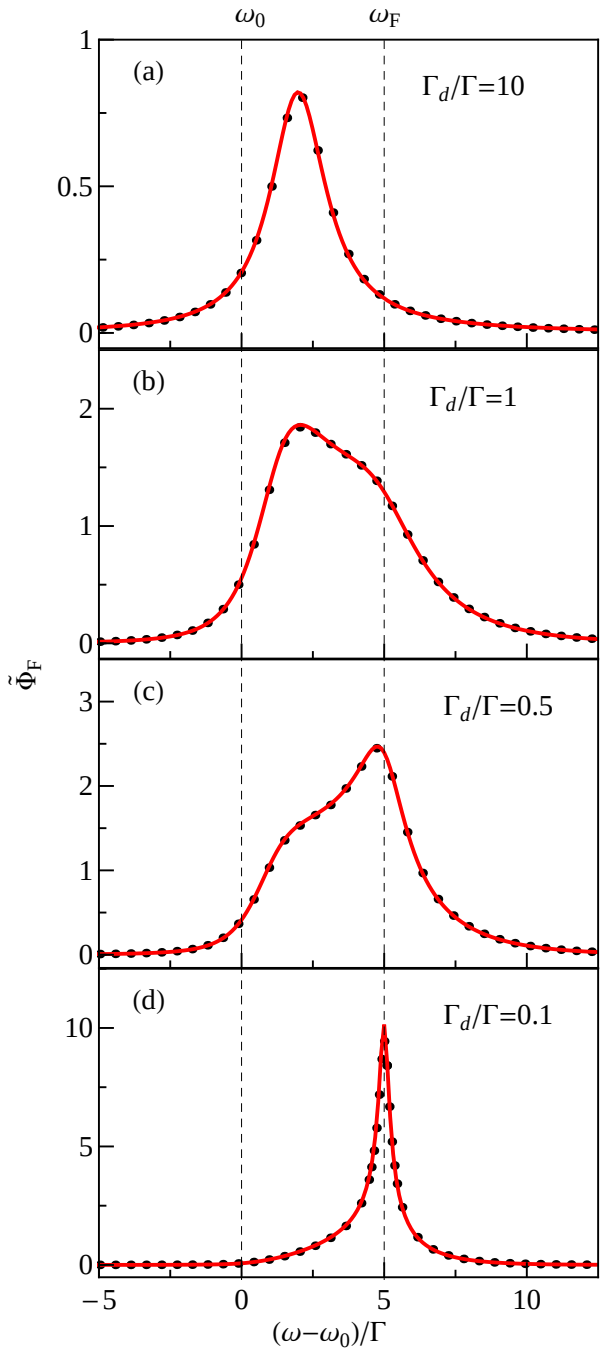

Figure 3.1 The scaled driving-induced part of the power spectrum of the driven mode dispersively coupled to another mode, which we call the d-mode. Thermal fluctuations of the d-mode lead to frequency fluctuations of the driven mode. Panels (a) to (d) show the change of the spectrum with the varying ratio Γ_d/Γ of the decay rates of the d-mode and the driven mode. The scaled strength (standard deviation) of the frequency noise is $\alpha_d\Gamma_d/\Gamma = 1$. The spectrum $\Phi_F(\omega)$ is scaled using the noise-free susceptibility $\chi_0(\omega_F)$, Eq. (3.40), $\tilde{\Phi}_F = 4\Gamma\Phi_F/|\chi_0(\omega_F)|^2$. The solid lines and the dots show the analytical theory and the numerical simulations, respectively.

Fig. 3.2 shows the evolution of the spectrum $\Phi_F(\omega)$ with the varying strength (standard deviation) $2\alpha_d\Gamma_d$ of the frequency noise. The frequency noise bandwidth $2\Gamma_d$ is chosen to be close to the decay rate of the driven mode Γ. The driving frequency ω_F is tuned away from resonance so that the two peaks of $\Phi_F(\omega)$ are well separated. An insight into the shape of the peaks can be gained from the aforementioned similarity of the spectrum $\Phi_F(\omega)$ with the spectrum of fluorescence and quasi-elastic light scattering by a periodically driven oscillating charge.

For weak frequency noise, curve 1 in Fig. 3.2 , the peaks are located near ω_F (quasi-elastic scattering) and ω_0 (fluorescence), cf. Eq. (3.37). As the noise strength increases, the peak near ω_0 becomes broader and the position of its maximum shifts to higher frequency (if $\gamma_d > 0$, as assumed in the figure). This resembles the evolution of the spectrum $\Phi_0(\omega)$ in the absence of driving with increasing α_d; this evolution is shown in the inset of Fig. 3.2. For $\alpha_d > 1$ the peak becomes non-Lorentzian and asymmetric.

In contrast, the shape of the peak located near ω_F stays almost the same with varying noise strength. This is consistent with the picture of quasi-elastic scattering, where the width of the peak is determined by the frequency noise bandwidth. To illustrate how persistent this behavior is, we scaled the spectra in Fig. 3.2 so that at their maxima at ω_F the spectra have the same height for different α_d.

3.6.3 Effect on $\Phi_F(\omega)$ of the detuning of the driving frequency

To provide more insight into the nature of the double-peak structure of the spectrum $\Phi_F(\omega)$ for $\Gamma \sim \Gamma_d$, we show in Fig. 3.3 the effect of detuning of the driving frequency ω_F from resonance. Panels (a), (b), and (c) refer to the driving frequency being red detuned, equal to, and blue detuned from the the maximum of the spectrum $\Phi_0(\omega)$ in the absence of driving, respectively. The results we show refer to the dispersive coupling constant $\gamma_d > 0$. For $\gamma_d < 0$, the plots should be mirror-reflected with respect to $\omega - \omega_0$, and $\omega_F - \omega_0$ should be replaced with $\omega_0 - \omega_F$.

The peak located near the frequency ω_F is well resolved in Fig. 3.3 (a). It moves along with ω_F as the latter varies. In Fig. 3.3 (a) one can also see a broader peak, which is located close to ω_0

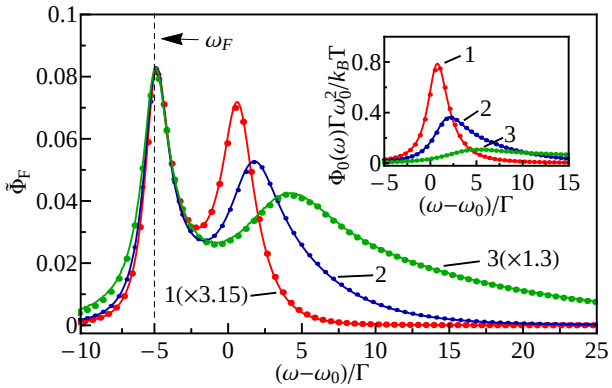

Figure 3.2 The evolution of the driving-induced part of the power spectrum with the varying strength of the frequency noise due to dispersive coupling. Curve 1 to 3 refer to the scaled standard deviation of the noise $\alpha_d\Gamma_d/\Gamma = 0.5$, 2.5, and 12.5, respectively. The ratio of the noise bandwidth to the decay rate of the driven mode is $2\Gamma_d/\Gamma = 1$. The scaled detuning of the driving frequency from the eigenfrequency of the driven mode is $\delta\omega_F/\Gamma = -5$. The spectrum is scaled using the noise-free susceptibility $\chi_0(\omega_F)$, Eq. (3.40), $\tilde{\Phi}_F = 4\Gamma\Phi_F/|\chi_0(\omega_F)|^2$. The curves 1 and 3 are additionally scaled by factors 3.15 and 1.3, respectively, so that the peaks near ω_F have the same height. The inset shows the spectrum $\Phi_0(\omega)$ in the absence of driving for the same values of the frequency noise strength $\alpha_d\Gamma_d/\Gamma$ as in the main panel. The solid lines and the dots show the analytical theory and the simulations, respectively.

and essentially does not change its position as ω_F changes. For small frequency-noise bandwidth, the peak at ω_F becomes narrow and is described by Eq. (3.39). However, it is well-resolved for large frequency detuning even where the noise bandwidth and the width of the spectrum $\Phi_0(\omega)$ are of the same order of magnitude. If the widths are close and ω_F is close to resonance, the peaks overlap and cannot be identified, as seen in panel (b). The areas of the peaks are dramatically different for red and blue detuning. This is due to the asymmetry of the spectrum $\Phi_0(\omega)$ in the presence of the frequency noise induced by dispersive coupling, see the inset of Fig. (3.2). As seen from Fig. 3.1, for very small Γ_d/Γ the peak near the oscillator eigenfrequency disappears; this was discussed earlier in the case of weak noise, but is also true in a general case.

3.6.4 The area of the driving induced power spectrum

The area S_F of the driving induced power spectrum $\Phi_F(\omega)$ is defined as $S_F = \int_0^\infty d\omega\Phi_F(\omega)$. The major contribution to the integral comes from the frequency range where $|\omega-\omega_F|, |\omega-\omega_0| \ll \omega_F$.

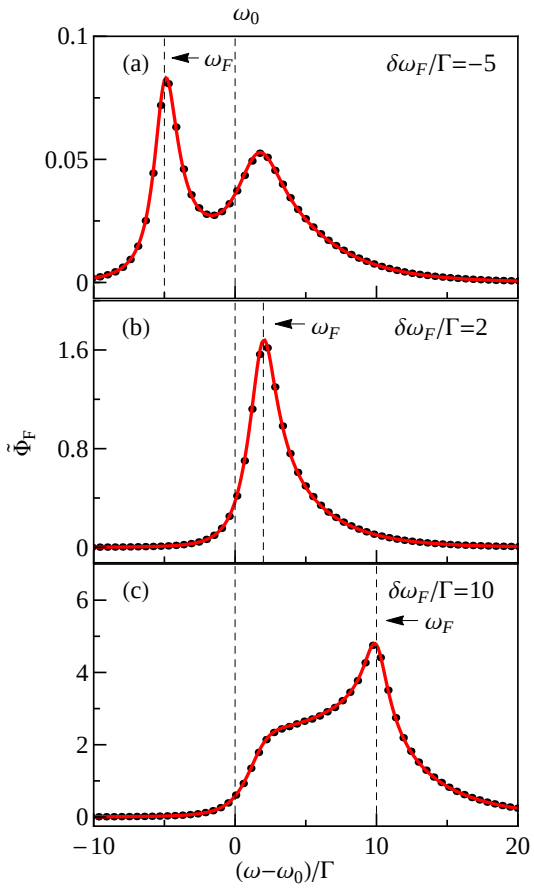

Figure 3.3 The evolution of the driving-induced part of the power spectrum with the varying detuning of the driving frequency ω_F. The scaled strength of the frequency noise induced by the dispersive coupling is $\alpha_d\Gamma_d/\Gamma = 2.5$. The ratio of the noise bandwidth to the decay rate of the driven mode is $2\Gamma_d/\Gamma = 1$. The spectrum is scaled using the noise-free susceptibility $\chi_0(\omega_F)$, Eq. (3.40), $\tilde{\Phi}_F = 4\Gamma\Phi_F/|\chi_0(\omega_F)|^2$. The solid lines and the dots show the analytical theory and the simulations, respectively.

Then integration over ω in Eq. (3.13) gives a factor $2\pi\delta(t)$. Further simplification comes from changing from integrating over t' and t_1' to integrating over t' and $t' - t_1'$ and using Eq. (3.12) for the susceptibility of the mode. The result reads

$$S_F = \frac{\pi}{4\omega_0\Gamma}\mathrm{Im}\chi(\omega_F) - \frac{\pi}{2}|\chi(\omega_F)|^2. \tag{3.41}$$

This reduces the calculation of the area S_F just to finding the susceptibility $\chi(\omega_F)$ of the mode. This susceptibility with account taken of the dispersive coupling is given by Eqs. (3.12) and (3.22).

The behavior of the area S_F can be found explicitly for small and large α_d. In the limit of small α_d, where the frequency noise is weak, from Eq. (3.37) $S_F \propto \alpha_d^2$. For large α_d, it is convenient

to write $\tilde{\chi}(t)$ in Eq. (3.22) as $\tilde{\chi}(t) \approx (2/\sqrt{i\alpha_d})\sum_{n=0}^{\infty}\exp[-2n(i\alpha_d)^{-1/2} - (2n+1)a_d t]$, where we assumed $\gamma_d > 0$; the ultimate result is independent of the sign of γ_d. The susceptibility $\chi(\omega_F)$ is given by the integral of $\tilde{\chi}(t)$ over t, Eq. (3.12). In the limit $\Gamma_d \alpha_d^{1/2} \gg |\Gamma - i\delta\omega_F|$ from Eq. (3.12) $\chi(\omega_F) \approx (2\omega_0\alpha_d\Gamma_d)^{-1}\sum\exp[-2n(i\alpha_d)^{-1/2}]/(2n+1)$. To the leading order in $1/\alpha_d$ this gives

$$\chi(\omega_F) \approx \left[\frac{1}{2}\ln(4\alpha_d) + i\frac{\pi}{4}\right]/4\omega_0\Gamma_d\alpha_d. \tag{3.42}$$

We see from Eqs. (3.41) and (3.42) that $S_F \propto \alpha_d^{-1}$ falls down with increasing α_d for large α_d.

The nonmonotonic dependence of the area S_F on the parameter α_d, which is expected from the above asymptotic expressions, is indeed seen in Fig. 3.4(a). This figure shows the area S_F as a function of the motional narrowing parameter α_d for different Γ_d/Γ. The position of the maximum of S_F sensitively depends on Γ_d/Γ.

In terms of a comparison with experiment, it is advantageous to scale the spectrum Φ_F, and in particular the area S_F, by the area of the δ-peak in the power spectrum of the driven mode. This area is given by the expression $S_\delta = (\pi/2)|\chi(\omega_F)|^2$, cf. Eq. (3.1). The quantities measured in the experiment are $F^2 S_F$ and $F^2 S_\delta$. The unknown scaled field intensity F^2 drops out from their ratio. From Eqs. (3.41) and (3.42) $S_F/S_\delta \propto \alpha_d/\ln^2\alpha_d$ increases with α_d for large α_d. For small α_d, $S_F/S_\delta \propto \alpha_d^2$ also increases with α_d. On the whole, we found that S_F/S_δ monotonically increases with α_d. This increase is seen in Fig. 3.4 (b).

3.7 Dispersive coupling to several modes

The results can be easily extended to the case of dispersive coupling to several modes rather than a single d-mode. We enumerate the modes by the subscript $\varkappa = 1, 2, \ldots$. The modes eigenfrequencies and decay rates are $\omega_\varkappa$ and $\Gamma_\varkappa$. The energy of the dispersive coupling is $(3/4)\sum_\varkappa \gamma_\varkappa q^2 q_\varkappa^2$. The contributions of different modes $\varkappa$ to the frequency fluctuations of the studied mode and therefore to the random accumulation of its phase are additive and mutually independent. To describe the driving-induced spectrum, one can use Eqs. (3.13) and (3.14) and average over the phase ac-

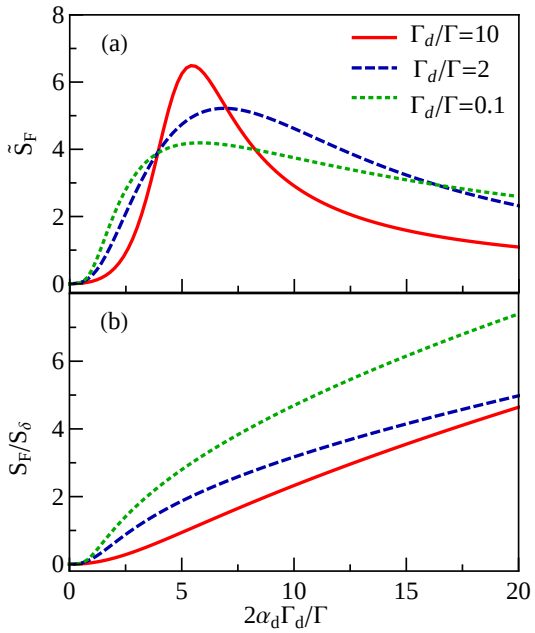

Figure 3.4 The area of the driving-induced part of the power spectrum as a function of α_d for different ratio of the frequency noise bandwidth to the decay rate of the driven mode $2\Gamma_d/\Gamma$. The red (solid), blue (dashed), and green (dotted) lines refer to $\Gamma_d/\Gamma = 10$, 2, and 0.1, respectively. The relative detuning of the driving frequency is $\delta\omega_F/\Gamma = 5$. In panel (a), the area S_F is scaled using the noise-free susceptibility $\chi_0(\omega_F)$, Eq. (3.40), $\tilde{S}_F = 2S_F/\pi|\chi_0(\omega_F)|^2$. In panel (b), S_F is scaled by the area of the δ peak in the power spectrum of the driven mode, $S_\delta = \pi|\chi(\omega_F)|^2/2$.

cumulation in Eq. (3.14) independently for each mode $\varkappa$. The result is the product of the averages [functions $G(t,t',t_1')$] calculated for each mode taken separately.

Perhaps of utmost physical interest are the cases where of significance is either dispersive coupling to one or very few modes, as for example in some optomechanical systems in which a radiation mode is dispersively coupled to a mechanical mode [50, 58], or where there is dispersive coupling to many modes, as may be the case in carbon nanotubes or graphene membranes [6, 7]. The present chapter is focused on the first case. The second case may be simpler, since the parameters $\gamma_\varkappa$ of coupling to individual modes are small; in particular, in nanomechanical systems this is a consequence of the difference of the spatial structure of the studied mode and the modes $\varkappa$. If the number of the $\varkappa$-modes is N, in the thermodynamic limit, $N \to \infty$, we would have $\gamma_\varkappa \propto 1/N$. In this limit the spectrum of the modes $\varkappa$ is almost continuous, and frequency fluctuations of the studied mode come from the coupling $\propto \sum_{\varkappa,\varkappa'} \gamma_{\varkappa\varkappa'} q^2 q_\varkappa q_{\varkappa'}$. This coupling leads to quasielastic

scattering of modes $\varkappa$ off the studied mode, which results in a broad-band frequency noise and in the Lorentzian spectrum $\Phi_0(\omega)$; [70, 71] the spectrum $\Phi_F(\omega)$ for a broad-band frequency noise is discussed in Chap. 2.

3.7.1 An intermediate number of modes: weak and effectively strong coupling

A more interesting situation can arise in the intermediate case of a large but limited number N of modes $\varkappa$. We assume that the mode frequencies are well separated, $|\omega_\varkappa - \omega_{\varkappa'}| \gg \Gamma_\varkappa, \Gamma_{\varkappa'}$, and the frequency differences do not resonate with $\omega_0, 2\omega_0$. Because N is large, the motional-narrowing parameters $\alpha_\varkappa = 3|\gamma_\varkappa| k_B T/8\omega_0\omega_\varkappa^2\Gamma_\varkappa$ can be small. However, $\alpha_\varkappa$ are not infinitesimally small. For a large N, one can think of a situation where the cumulative effect of the coupling to many modes is effectively strong.

For a multimode coupling, the factor $\tilde{\chi}(t)$ in the average susceptibility $\langle \chi_{\rm sl}(t,0)\rangle$ (3.22) is given by the product of the expressions (3.22) for $\tilde{\chi}(t)$ calculated for each mode $\varkappa$.[59] For $\alpha_\varkappa \ll 1$

$$\tilde{\chi}(t) \approx \exp\sum_\varkappa g_\varkappa(t), \qquad g_\varkappa(t) = -2i\alpha_\varkappa\Gamma_\varkappa t\,\mathrm{sgn}\gamma_\varkappa + \alpha_\varkappa^2[1 - 2\Gamma_\varkappa t - \exp(-2\Gamma_\varkappa t)]. \tag{3.43}$$

For large N, the most simple relevant case is the case of weak coupling, where $\sum_\varkappa \alpha_\varkappa^2 \ll 1$. In this case the power spectrum $\Phi_0(\omega) = (2k_BT/\omega_0)\mathrm{Im}\,\chi(\omega)$ is close to Lorentzian. From Eqs. (3.12), (3.22), and (3.43), to the leading order in $\sum_\varkappa \alpha_\varkappa^2$,

$$\mathrm{Im}\,\chi(\omega) \approx \tilde{\Gamma}/\left\{2\omega_0[\tilde{\Gamma}^2 + (\omega - \tilde{\omega}_0)^2]\right\},$$
$$\tilde{\omega}_0 = \omega_0 + 2\sum_\varkappa \alpha_\varkappa\Gamma_\varkappa\,\mathrm{sgn}\gamma_\varkappa, \quad \tilde{\Gamma} = \Gamma + 2\sum_\varkappa \alpha_\varkappa^2\Gamma_\varkappa. \tag{3.44}$$

In contrast to the previous work,[59] we do not assume here that the halfwidth of the spectrum is close to Γ; even for small $\alpha_\varkappa$ the dispersive-coupling induced spectral broadening may become comparable to the decay rate of the studied mode for $\Gamma_\varkappa \gg \Gamma$. For $\tilde{\Gamma} - \Gamma \ll \Gamma$ one should keep in $\mathrm{Im}\,\chi(\omega)$ other corrections $\propto \alpha_\varkappa^2$, which make the spectrum slightly non-Lorentzian.[59].

Even where $\alpha_\varkappa \ll 1$, the sum $\sum_\varkappa \alpha_\varkappa^2$ is not necessarily small. We will now consider the case where $\sum_\varkappa \alpha_\varkappa^2 \Gamma_\varkappa^2$ greatly exceeds the scaled squared decay rates of the involved modes $\Gamma_\varkappa^2(1+2\alpha_\varkappa)^2$ (typically, this requires that $\sum_\varkappa \alpha_\varkappa^2 \gg 1$) and $\sum_\varkappa \alpha_\varkappa^2 \Gamma_\varkappa^2 \gg \Gamma^2$. This is the case of cumulatively strong coupling, where the coupling becomes strong because of the large number of modes involved. One can see that the major contribution to the Fourier transform of $\tilde{\chi}(t)$ in Eq. (3.22) [and in Eq. (3.43), for $\alpha_\varkappa \ll 1$] comes from the time range $t \lesssim (\sum_\varkappa \alpha_\varkappa^2 \Gamma_\varkappa^2)^{-1/2}$. In this range $\tilde{\chi}(t)$ is given by Eq. (3.43) with the exponent expanded to second order in $\Gamma_\varkappa t$. Then the power spectrum in the absence of driving $\Phi_0(\omega) = (2k_BT/\omega_0)\mathrm{Im}\ \chi(\omega)$ has a Gaussian spectral peak. From Eqs. (3.12), (3.22), and (3.43) ,

$$\mathrm{Im}\ \chi(\omega) \approx (\pi/8\omega_0^2\sigma^2)^{1/2} \exp[-(\omega-\tilde{\omega}_0)^2/2\sigma^2],$$
$$\sigma^2 = 4\sum_\varkappa \alpha_\varkappa^2 \Gamma_\varkappa^2. \tag{3.45}$$

A Gaussian shape of the spectrum in the case of multi-mode dispersive coupling was proposed to describe the spectra of vibrational modes in carbon nanotubes.[6] This shape was justified[6] in numerical simulations of a model where all $\Gamma_\varkappa$ were the same. The numerical analysis [6] further showed that the tails of the spectrum are Lorentzian, which is generic for nonlinearly coupled modes[59] and is seen from Eq. (3.43).

3.7.1.1 The driving-induced spectrum

The spectrum $\Phi_F(\omega)$ is determined by the Fourier transform of function $G^2(t,t',t_1')$ which, as indicated earlier, is given by the product of expressions (3.23) calculated for each mode $\varkappa$. For small $\alpha_\varkappa$

$$G^2(t,t',t_1') \approx \exp\big[g_\varkappa(\tau_1) + g_\varkappa'(\tau_3) + \mathrm{sgn}(t'-t_1')$$
$$\times \sum_\varkappa \alpha_\varkappa^2 e^{-2\Gamma_\varkappa\tau_2}\left(1-e^{-2\Gamma_\varkappa\tau_1}\right)\left(1-e^{-2\Gamma_\varkappa\tau_3}\right)\big], \tag{3.46}$$

where $g_\varkappa$ is given by Eq. (3.43), whereas $g_\varkappa' = g_\varkappa$ for $t' < t_1'$ and $g_\varkappa' = g_\varkappa^*$ for $t' > t_1'$; the relation between $\tau_{1,2,3}$ and t,t',t_1' is explained below Eq. (3.23), see also Sec. 3.7.1.2.

For small $\sum_\varkappa \alpha_\varkappa^2$ and small frequency-noise induced spectral broadening, $\sum_\varkappa \alpha_\varkappa^2 \Gamma_\varkappa \ll \Gamma$ and $\sum_\varkappa \alpha_\varkappa^2 \Gamma_\varkappa^2 \ll \Gamma^2$, the driving-induced spectrum is given by Eq. (3.37) in which the factor $\alpha_d^2 \Gamma_d^3/[(\omega - \omega_F)^2 + 4\Gamma_d^2]$ is replaced by $\sum_\varkappa \alpha_\varkappa^2 \Gamma_\varkappa^3/[(\omega-\omega_F)^2 + 4\Gamma_\varkappa^2]$ and $\tilde{\omega}_0$ is given by Eq. (3.44). In the case where $\sum_\varkappa \alpha_\varkappa^2 \Gamma_\varkappa \gtrsim \Gamma$, the spectrum $\Phi_F(\omega)$ has a Lorentzian peak near $\tilde{\omega}_0$ described by Eq. (3.38) in which one should use Eq. (3.44) for $\tilde{\Gamma}, \tilde{\omega}_0$, and $\chi(\omega)$, and should replace in the numerator $\alpha_d^2 \Gamma_d$ with $\sum_\varkappa \alpha_\varkappa^2 \Gamma_\varkappa$.

The driving-induced term $\Phi_F(\omega)$ arises also in the case of the effectively strong coupling where $\sum_\varkappa \alpha_\varkappa^2 \Gamma_\varkappa^2$ largely exceeds the scaled squared decay rates $\Gamma^2, \Gamma_\varkappa^2 (1+2\alpha_\varkappa)^2$. In this case one should keep in the exponent in G^2 in Eq. (3.46) only terms up to second order in τ_1, τ_3. Function G^2 then should be expanded in a series in $\sum_\varkappa \alpha_\varkappa^2 \Gamma_\varkappa^2 \tau_1 \tau_3 \exp[-2\Gamma_\varkappa \tau_2]$. The result of the calculation is given in Sec. 3.7.1.2. The general expressions simplify in the important case where the decay rate of the considered mode is small compared to the decay rates of the $\varkappa$-modes, $\Gamma \ll \Gamma_\varkappa$. In this case

$$\Phi_F(\omega) \approx (2\Gamma)^{-1} \mathrm{Im}\chi(\omega)\, \mathrm{Im}\chi(\omega_F). \tag{3.47}$$

Equations (3.45) and (3.47) show that, for frequency noise with the correlation time small compared to the mode lifetime Γ^{-1}, the leading-order term in the driving-induced power spectrum $\Phi_F(\omega)$ has the same shape as the peak in the power spectrum in the absence of driving $\Phi_0(\omega)$. This behavior was found earlier in Chap. 2 for a general frequency noise provided the noise spectrum is much broader than the width of the spectral peak of $\Phi_0(\omega)$ and the standard deviation of the noise, in which case the spectrum $\Phi_0(\omega)$ is Lorentzian; cf. also Eq. (3.38). In the present case the coupling is strong and the width of the noise spectrum $\sim \max \Gamma_\varkappa$ is smaller than the standard deviation σ, and as a result $\Phi_F(\omega)$ is not proportional to the squared coupling parameter as in Eq. (3.38).

Other terms in the expression for $\Phi_F(\omega)$ obtained in Sec. 3.7.1.2 show that the driving-induced spectrum is nonmonotonic also near the driving frequency. The structure of the spectrum sensitively depends on the coupling and the decay rates of the $\varkappa$-modes.

The general expressions (3.48) and (3.50) simplify if all $\varkappa$ modes have the same decay rate. In

this case it is also possible to simulate the spectra numerically. We have checked that the analytical results are in excellent agreement with the simulations. It is important that the dispersive-coupling induced term in the power spectrum of the driven mode $\Phi_F(\omega)$ is always positive, whether the dispersive coupling is mostly to one mode or to many modes.

3.7.1.2 Driving-induced spectrum for an effectively strong dispersive coupling to a large number of modes

Calculation of the driving-induced power spectrum involves a triple integral over time, as seen from Eq. (3.13). It is convenient to evaluate the integrals over t', t_1' separately in three regions, $A1$, $A2$, and $A3$. Region $A1$ corresponds to $-\infty < t' \le t_1', -\infty < t_1' \le 0$; then in Eq. (3.46) $\tau_1 = t, \tau_2 = -t_1', \tau_3 = t_1' - t'$. Region $A2$ corresponds to $-\infty < t_1' \le t', -\infty < t' \le 0$; then in Eq. (3.46) $\tau_1 = t, \tau_2 = -t', \tau_3 = t' - t_1'$. Region $A3$ corresponds to $0 < t' \le t, -\infty < t_1' \le 0$; then in Eq. (3.46) $\tau_1 = t - t', \tau_2 = t', \tau_3 = -t_1'$. Expanding the exponentials in $G^2(t, t', t_1')$ as described in Sec. 3.7.1 and integrating G^2 with weight $\exp[-(\Gamma - i\delta\omega_F)(t - t') + (\Gamma + i\delta\omega_F)t_1']$ [see Eq. (3.13)], we obtain the contributions of the regions $A1$ and $A2$ in the form

$$\begin{aligned}
\Phi_F^{(A1)}(\omega) &\approx -\frac{1}{2}\mathrm{Re}\sum_{n=0}^{\infty} \mathscr{K}_n \frac{\partial^n \chi(\omega)}{\partial \omega^n}\frac{\partial^n \chi(\omega_F)}{\partial \omega_F^n}, \\
\mathscr{K}_{n>0} &= \frac{4^n}{n!}\sum_{\varkappa_1,\ldots,\varkappa_n} \alpha_{\varkappa_1}^2 \ldots \alpha_{\varkappa_n}^2 \Gamma_{\varkappa_1}^2 \ldots \Gamma_{\varkappa_n}^2 [2\Gamma + 2\sum_{i=1}^{n}\Gamma_{\varkappa_i}]^{-1} \\
\Phi_F^{(A2)}(\omega) &\approx \frac{1}{2}\mathrm{Re}\sum_{n=0}^{\infty} \mathscr{K}_n \frac{\partial^n \chi(\omega)}{\partial \omega^n}\frac{\partial^n \chi^*(\omega_F)}{\partial \omega_F^n}.
\end{aligned} \tag{3.48}$$

In this equation $\mathscr{K}_0 = 1/2\Gamma$. The susceptibility

$$\chi(\omega) = (i/2\omega_0)\int_0^{\infty} dt e^{i(\omega - \tilde{\omega}_0)t - \Gamma t - \sigma^2 t^2/2} \tag{3.49}$$

can be easily expressed in terms of the error function; $\tilde{\omega}_0$ and σ^2 are given by Eqs. (3.44) and (3.45).

In the region $A3$ it is convenient first to change from integration over t' to integration over $\tilde{t}' = t - t'$. To find the spectrum Φ_F, it is convenient to integrate G^2 with the appropriate weight

first over t and then over $\tilde{t}'$. One should take into account that $\tilde{t}' \lesssim 1/\sigma \ll 1/\Gamma_\varkappa$, but the range of the values of t that contribute to the integral is not limited to $\lesssim 1/\sigma$. The result of integration reads

$$\Phi_F^{(A3)}(\omega) \approx -\mathrm{Im}[\chi(\omega)\chi^*(\omega_F)]/[2(\omega-\omega_F)] + \frac{1}{2}\mathrm{Re}\sum_{n=1}^{\infty} \mathscr{K}_n' \frac{\partial^n \chi(\omega)}{\partial \omega^n} \frac{\partial^n \chi^*(\omega_F)}{\partial \omega_F^n}. \tag{3.50}$$

Here, the coefficients $\mathscr{K}_n'$ are given by the expression (3.48) for $\mathscr{K}_n$ in which 2Γ is replaced by $-i(\omega-\omega_F)$. We note that $\Phi_F^{(A3)}$ is not singular at $\omega=\omega_F$, since Im $|\chi(\omega_F)|^2 = 0$ and $\chi(\omega)$ is a smooth function of frequency; the corresponding term is important primarily where either ω or ω_F are on the tail of the spectral peak $\Phi_0(\omega)$.

The series over n in Eqs. (3.48) and (3.50) generally converges slowly if the decay rates of the $\varkappa$ modes $\Gamma_\varkappa \lesssim \Gamma$. For large n, in Eq. (3.50) the derivative $\partial^n\chi(\omega)/\partial\omega^n$ should be calculated with the decay rate Γ replaced with $\Gamma + 2\sum_{i=1}^n \Gamma_{\varkappa_i}$ in Eq. (3.49). The summation over the modes $\varkappa_i$ in the coefficients $\mathscr{K}_n'$ should now be extended to include the modified $\chi(\omega)$, which now itself depends on $\varkappa_i$. We note that $\chi^*(\omega_F)$ in Eq. (3.50) should still be calculated using Eq. (3.49).

The overall driving-induced term in the power spectrum $\Phi_F(\omega) = \Phi_F^{(A1)}(\omega) + \Phi_F^{(A2)}(\omega) + \Phi_F^{(A3)}(\omega)$ has peaks and, generally, more complicated features near both the oscillator eigenfrequency and the driving frequency.

3.8 Power spectrum of a driven nonlinear oscillator

An important contribution to the broadening of the spectra of mesoscopic oscillators can come from their internal nonlinearity.[4] The vibration frequency of a nonlinear oscillator depends on the vibration amplitude. Therefore thermal fluctuations of the amplitude lead to frequency fluctuations. The analysis of the spectra is complicated by the interplay of the frequency fluctuations that come from the amplitude fluctuations and the frequency uncertainty that comes from the oscillator decay. Nevertheless the linear susceptibility could be found for an arbitrary relation between the standard

deviation of the frequency $\Delta\omega$ and the decay rate Γ.[59]. The power spectrum of a nonlinear oscillator in the absence of driving is generally asymmetric and non-Lorentzian.

Finding the driving-induced terms in the power spectrum is still more complicated. The oscillator displacement is nonlinear in the driving field amplitude F, and the driving-induced part of the power spectrum $\Phi(\omega)$ is not quadratic in F. However, if the field is weak, Eq. (3.1) for $\Phi(\omega)$ applies. In the calculation of $\Phi_F(\omega)$ one should take into account terms in the oscillator displacement that are quadratic in F, which is generic for nonlinear systems.[16]

We assume that the nonlinear part of the oscillator energy is small compared to the linear part. Then the nonlinear term in the oscillator energy can be taken in the form of $\gamma q^4/4$.[72] The oscillator equation of motion in the rotating wave approximation is given by Eq. (3.7) with $\gamma_d = 0$,

$$\dot{u} = -(\Gamma + i\delta\omega_F)u + \frac{3i\gamma}{2\omega_0}|u|^2 u - i\frac{F}{4\omega_0} + f(t). \tag{3.51}$$

In this section we do not discuss the effect of dispersive coupling, and the frequency noise that comes from this coupling is not included into Eq. (3.51).

To find $\Phi_F(\omega)$, we first consider the dynamics of a driven nonlinear oscillator without fluctuations and then take fluctuations into account. The stationary solution $u_{\rm st}$ of Eq. (3.51) in the absence of the noise $f(t)$ can be found by setting $\dot{u} = 0$. For weak driving, $u_{\rm st}$ is a series in F, which contains only odd powers of F. Since we are interested in the terms which are linear or quadratic in F, it is sufficient to keep only the leading term, $u_{\rm st} = F/4i\omega_0(\Gamma + i\delta\omega_F)$. One then substitutes into Eq. (3.51) $u(t) = u_{\rm st} + \delta u(t)$. The deviation $\delta u(t)$ is due only to the noise,

$$\begin{aligned}\delta\dot{u} = &-(i\delta\omega_F + \Gamma)\delta u + \frac{3i\gamma}{2\omega_0}\Big(|\delta u|^2\delta u + 2u_{\rm st}|\delta u|^2 + u_{\rm st}^*\delta u^2 \\ &+2|u_{\rm st}|^2\delta u + u_{\rm st}^2\delta u^*\Big) + f(t).\end{aligned} \tag{3.52}$$

Time evolution of $\delta u(t)$ depends on the driving field in terms of $u_{\rm st}$. We find this time evolution in the two limiting cases.

3.8.1 Weak nonlinearity

The analysis of the dynamics simplifies in the case of small nonlinearity-induced spread of the oscillator frequency $\Delta\omega$ compared to the decay rate Γ. As seen from Eq. (3.51), in the absence of driving the frequency shift is quadratic in the vibration amplitude $\propto |u|^2$,[72], and therefore the frequency spread is determine by the standard deviation of $|u|^2$ due to the thermal noise. This gives $\Delta\omega = 3|\gamma|k_BT/8\omega_0^3$.

For $\Delta\omega \ll \Gamma$, it is sufficient to keep only the linear in δu terms in Eq. (3.52).[73, 74] A straightforward calculation then gives a simple expression for the the driving-induced power spectrum,

$$\Phi_F(\omega) \approx \frac{3\gamma k_B T}{8\omega_0^5} \frac{(\omega-\omega_0)\Gamma}{(\Gamma^2+\delta\omega_F^2)[\Gamma^2+(\omega-\omega_0)^2]^2}. \tag{3.53}$$

The spectrum (3.53) is proportional to the derivative of the Lorentzian spectrum of the harmonic oscillator $\Phi_0(\omega) \propto 1/[\Gamma^2+(\omega-\omega_0)^2]$ over ω. It has a characteristic dispersive shape, being of the opposite signs on the other sides of ω_0. This is the result of the shift of the oscillator vibration frequency $\propto \gamma F^2$ due to the driving. Such shift is the main effect of the driving for small $\Delta\omega/\Gamma$.

3.8.2 Large detuning of the driving field frequency

For arbitrary $\Delta\omega/\Gamma$, the analysis is simplified if the detuning of the driving field frequency from the small-amplitude oscillator frequency $|\delta\omega_F| \gg \Gamma, \Delta\omega$. In this case, one can change variables in Eq. (3.52) to $\delta\tilde{u}(t) = \delta u(t)e^{i\delta\omega_F t}$. The right-hand side of the resulting equation for $\delta\tilde{u}$, besides the noise term, has terms that smoothly depend on time on the scale $|\delta\omega_F|^{-1}$ and terms that oscillate as $\exp(\pm i\delta\omega_F t), \exp(2i\delta\omega_F t)$. These oscillating terms can be considered a perturbation. To the first order of the perturbation theory, the equation for the smooth terms takes the form

$$\delta\dot{\tilde{u}} = -\Gamma\delta\tilde{u} + \frac{3i\gamma}{\omega_0}|u_{\rm st}|^2\delta\tilde{u} + \left(1+\frac{9\gamma|u_{\rm st}|^2}{\omega_0\delta\omega_F}\right)\frac{3i\gamma}{2\omega_0}|\delta\tilde{u}|^2\delta\tilde{u} + \tilde{f}(t), \tag{3.54}$$

where $\tilde{f}(t) = f(t)e^{i\delta\omega_F t}$. We keep in this equation the terms $\propto |u_{\rm st}|^2 \propto F^2$. These terms contribute to the spectrum $\Phi_F(\omega)$. The terms of higher oder in $|u_{\rm st}|^2$ have been discarded.

Equation (3.54) has the same form as the equation of motion for the complex amplitude $u(t)$ in the absence of driving, i.e., Eq. (3.51) with $F = 0$. The noise $\tilde{f}(t)$ has the same correlation function as $f(t)$. Therefore the power spectrum of $\delta\tilde{u}(t)$ is the same as the power spectrum of a nonlinear oscillator found earlier,[59] with the renormalized parameters: the eigenfrequency is shifted by $3\gamma|u_{\rm st}|^2/\omega_0$ and the nonlinearity parameter is multiplied by the factor $1+9\gamma|u_{\rm st}|^2/\omega_0\delta\omega_F$. We note that the correction $\propto |u_{\rm st}|^2$ in this factor, which comes from the perturbation theory in $1/\delta\omega_F$, is small.

To find $\Phi_F(\omega)$ we have to expand the result[59] with the appropriately renormalized parameters to the first order in $|u_{\rm st}|^2$. This gives

$$F^2\Phi_F(\omega) = \beta\{\partial_\beta[\Phi_0(\omega - 2\beta\delta\omega_F; \Delta\omega(1+6\beta))]\}_{\beta=0},$$
$$\Phi_0(\omega;\Delta\omega) = \frac{k_BT}{\omega_0^2}\Re\int_0^\infty dt\exp\{[i(\omega-\omega_0)+\Gamma]t\}$$
$$\times[\cosh(at)+(\Gamma/a)(1+2i\alpha\,\mathrm{sgn}\gamma)\sinh(at)]^{-2}. \qquad (3.55)$$

The parameters α and a have the same structure and the same physical meaning as the parameters α_d and a_d used before, $\alpha = \Delta\omega/\Gamma$ and $a = \Gamma(1+4i\alpha\,\mathrm{sgn}\gamma)^{1/2}$, whereas $\beta = 3\gamma F^2/32\omega_0^3(\delta\omega_F)^3$ is the scaled intensity of the driving field.

The major contribution to $\Phi_F(\omega)$ as given by Eq. (3.55) for large $|\delta\omega_F|/\Delta\omega$ comes from the frequency shift of the spectrum without driving $\Phi_0(\omega)$ and is determined by $-2\delta\omega_F\partial_\omega\Phi_0(\omega;\Delta\omega)$. Physically, this results again corresponds to the shift of the oscillator eigenfrequency associated with the forced vibrations, and the spectrum Φ_F again has the characteristic shape of a dispersive curve. To the next order in $1/\delta\omega_F$, the driving broadens or narrows the spectrum depending on the sign of $\gamma/\delta\omega_F$ by renormalizing the nonlinearity-induced standard deviation of the oscillator frequency $\Delta\omega$.

3.8.3 Numerical simulations

The analytical results on the spectra of the modulated nonlinear oscillator, Eq. (3.55), are compared with the results of numerical simulations in Fig. 3.5. The spectrum $\Phi_F(\omega)$ generally has a positive

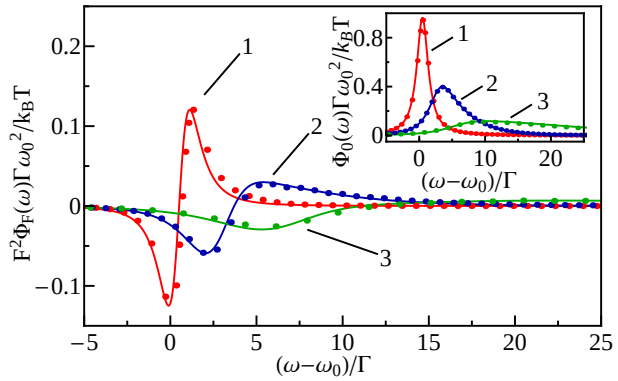

Figure 3.5 The driving-induced part of the power spectrum of a nonlinear oscillator for large detuning of the driving frequency, $\delta\omega_F/\Delta\omega = 40$. The solid curves and the dots show the analytical expressions and the results of simulations, respectively. The values of the nonlinearity parameter and the scaled driving strength for the curves 1 to 3 are, respectively, $\alpha \equiv \Delta\omega/\Gamma = 0.125$, 1.25, and 5, and $\beta \equiv 3\gamma F^2/32\omega_0^3\delta\omega_F^3 =$ 0.016, 0.004, and 0.004. The inset shows the change of the power spectrum in the absence of driving with varying $\Delta\omega/\Gamma$.

and negative parts, in a dramatic distinction from the case of a linear oscillator dispersively coupled to another oscillator. As $\Delta\omega/\Gamma$ increases, the shape of $\Phi_F(\omega)$ becomes more complicated, in particular, the positive and negative parts become asymmetric.

The simulations were performed in the same way as for the dispersively coupled modes by integrating the stochastic differential equations (3.51). We verified that the values of the modulating field amplitude F were in the range where the driving-induced term in the power spectrum was quadratic in F. As seen from this figure, the simulations are in excellent agreement with the analytical results.

In the intermediate range, where the nonlinearity is not weak and the driving is not too far detuned, i.e., $|\delta\omega_F| \sim \max(\Gamma, \Delta\omega)$, we obtained the spectrum $\Phi_F(\omega)$ by running numerical simulations. These results are presented in Fig. 3.6. They show that the general trend seen in Fig. 3.5 that $\Phi_F(\omega)$ changes signs and is asymmetric for a nonlinear oscillator persists in this case as well.

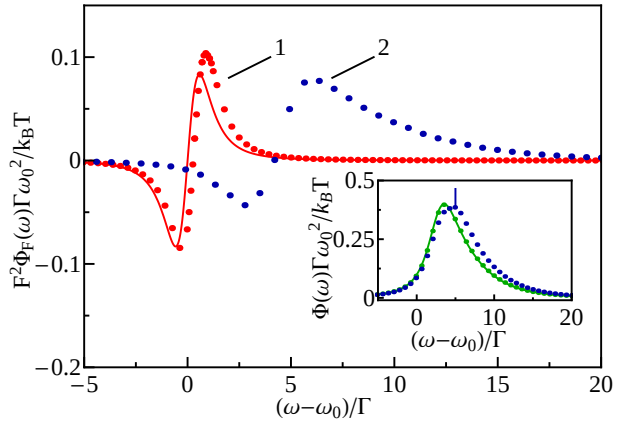

Figure 3.6 The driving-induced part of the spectrum of a nonlinear oscillator for small detuning of the driving frequency. The solid curve (red) shows the analytical results for $\Phi_F(\omega)$ for small $\Delta\omega/\Gamma$ for the same parameters as the dotted curve 1. The dots show the results of simulations. The scaled values of the nonlinearity parameter, the detuning, and the driving strength on the curves 1 and 2 are, respectively, $\alpha \equiv \Delta\omega/\Gamma = 0.05$, and 1.25, $\delta\omega_F/\Gamma = 0.5$ and 5, and $\beta \equiv 3\gamma F^2/32\omega_0^3(\delta\omega_F)^3 = 0.64$ and 0.01. The inset shows the full spectrum for the parameters of curve 2 (blue dots, simulations); the spectrum without driving for the same $\Delta\omega/\Gamma$ is shown by the solid line (analytical) and (green) dots on top of this line, which are obtained by simulations.

3.9 Conclusions

In terms of experimental studies of mesoscopic vibrational systems, the major result of this chapter is the suggestion of a way to single out and characterize the dispersive (nonresonant) coupling between vibrational modes. The proposed method allows revealing dispersive coupling even where there is no access to the mode coupled to the studied one. We have shown that dispersive coupling leads to a specific, generally double-peak extra structure in the power spectrum of a mode when this mode is driven close to resonance. The dispersive-coupling induced part of the power spectrum is quadratic in the driving field amplitude. It varies significantly with the detuning of the driving frequency from the mode eigenfrequency.

The "tune off to read off" approach, which relies on changing the driving frequency, allows one to study separately two effects. One is the dispersive-coupling induced broadening of the spectral peak of the linear response, which is of significant interest for mesoscopic modes.[6, 55, 49, 7, 56] The other is the decay of the “invisible" mode that is dispersively coupled to the studied mode. The double-peak structure of the driving-induced power spectrum sensitively depends both on the

strength of the dispersive coupling and the parameters of the invisible mode.

Another important feature of the driving-induced spectrum is the qualitative difference between the effects of nonlinear dispersive coupling to other modes and the internal nonlinearity of the studied mode. Both nonlinearities are known to broaden, in a somewhat similar way,[59] the linear response spectrum in the presence of thermal fluctuations. However, in the case of internal nonlinearity, the driving-induced part of the power spectrum changes sign as a function of frequency, i.e., it has peaks of the opposite signs and is similar (and is close, in a certain parameter range) to the derivative of the power spectrum without driving.

We have extended the results to the case of dispersive coupling to several modes. The contributions of different modes to the frequency fluctuations of the studied mode, and therefore to the random accumulation of its phase, are additive and mutually independent. Then the averaging over the phase accumulation can be done independently for each mode. The extension to the case of a few modes is therefore straightforward. New features emerge if there are many, but not too many modes. The cumulative effect of weak dispersive coupling to many modes may lead to an effectively strong coupling. As a result, the spectrum without driving becomes close to Gaussian in the central part, as was suggested in Ref. [6]. The driving-induced part of the power spectrum displays a characteristic structure, which sensitively depends both on the parameters of the dispersive coupling and the dissipation parameters of the involved modes.

In terms of the theory, the chapter describes a path-integral method that enables finding in an explicit form the spectrum of a driven oscillator in the presence of non-Gaussian fluctuations of its frequency, which result from dispersive coupling to other modes. The results apply for an arbitrary ratio between the relevant parameters of the system. These parameters are the magnitude (standard deviation) of the frequency fluctuations $\Delta\omega$, their reciprocal correlation time, which is given by the decay rate of the dispersively-coupled mode that causes the fluctuations, the decay rate of the driven mode itself, and the detuning of the driving frequency.

It is the presence of several parameters that makes it complicated to identify the broadening mechanisms from the linear response spectra. The results of the chapter show the qualitative

difference between the effects of these parameters on the power spectrum when the oscillator is driven. This enables their identification.

Generally, in mesoscopic vibrational systems, and in particular in nanomechanical systems, the internal (Duffing) and dispersive nonlinearities can be of the same order of magnitude. If the studied mode has a much higher frequency than the mode to which it is dispersively coupled, its fluctuations can be comparatively weaker making the effect of the dispersive coupling stronger. Also if there are several modes dispersively coupled to the mode of interest, their cumulative effect can be stronger than the effect of the internal nonlinearity. This makes it even more important to be able to distinguish the effects, which the proposed approach allows.

The results immediately extend to the parameter range where the driven mode has high frequency and is in the quantum regime, $\hbar\omega_0 > k_B T$. This is because, as long as the mode itself is linear, its displacement is a superposition of the displacement without driving, which is affected by quantum fluctuations, and the classical driving-induced displacement. The effect of dispersive coupling to a classical mode ($\hbar\omega_d \ll k_B T$) on the driving-induced displacement is independent of $\hbar\omega_0/k_B T$. Dispersive coupling of a quantum mode to a classical mode is of particular interest for optomechanics, where the high-frequency optical cavity mode can be dispersively coupled to a low-frequency mechanical mode.[50, 58] Driving the cavity mode leads in this case to a characteristic radiation described in this chapter.

CHAPTER 4

FLUCTUATION SPECTRA OF DRIVEN OVERDAMPED NONLINEAR SYSTEMS

4.1 Introduction

Fluctuation spectra and spectra of response to periodic driving are major tools of characterizing physical systems. The spectra are conventionally used to find system frequencies and relaxation rates and to characterize fluctuations in the system. For example, optical absorption spectra give the transition frequencies of atomic systems and the lifetimes of the excited states, and the spectrum of spontaneous radiation is a well-known example of the fluctuation (power) spectrum [75]. In macroscopic systems the spectra are often complicated by the effects of inhomogeneous broadening. Recent progress in nanoscience has made it possible to study the spectra of individual dynamical systems. A well-known example is provided by optically trapped Brownian particles and biomolecules [76, 77], where the power spectra are a major tool for characterizing the motion in the trap [78, 79]. Spectra of various types of individually accessible mesoscopic systems are studied nowadays in optics [80, 81], nanomechanics and circuit quantum electrodynamics, cf. [4], biophysics, cf. [82, 83], and many other areas; the technique based on spectral measurements has found various applications, photonic force microscopy being a recent example, see Ref. [84].

A familiar effect of weak periodic driving is forced vibrations of the system. When ensemble-averaged, they are also periodic and occur at the driving frequency ω_F. They lead to a δ-shape peak at frequency ω_F in the system power spectrum. However, the driving also modifies the power spectrum away from ω_F. A textbook example is inelastic light scattering and resonance fluorescence. In the both cases, the system driven by a periodic electromagnetic field emits radiation at frequencies that differ from the driving frequency [10]. This radiation is one of the major sources of information about the system in optical experiments.

In this chapter we study the spectra of periodically driven nonlinear systems. We show that,

in the presence of noise, along with the δ-shape peak at the driving frequency ω_F, these spectra display a characteristic structure. We are interested in the regime of relatively weak driving, where the driving-induced change of the power spectrum is quadratic in the amplitude of the driving, as in inelastic light scattering.

In view of the significant interest in the power spectra of systems optically trapped in fluids, we consider systems where inertial effects play no role. In the absence of driving the power spectra of such systems usually have a peak at zero frequency. In particular it is this peak that is used to characterize the dynamics of optically trapped particles.

For a linear system, like a Brownian particle in a harmonic trap, the δ-shape peak at ω_F is the only effect of the driving on the power spectrum. This is because motion of such a system is a linear superposition of forced vibrations at ω_F and fluctuations in the absence of driving. The amplitude and phase of the forced vibrations depend on the parameters of the system and determine the standard linear susceptibility [85]. In nonlinear systems forced vibrations become random, because the parameters of the system are fluctuating. The power spectrum of such random vibrations is no longer just a δ-shape peak (although the δ-shape peak is necessarily present). The driving-induced spectral features away from ω_F result from mixing of fluctuations and forced vibrations in a nonlinear system.

4.1.1 Qualitative picture

The idea of the driving-induced change of the power spectrum can be gained by looking at a Brownian particle fluctuating in a confining potential, a typical situation for optical trapping. The motion of the particle, after proper rescaling of time and particle coordinate q, is described by the Langevin equation [86]

$$\dot{q} = -U'(q) + f(t), \qquad U'(q) \equiv dU/dq, \tag{4.1}$$

where $U(q)$ is the scaled potential and $f(t)$ is thermal noise. If potential $U(q)$ is parabolic and the system is additionally driven by a force $F\cos\omega_F t$, forced vibrations are described by the textbook

expression

$$\langle q(t)\rangle = \frac{1}{2}F\chi(\omega_F)\exp(-i\omega_F t) + \text{c.c.}, \qquad \chi(\omega) = [U''(q_{\text{eq}}) - i\omega]^{-1}, \tag{4.2}$$

where q_{eq} is the equilibrium position [the minimum of $U(q)$] and $\chi(\omega)$ is the susceptibility.

For a nonlinear system the potential $U(q)$ is nonparabolic. Because of thermal fluctuations, the local curvature of the potential $U''(q)$ is fluctuating. Intuitively, one can think of the effect of thermal fluctuations on forced vibrations as if $U''(q_{\text{eq}})$ in Eq. (4.2) for the susceptibility were replaced by a fluctuating curvature, see Fig. 4.1. If the driving frequency ω_F largely exceeds the reciprocal correlation time of the fluctuations t_c^{-1}, the fluctuations would lead to the onset of a structure in the power spectrum near frequency ω_F with typical width t_c^{-1}. The quantity t_c^{-1} also gives the typical width of the peak in the power spectrum at zero frequency in the absence of driving [for a linear system, $t_c^{-1} = U''(q_{\text{eq}})$].

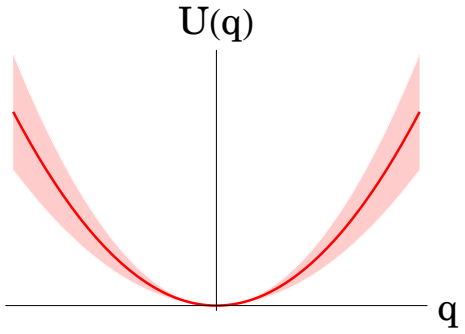

Figure 4.1 Sketch of a potential of a nonlinear system near the potential minimum. Because of the interplay of nonlinearity and fluctuations, the curvature of the potential fluctuates. These fluctuations are shown as the smearing of the solid line, which represents the potential in the absence of fluctuations.

Another effect of the interplay of driving, nonlinearity, and fluctuations can be understood by noticing that the periodic force causes a periodic change in the system coordinate. For a nonlinear system, roughly speaking, this leads to a periodic modulation of the local curvature, and thus of t_c^{-1}. Since t_c^{-1} determines the shape of the zero-frequency peak in the power spectrum, such modulation causes a change of this peak proportional to F^2, to the lowest order in F.

Even from the above simplistic description it is clear that the driving-induced change of the spectrum is sensitive to the parameters of the system and the noise and to the nonlinearity mechanisms. Explicit examples given below demonstrate this sensitivity and suggest that the effects we discuss can be used for characterizing a system beyond the conventional linear analysis. After formulating how the power spectrum can be evaluated in Section 4.2, we demonstrate the effects of the interplay of driving and fluctuations for three very different types of nonlinear systems: an overdamped Brownian particle (Section 4.3), a system that switches at random between coexisting stable states (Section 4.4), and a threshold detector (Section 4.5). All these systems are of broad interest, and all of them display a significant driving-induced change of the power spectrum.

4.2 General formulation

We consider fluctuating systems driven by a periodic force $F\cos(\omega_F t)$ and assume that fluctuations are induced by a stationary noise, like in the case of an optically trapped Brownian particle, for example. After a transient time such system reaches a stationary state. The stationary probability distribution of the system with respect to its dynamical variable q, $\rho_{\rm st}(q,t)$, is periodic in time t with the driving period $\tau_F = 2\pi/\omega_F$. The two-time correlation function $\langle q(t_1)q(t_2)\rangle$ [$\langle\cdot\rangle$ implies ensemble averaging] is a function of $t_1 - t_2$ and a periodic function of t_2 with period τ_F. The power spectrum usually measured in experiment is of the form

$$\Phi(\omega) = 2{\rm Re}\int_0^\infty dt e^{i\omega t}\langle\langle q(t+t')q(t')\rangle\rangle,$$
$$\langle\langle q(t+t')q(t')\rangle\rangle = \frac{1}{\tau_F}\int_0^{\tau_F} dt'\langle q(t+t')q(t')\rangle. \tag{4.3}$$

The correlation function in Eq. (4.3) can be expressed in terms of $\rho_{\rm st}(q,t)$ and the transition probability density $\rho(q_1,t_1|q_2,t_2)$ that the system that was at position q_2 at time t_2 is at q_1 at time $t_1 \geq t_2$,

$$\langle q(t_1)q(t_2)\rangle = \int dq_1 dq_2\, q_1 q_2\, \rho(q_1,t_1|q_2,t_2)\rho_{\rm st}(q_2,t_2). \tag{4.4}$$

For weak driving, function $\rho_{\rm st}(q,t_2)$ can be expanded in a series in $F\exp(\pm i\omega_F t_2)$ with time-independent coefficients, whereas $\rho(q_1,t_1|q_2,t_2)$ can be expanded in $F\exp(\pm i\omega_F t_2)$ with coefficients that depend on t_1-t_2. Therefore the power spectrum (4.3) does not have terms linear in F. To the second order in F for $\omega\geq 0$ we have

$$\Phi(\omega)=\Phi_0(\omega)+\frac{\pi}{2}F^2|\chi(\omega_F)|^2\delta(\omega-\omega_F)+F^2\Phi_F(\omega). \tag{4.5}$$

The term $\Phi_0(\omega)$ describes the power spectrum of the system in the absence of driving. The term $\propto\delta(\omega-\omega_F)$ describes the conventional linear response, cf. Eq. (4.2). However, the expression for the susceptibility $\chi(\omega)$ in nonlinear systems is far more complicated than Eq. (4.2); generally, the susceptibility is determined by the linear in F term in $\rho_{\rm st}(q,t)$. In the optical language, the term $\propto\delta(\omega-\omega_F)$ in (4.5) corresponds to elastic scattering of the field $F\cos\omega_F t$ by the system.

Of primary interest to us is the term $\Phi_F(\omega)$. This term is often disregarded in the analysis of the power spectra of driven systems, while the major emphasis is placed on the δ-function in Eq. (4.5). Function $\Phi_F(\omega)$ describes the interplay of fluctuations and driving in a nonlinear system beyond the trivial linear response. In the considered lowest-order approximation in the driving amplitude, Φ_F does not contain a δ-peak at $2\omega_F$. However, it may contain a δ-peak at $\omega=0$, which corresponds to the static driving-induced shift of the average position of the system. In what follows we do not consider this peak, as the static equilibrium position can be measured independently.

Function Φ_F can be found from Eq. (4.4) by calculating the transition probability density and the stationary probability distribution. This can be done for Markov systems numerically and also, in the case of weak noise, analytically, see Secs. 4.3 and 4.4. Alternatively, function Φ_F can be related to fluctuations of linear and nonlinear response of the system and expressed in terms of the fluctuating linear and nonlinear susceptibility, see Sec. 4.6. We emphasize that the nonlinear response has to be taken into account when fluctuations are considered even though we are not interested in the behavior of the power spectrum near $2\omega_F$ or higher overtones or subharmonics of ω_F.

4.3 Power spectrum of a driven Brownian particle

A simple example of a system where $\Phi_F(\omega)$ displays a nontrivial behavior is a periodically driven overdamped Brownian particle in a nonlinear confining potential $U(q)$, see Eq. (4.1). This model immediately relates to many experiments on optically trapped particles and molecules. We will assume that thermal noise $f(t)$ is white and Gaussian and that it is not strong, so that it suffices to keep the lowest-order nontrivial terms in the potential,

$$U(q) = \frac{1}{2}\kappa q^2 + \frac{1}{3}\beta q^3 + \frac{1}{4}\gamma q^4 + \ldots, \qquad \langle f(t) f(t')\rangle = 2D\delta(t-t'), \tag{4.6}$$

where $D \propto k_B T$ is the noise intensity. In the absence of driving the stationary probability distribution is of the Boltzmann form, $\rho_{\rm st}^{(0)} \propto \exp[-U(q)/D]$.

For small D and weak driving force equation of motion $\dot{q} = -U'(q) + f(t) + F\cos\omega_F t$ can be solved directly by perturbation theory in the noise $f(t)$ and in F, as indicated in Sec. 4.6. Here we develop a different method, which is particularly convenient if one wants to go to high orders of the perturbation theory in D and F.

4.3.1 Method of Moments

Systems in which fluctuations are induced by white noise can be studied using the Fokker-Planck equation

$$\partial_t \rho = -\partial_q \left\{ \left[-U'(q) + F\cos\omega_F t \right] \rho \right\} + D\partial_q^2 \rho. \tag{4.7}$$

This equation can be solved numerically. A convenient analytical approach is based on the method of moments, which are defined as

$$M_n(\omega;t') = \int_0^\infty dt e^{i\omega t} \int dq q^n \int dq' \rho(q,t+t'|q',t') q' \rho_{\rm st}(q',t'). \tag{4.8}$$

From Eq. (4.5), the power spectrum is $\Phi(\omega) = (2/\tau_F)\mathrm{Re}\int_0^{\tau_F} dt' M_1(\omega;t')$.

The moments M_n satisfy a set of simple linear algebraic equations

$$\begin{aligned} &-i\omega M_n(\omega) + n\hat{\mathscr{F}}[M_n(\omega)] = Dn(n-1)M_{n-2}(\omega) \\ &+\frac{1}{2}F\left[e^{i\omega_F t'} n M_{n-1}(\omega+\omega_F) + e^{-i\omega_F t'} n M_{n-1}(\omega-\omega_F) \right] + Q_{n+1}(t'). \end{aligned} \tag{4.9}$$

Here, we skipped the argument t' in M_n and introduced function $\hat{\mathscr{F}}[M_n] \equiv \kappa M_n + \beta M_{n+1} + \gamma M_{n+2}$.. Functions

$$Q_n(t) = \int dq q^n \rho_{\rm st}(q,t) \tag{4.10}$$

in the right-hand side of Eq. (4.9) can themselves be found from a set of linear equations similar to (4.9). They follow from Eq. (4.7), if one sets $\rho = \rho_{\rm st}(q,t)$ and takes into account that $\rho_{\rm st}(q,t)$ is periodic in t. To the lowest order in F it suffices to keep in $Q_n(t)$ only terms that are independent of t or oscillate as $\exp(\pm i\omega_F t)$; respectively, in Eq. (4.10) $Q_n(t) \approx Q_n^{(0)} + \left[Q_n^{(1)} \exp(i\omega_F t) + \text{c.c.}\right]$, and

$$\begin{aligned} \hat{\mathscr{F}}[Q_n^{(0)}] &= D(n-1)Q_{n-2}^{(0)} + F\,\mathrm{Re}\, Q_{n-1}^{(1)}, \\ i\omega_F Q_n^{(1)} + n\hat{\mathscr{F}}[Q_n^{(1)}] &= Dn(n-1)Q_{n-2}^{(1)} + \frac{1}{2}nFQ_{n-1}^{(0)}. \end{aligned} \tag{4.11}$$

The system of coupled linear equations for the moments M_n and Q_n can be quickly solved with conventional software to a high order in the noise intensity D. Nontrivial results emerge already if we keep terms $\propto DF^2$: these are the terms that contribute to the power spectrum $\Phi_F(\omega)$ to the lowest order in D. To find them it suffices to consider terms M_n with $n \leq 3$ and Q_n with $n \leq 4$. This gives

$$\begin{aligned} \Phi_F(\omega) \;\approx\; & \frac{2D}{(\kappa^2+\omega_F^2)(\kappa^2+\omega^2)^2} \left\{ 2\beta^2 \frac{(4\kappa^2+\omega_F^2)(\kappa^2+\omega^2+\omega_F^2)}{[\kappa^2+(\omega-\omega_F)^2][\kappa^2+(\omega+\omega_F)^2]} \right. \\ & \left. -3\gamma\kappa \right\}. \end{aligned} \tag{4.12}$$

This expression refers to $|\omega| > 0$; function $\Phi_F(\omega)$ contains also a δ-peak at $\omega = 0$, which comes from the driving-induced shift of the average static value of the coordinate.

The solution of the equations for the moments in the considered approximation gives a correction $\propto D^2$ to the power spectrum in the absence of driving $\Phi_0(\omega)$. To the lowest order in D this function displays a Lorentzian peak at $\omega = 0$, $\Phi_0(\omega) = 2D/(\kappa^2+\omega^2)$. This peak is used in the analysis of optical traps for Brownian particles [78, 79]; with account taken of the term $\propto D^2$ the zero-frequency peak of $\Phi_0(\omega)$ becomes non-Lorentzian.

4.3.2 Power spectrum for comparatively large driving frequency

The interpretation of Eq. (4.12) is simplified in the case where the driving frequency exceeds the decay rate, $\omega_F \gg \kappa$. In this case, periodic driving leads to two well-resolved features in the spectrum Φ_F. One is located at $\omega = 0$ and has the form

$$\Phi_F(\omega) \approx (2D/\omega_F^2)(2\beta^2 - 3\gamma\kappa)(\kappa^2 + \omega^2)^{-2} \quad (\omega \ll \omega_F). \tag{4.13}$$

This equation can be easily obtained directly by solving the equation of motion $\dot{q} = -U'(q) + F\cos\omega_F t + f(t)$ by perturbation theory in which $q(t)$ is separated into a part oscillating at high frequency ω_F (and its overtones) and a slowly varying part. To the lowest order in F and D, the fast oscillating part renormalizes the decay rate of the slowly varying part of $q(t)$, with $\kappa \to \kappa - (F/\omega_F)^2\left[\kappa^{-1}\beta^2 - (3/2)\gamma\right]$. Using this correction in the expression for the power spectrum of a linear system $\Phi_0^{(0)}(\omega) = 2D/(\kappa^2 + \omega^2)$, one immediately obtains Eq. (4.13) to the leading order in κ/ω_F.

Interestingly, Eq. (4.13) describes a peak or a dip depending on the sign of $2\beta^2 - 3\gamma\kappa$. That is, the sign of Φ_F is determined by the competition of the cubic and quartic nonlinearity of the potential $U(q)$. This shows high sensitivity of the spectrum to the system parameters. The typical width of the peak/dip of Φ_F near $\omega = 0$ is κ; the shape of the peak/dip is non-Lorentzian.

The other spectral feature is located at ω_F and near the maximum has the form of a Lorentzian peak, $\Phi_F(\omega) \approx (D\beta^2/\omega_F^4)[\kappa^2 + (\omega - \omega_F)^2]^{-1}$. The height of this peak is smaller by a factor $\kappa^2/\omega_F^2 \ll 1$ than the height of the feature near $\omega = 0$. We note that the height of the peak at ω_F is proportional to the squared parameter of the cubic nonlinearity of the potential β, but is independent of the quartic-nonlinearity parameter γ, to the leading order in the noise intensity D.

In Fig. 4.2 we compare the analytical expression (4.12) with the results of numerical simulations. The simulations were done by integrating the stochastic differential equation $\dot{q} = -U'(q) + f(t) + F\cos\omega_F t$ using the Heun scheme (cf. [69]). Panel (a) shows that the cubic nonlinearity of the potential leads to a peak at $\omega = 0$ and a comparatively small peak at ω_F. The spectrum becomes more interesting in the generic case where both cubic and quartic terms in the potential

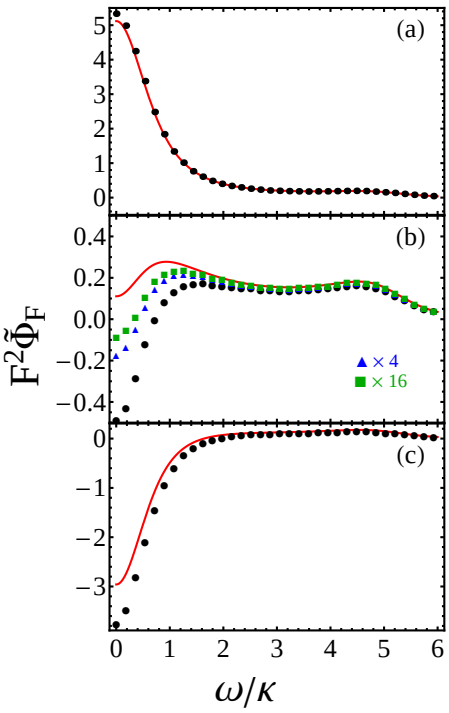

Figure 4.2 Scaled driving induced terms in the power spectrum of an overdamped Brownian particle moving in the quartic potential $U(q)$ given by Eq. (4.6), $\tilde{\Phi}_F(\omega) = 10^2\kappa^2\Phi_F(\omega)/2D$. Panels (a), (b), and (c) refer to the scaled cubic nonlinearity $\beta^2 D/\kappa^3 = 0.002$ and quartic nonlinearity $\gamma D/\kappa^2 = 0.0006$, 0.00147, and 0.002, respectively. The black dots and red solid curves correspond to the numerical simulations and Eq. (4.12). The scaled driving frequency is $\omega_F/\kappa = 5$ and the driving strength is $\kappa F^2/\omega_F^2 D = 20$. For this driving strength and the noise intensity, the simulation results in panels (b) and (c) deviate from the theoretical curve. The deviation decreases for weaker driving. This is seen from the simulation data in panel (b) that refer to $\kappa F^2/\omega_F^2 D = 5$ (blue triangles) and 1.25 (green squares). The corresponding spectra are scaled up by factors 4 and 16, respectively.

.

are present and β^2 is comparable to $\gamma\kappa$. Here, as seen from panel (b), as a result of the competition between these terms, $\Phi_F(\omega)$ can have a dip at $\omega = 0$ and two peaks, one near ω_F and the other with the position determined by $\beta^2/\gamma\kappa$ and ω_F/κ. Where the quartic nonlinearity dominates, $\gamma\kappa \gg \beta^2$, see panel (c), it is hard to detect the peak at ω_F for small noise intensity. Our analytical calculations and numerical simulations show that, for larger noise intensity, this peak becomes more pronounced.

A significant deviation of simulations and the asymptotic expression (4.12) in panel (b) for small ω is a consequence of the near compensation of the contributions to $\Phi_F(\omega)$ from the cubic

and quartic nonlinear terms in $U(q)$ to the lowest order in F^2 and D. The terms of higher-order in D and F^2 become then substantial. Panel (b) illustrates how the difference is reduced if F^2 is reduced. We checked that by reducing also the noise intensity we obtain a quantitative agreement of simulations with Eq. (4.12).

In some cases the confining potential of an overdamped system has inversion symmetry, and then $\beta = 0$ in Eq. (4.6). In such cases spectral features of Φ_F at the driving frequency are $\propto (\gamma D)^2$. They can be found by solving the equations for the moments M_n with $n \leq 5$ and Q_n with $n \leq 6$ or by solving the equations of motion by perturbation theory to the second order in γ, see Sec. 4.6.

4.4 Power spectrum of a driven two-state system

We now consider the effect of driving on a two-state system. Various types of such systems are studied in physics, from spin-1/2 systems to two-level systems in disordered solids to classical Brownian particles mostly localized at the minima of double-well potentials. We will assume that the system dynamics are characterized by the rates W_{ij} of interstate $i \to j$ switching, where $i, j = 1, 2$. In the case of quantum systems, this means that the decoherence rate largely exceeds W_{ij}; in other words, the typical duration of an interstate transition is small compared to $1/W_{ij}$. For classical systems, this description means that small fluctuations about the stable states are disregarded.

4.4.1 The model: modulated switching rates

A major effect of periodic driving is modulation of the switching rates. It can be quite strong already for comparatively weak driving. Indeed, if the rates are determined by the interstate tunneling, since the field changes the tunneling barrier, its effect can be exponentially strong. Similarly, it may be exponentially strong in the classical limit if the switching is due to thermally activated overbarrier transitions, because the driving changes the barriers heights. Nevertheless, for weak sinusoidal driving $F \cos \omega_F t$ the modulated rates $W_{ij}^{(F)}(t)$ can still be expanded in the driving am-

plitude,

$$W_{ij}^{(F)} \approx W_{ij} - \alpha_{ij} F \cos \omega_F t, \qquad i,j = 1,2. \tag{4.14}$$

This equation is written in the adiabatic limit, where the driving frequency ω_F is small compared to the reciprocal characteristic dynamical times, like the imaginary time of motion under the barrier in the case of tunneling [87] or the periods and relaxation times of vibrations about the potential minima in the case of activated transitions. The rates W_{ij} are also assumed to be small compared to the reciprocal dynamical times. The driving frequency ω_F is of the order of W_{ij}.

Parameters α_{ij} in Eq. (4.14) describe the response of the switching rates to the driving. They contain factors $\sim W_{ij}$. Indeed, for activated processes $W_{ij} \propto \exp(-\Delta U_i / k_B T)$, where ΔU_i is the height of the potential barrier for switching from the state i. If $F \cos \omega_F t$ is the force that drives the system, then $\alpha_{ij} \approx W_{ij} d_i / k_B T$, where d_i is the position of the ith potential well counted off from the position of the barrier top [88]. The terms $\propto F^2$, which have been disregarded in Eq. (4.14), are $\propto W_{ij} (d_i / k_B T)^2$ in this case; a part of these terms that are $\propto \cos 2\omega_F t$ do not contribute to $\Phi_F(\omega)$ to the second order in F, whereas the contribution of the time-independent terms $\propto F^2$ comes to renormalization of the parameters W_{ij} in $\Phi_0(\omega)$, see below. For incoherent interstate quantum tunneling, $\alpha_{ij} \propto W_{ij}$, too.

We will use quantum notations $|i\rangle$ $(i = 1,2)$ for the states of the system. One can associate these states with the states of a spin-1/2 particle by setting $|1\rangle \equiv |\uparrow\rangle$ and $|2\rangle \equiv |\downarrow\rangle$. The system dynamics is most conveniently described by the dynamical variable q defined as

$$q = |1\rangle\langle 1| - |2\rangle\langle 2| \equiv \sigma_z, \tag{4.15}$$

where σ_z is the Pauli matrix. For a particle in a double-well potential, q is the coordinate that takes on discrete values 1 and -1 at the potential minima 1 and 2, respectively.

The power spectra of driven two-state systems have been attracting much interest in the context of stochastic resonance, see [89, 90, 91, 92] for reviews. By now it has been generally accepted that, for weak driving, the power spectrum of a system has a δ-peak at the driving frequency with area $\propto F^2$, which is described by the standard linear response theory [93]. This peak is of central

interest for signal processing. However, as we show in this Section, along with this peak, the spectrum has a characteristic extra structure, which is also $\propto F^2$, to the leading order in F.

4.4.2 Kinetic equation and its general solution

It is convenient to write the analog of Eq. (4.4) for the correlation function of the discrete variable q as

$$\langle q(t_1)q(t_2)\rangle = \sum_{i,j}\langle i|\sigma_z\hat{\rho}(t_1|t_2)\sigma_z\hat{\rho}_{\rm st}(t_2)|j\rangle \tag{4.16}$$

Here, $\hat{\rho}(t_1|t_2)$ is the transition density matrix, $\hat{\rho}(t_1|t_2)\equiv\sum|i\rangle\rho_{ij}(t_1|t_2)\langle j|$, and $\hat{\rho}_{\rm st}\equiv\sum|i\rangle(\rho_{\rm st})_{ii}\langle i|$ is the stationary density matrix. By construction (in particular, because of the decoherence in the quantum case) the stationary density matrix is diagonal. Its matrix elements $(\rho_{\rm st})_{ii}$ give the populations of the corresponding states and periodically depend on time, $\hat{\rho}_{\rm st}(t+2\pi/\omega_F)=\hat{\rho}_{\rm st}(t)$. The transition matrix elements $\rho_{ij}(t_1|t_2)$ give the probability to be in state i at time t_1 given that the system was in state j at time t_2. At equal times we have $\hat{\rho}(t_2|t_2)=\hat{I}$, where $\hat{I}$ is the unit matrix.

Equation (4.16) does not have the form of a trace over the states $|i\rangle$; rather it expresses the correlator in terms of the joint probability density to be in state $|j\rangle$ at time t_2 and in state $|i\rangle$ at time t_1, with summation over i,j [94]. In the quantum formulation, the applicability of this expression is a consequence of the decoherence and Markovian kinetics.

Matrix elements $\rho_{ij}(t|t')$ satisfy a simple balance equation, which in the presence of driving reads

$$\partial_t\rho_{1j}(t|t') = -W_{12}^{(F)}(t)\rho_{1j}+W_{21}^{(F)}(t)\rho_{2j},\quad \rho_{1j}+\rho_{2j}=1, \tag{4.17}$$

where $j=1,2$. Equation for the matrix elements of $\hat{\rho}_{\rm st}(t)$ has the same form, except that subscript j has to be set equal to the first subscript.

From Eqs. (4.16) and (4.17) we obtain a general expression for the correlator of interest,

$$\langle q(t_1)q(t_2)\rangle = \exp\left[-\int_{t_2}^{t_1}dtW_+^{(F)}(t)\right]+\langle\sigma_z(t_2)\rangle_{\rm st}\int_{t_2}^{t_1}dt\left\{W_-^{(F)}(t)\right.$$
$$\left.\times\exp\left[-\int_t^{t_1}dt'W_+^{(F)}(t')\right]\right\},\qquad W_\pm^{(F)}(t)=W_{21}^{(F)}(t)\pm W_{12}^{(F)}(t). \tag{4.18}$$

Here, $\langle\sigma_z(t)\rangle_{\rm st} \equiv \langle q(t)\rangle_{\rm st} \equiv {\rm Tr}\,[\sigma_z\hat{\rho}_{\rm st}(t)]$ is the time-dependent difference of the state populations in the stationary state. Generally , $\langle\sigma_z(t)\rangle_{\rm st}$ is nonzero even in the absence of driving unless the switching rates are equal, $W_{12} = W_{21}$. In the presence of driving there emerges a periodic term in $\langle\sigma_z(t)\rangle_{\rm st}$, which describes the linear response, for weak driving.

Disregarding terms oscillating as $\exp(\pm 2i\omega_F t)$, to the second order in F we obtain from the balance equation (4.17) written for $(\rho_{\rm st})_{ii}$

$$\langle\sigma_z(t)\rangle_{\rm st} \approx \frac{W_-}{W_+} + \frac{F}{2}\left[\chi_1(\omega_F)e^{-i\omega_F t} + \text{ c.c.}\right] + \frac{\alpha_+ F^2}{2W_+}{\rm Re}\,\chi_1(\omega_F),$$
$$\chi_1(\omega) = 2\left(\alpha_{12}W_{21} - \alpha_{21}W_{12}\right)/\left[W_+\left(W_+ - i\omega\right)\right]. \tag{4.19}$$

Here we introduced notations

$$\alpha_\pm = \alpha_{21} \pm \alpha_{12}, \qquad W_\pm = W_{21} \pm W_{12}. \tag{4.20}$$

Function $\chi_1(\omega)$ gives the linear susceptibility. In the case of thermally activated transitions, Eq. (4.19) for χ_1 coincides with the classical result [88]. The term W_-/W_+ gives the difference of the state populations in the absence of driving, whereas the term $\propto F^2$ gives the time independent part of the driving-induced correction to this difference.

4.4.3 The driving-induced part of the power spectrum

Equation (4.18) allows one to calculate the period-averaged correlator $\langle\langle q(t_1)q(t_2)\rangle\rangle$ in the explicit form and to obtain the power spectrum. As before, we will not consider the δ-peak in $\Phi(\omega)$ for $\omega = 0$. The spectrum is an even function of ω, and we will consider it for $\omega > 0$:

$$\Phi_0(\omega) = 8\frac{W_{12}W_{21}}{W_+^2}\,\frac{W_+}{W_+^2+\omega^2}, \qquad \Phi_F(\omega) = \Phi_F^{(\rm r)}(\omega) + \Phi_F^{(\rm c)}(\omega),$$
$$\Phi_F^{(\rm r)}(\omega) = \alpha_+ \textstyle\sum_{\mu,\nu=\pm}\phi_F(\mu\omega, \nu\omega_F),$$
$$\phi_F(\omega,\omega_F) = -[W_+ - i(\omega-\omega_F)]^{-1}\left[\frac{\alpha_+ W_{12}W_{21}}{\omega_F^2 W_+^2} + i\frac{W_-}{2\omega_F W_+}\chi_1^*(\omega_F)\right]. \tag{4.21}$$

The term Φ_0 is the familiar power spectrum of a two-state system in the absence of driving [88]. It has a peak at $\omega = 0$ with halfwidth W_+ equal to the sum of the switching rates. The term $\Phi_F^{(\rm c)}$

describes the driving-induced modification of the peak centered at $\omega = 0$,

$$\Phi_F^{(c)}(\omega) = (\alpha_+^2/2\omega_F^2)\Phi_0(\omega) - |\chi_1(\omega_F)|^2 W_+/(W_+^2 + \omega^2). \tag{4.22}$$

Of major interest to us is the part $\Phi_F^{(r)}(\omega)$ of the driving-induced term in the power spectrum (4.21). For $\omega > 0$, it shows a resonant peak (or a dip, depending on the parameters) at the driving frequency ω_F. In contrast to the δ-peak of the linear response, the peak has a finite halfwidth $\sim W_+ = W_{12} + W_{21}$. It is well separated from the peak at $\omega = 0$ for $\omega_F \gg W_+$ and generally is of a non-Lorentzian shape. We stress that, to the order of magnitude, the peak has the same overall area as the δ-peak of the linear response (in the case of a dip, the absolute value of the area should be considered). Another important feature of the peak/dip seen from Eq. (4.21) is that it is proportional to the parameter $\alpha_+ = \alpha_{12} + \alpha_{21}$. This parameter describes the change of the sum of the switching rates due to the driving.

For activated switching between potential minima considered in the classical stochastic resonance theory, $\alpha_+ = (k_B T)^{-1}(W_{12} d_1 + W_{21} d_2)$. For a symmetric potential $\alpha_+ = 0$, since $W_{12} = W_{21}$ and $d_1 = -d_2$. Then $\Phi_F^{(r)} = 0$, in agreement with [95] where a symmetric potential was considered. On the other hand, for strong driving it was found [96] that the power spectrum for an asymmetric potential displays peaks close to odd multiples of the driving frequency and dips close to even multiples of driving frequency. In our weak-driving analysis we do not consider peaks/dips near the overtones of ω_F; however, as seen from Eq. (4.21), the sign of $\Phi_F^{(r)}(\omega)$ near ω_F can be positive or negative, depending on the parameters.

Examples of the driving-induced spectra $\Phi_F(\omega)$ are shown in Fig. 4.3. One can clearly see the peaks or dips both at $\omega = 0$ and at the driving frequency ω_F. In agreement with Eqs. (4.21) and (4.22), the signs of the features of Φ_F are determined by the interrelation between the parameters of the two-states system. For illustration purpose we chose the values of the ratio of the response parameters α_{21}/α_{12} to lie between plus and minus the ratio of the switching rates in the absence of driving, W_{21}/W_{12}. As seen from Fig. 4.3, the spectra are very sensitive to the ratio α_{21}/α_{12}. We have seen this sensitivity also for different values of W_{21}/W_{12}.

Unexpectedly, a finite-height spectrum $\Phi_F(\omega)$ emerges even where the linear susceptibility is equal to zero, which happens for $\alpha_{12}W_{21} = \alpha_{21}W_{12}$. This is seen from Eq. (4.21) and also from Fig. 4.3. The red line with $\alpha_{21}/\alpha_{12} = 7/3$ refers to this case, and the area of δ-peak in the spectrum is zero. As seen from the figure, numerical simulations are in excellent agreement with the analytical expressions.

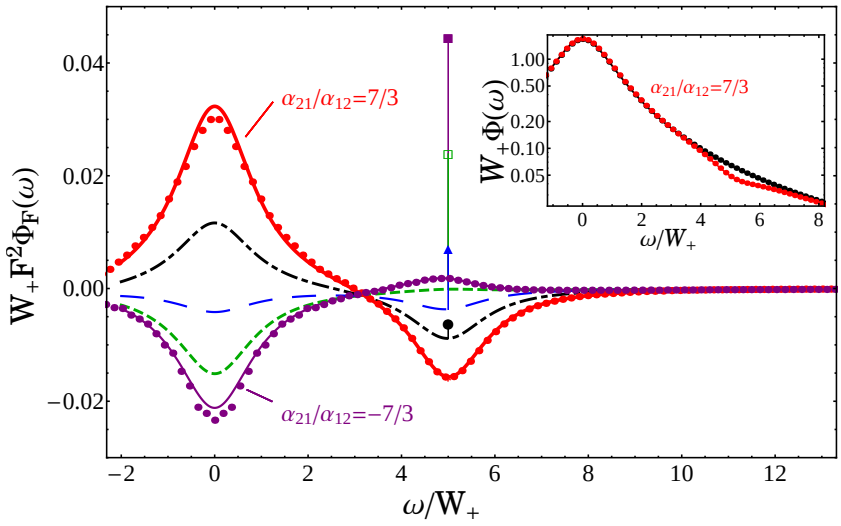

Figure 4.3 The driving induced terms in the power spectrum of the two-state system for the ratio of the switching rates $W_{21}/W_{12} = 7/3$. The scaled driving frequency and amplitude are $\omega_F/W_+ = 5$ and $F\alpha_{12}/W_{12} = 1$. On the thick solid (red), dot-dashed (black), long-dashed (blue), short-dashed (green), and thin solid (purple) lines the ratio α_{21}/α_{12} is 7/3, 7/6, 0 , $-7/6$, and $-7/3$. The vertical line at ω_F shows the position of the δ-peak at ω_F. The areas of the δ-peaks for different α_{21}/α_{12} are given by the heights of the vertical segments. The heights are counted off from the lines to the symbols of the same color, i.e., to the circle, triangle, and open and full square, in the order of decreasing α_{21}/α_{12}; there is no symbol for $\alpha_{21}/\alpha_{12} = 7/3$ as there is no δ-peak in this case. The inset shows the full spectrum with (red) and without (black) driving for $\alpha_{21}/\alpha_{12} = 7/3$. The curves and the dots show the analytical theory and the simulations, respectively.

The structure of the spectrum near $\omega = 0$ will be modified if one takes into account terms $\propto F^2$ in the expressions for the switching rates (4.14). In the considered leading-order approximation in F these terms have to be averaged over the driving period and are thus independent of time. The correction due to these terms can be immediately found from Eq. (4.21) for $\Phi_0(\omega)$ by expanding Φ_0 to the first order in the corresponding increments of W_{ij}; this correction is of a non-Lorentzian form.

4.5 Threshold detector

An insight into the dynamical nature of the driving-induced change of the power spectrum can be gained from the analysis of the spectrum of a threshold detector. Such detectors are broadly used in science and engineering, and their analogs play an important role in biosystems. We will employ the simplest model where the output of a threshold detector is $q = -1$ if the signal at the input is below a threshold value η, whereas $q = 1$ otherwise, and will consider the case where the input signal is a sum of the periodic signal $F\cos\omega_F t$ and noise $\xi(t)$,

$$q(t) = 2\Theta\left[F(t) + \xi(t) - \eta\right] - 1, \tag{4.23}$$

where $\Theta(x)$ is the Heaviside step function. To avoid singularities related to non-differentiability of the Θ-function, we will model the output by

$$q(t) = \tanh\left[\Lambda\big(F(t) + \xi(t) - \eta\big)\right], \qquad \Lambda \gg 1, \tag{4.24}$$

and in the final expressions will go to the limit $\Lambda \to \infty$. Much work on the interplay of noise and driving in threshold detectors has been done in the context of stochastic resonance, cf. [97, 98, 99]. In these papers of primary interest was the signal to noise ratio; the issues we are considering here, i.e., the occurrence of the effective “inelastic scattering" and “fluorescence" as a result of interplay of nonlinearity and noise, have not been addressed, to the best of our knowledge.

In the absence of noise, the power spectrum of $q(t)$ is a series of δ-peaks at ω_F and its overtones (including $\omega = 0$), provided the driving amplitude $F > \eta$, whereas for $F < \eta$ we have $q = -1$ and the power spectrum is just a δ-peak at $\omega = 0$. On the other hand, if $F = 0$ and $\xi(t)$ is white noise, in the limit $\Lambda \to \infty$ in Eq. (4.24) the correlator $\langle q(t)q(t')\rangle = 0$ for $t \neq t'$, since the values of $q(t)$ at different instants of time are uncorrelated and $\langle q\rangle \to 0$, whereas $\langle q^2\rangle \to 1$.

The singular behavior of the correlator $\langle q(t)q(t')\rangle$ in the case of white noise persists also in the presence of driving. This is a consequence of the absence of *d*ynamics, i.e., any memory effects in the variable $q(t)$ (4.23), and the singular distribution of white noise, where the intensity $\langle \xi^2(t)\rangle$ diverges.

Dynamics can be brought into the system by the noise color. Such noise can be thought of as coming from a dynamical system with retarded response, which is driven by white noise. We will be interested in the correlator $\langle q(t)q(t')\rangle$ and the power spectrum $\Phi(\omega)$ for weak driving, where the driving amplitude is $F \ll \eta$ (subthreshold driving), and for a simple colored noise, the Ornstein-Uhlenbeck noise. This is Gaussian noise with correlator

$$\langle \xi(t)\xi(t')\rangle = (D/\kappa)\exp(-\kappa|t-t'|). \tag{4.25}$$

Parameter κ characterizes the decay rate of noise correlations.

Because the threshold detector has no dynamics on its own, the value of the variable $q(t)$ is determined by the instantaneous value of the noise $\xi(t)$. We can write $q(t) \equiv \tilde{q}\big(t,\xi(t)\big)$, where $\tilde{q}(t,\xi)$ is given by Eqs. (4.23), (4.24) with $\xi(t)$ replaced with ξ. Then the general expression for the correlator of $q(t)$, Eq. (4.4), can be rewritten as

$$\langle q(t_1)q(t_2)\rangle = \int d\xi_1 d\xi_2\, \tilde{q}(t_1,\xi_1)\tilde{q}(t_2,\xi_2)\,\rho^{(\xi)}(\xi_1,t_1|\xi_2,t_2)\rho_{\rm st}^{(\xi)}(\xi_2,t_2). \tag{4.26}$$

Here, the superscript ξ indicates that the corresponding transition probability density and the stationary distribution refer to the random process $\xi(t)$.

The form of the transition probability for the process (4.25) is well-known [100],

$$\rho^{(\xi)}(\xi_1,t_1|\xi_2,t_2) = \sqrt{\frac{\kappa}{2\pi D(1-e^{-2\kappa|t_1-t_2|})}}\exp\left\{-\frac{\kappa(\xi_1-\xi_2 e^{-\kappa|t_1-t_2|})^2}{2D(1-e^{-2\kappa|t_1-t_2|})}\right\}. \tag{4.27}$$

The stationary distribution $\rho_{\rm st}^{(\xi)}(\xi_1,t_1)$ is given by the same expression with $t_2 \to -\infty$. Substituting these expressions into Eq. (4.26) and expanding $\tilde{q}(t,\xi)$ in $F(t)$, after averaging over the driving period we obtain to second order in $F(t)$ for $t_1 > t_2$

$$\begin{aligned}\langle\langle q(t_1)q(t_2)\rangle\rangle = C+ \quad & 4\int_\eta^\infty d\xi_1 \int_\eta^\infty d\xi_2 \left[\rho^{(\xi)}(\xi_1,t_1|\xi_2,t_2) - \rho_{\rm st}^{(\xi)}(\xi_1)\right]\rho_{\rm st}^{(\xi)}(\xi_2) \\ & +2F^2\cos\omega_F(t_1-t_2)\rho^{(\xi)}(\eta,t_1|\eta,t_2)\rho_{\rm st}^{(\xi)}(\eta) \\ & -2F^2\int_\eta^\infty d\xi_2 \rho_{\rm st}^{(\xi)}(\xi_2)\tfrac{d}{d\eta}\left[\rho^{(\xi)}(\eta,t_1|\xi_2,t_2) - \rho_{\rm st}^{(\xi)}(\eta)\right].\end{aligned} \tag{4.28}$$

Here, C is a constant independent of time; it leads to a δ peak at $\omega = 0$ in the power spectrum and will not be considered in what follows. The remaining terms are time-dependent. They decay

with increasing $|t_1 - t_2|$, except for the term that oscillates as $\exp[\pm i\omega_F(t_1-t_2)]$ and describes the standard linear response to periodic driving. As seen from Eq. (4.28), this term has the form

$$2F^2 \cos\omega_F(t_1-t_2)\left[\rho_{\rm st}^{(\xi)}(\eta)\right]^2 \equiv \tfrac{1}{2}F^2|\chi(\omega_F)|^2\cos\omega_F(t_1-t_2),$$
$$\chi(\omega) = 2\rho_{\rm st}^{(\xi)}(\eta) \equiv (2\kappa/\pi D)^{1/2}\exp[-\kappa\eta^2/2D), \tag{4.29}$$

where $\chi(\omega)$ is the standard linear susceptibility [85] of the threshold detector. Interestingly, this susceptibility is independent of frequency. This is because the detector has no dynamics, its response to the driving is instantaneous. An alternative derivation of the expression for the susceptibility, which provides a useful insight into the response of the threshold detector, is given in Sec. 4.6. It also shows how to deal with the singularities in Eq. (4.28) for $t_1 \to t_2$, which emerge after the transition $\Lambda \to \infty$ in Eqs. (4.24) and (4.26).

The power spectrum $\Phi(\omega)$ is obtained from Eq. (4.28) by a Fourier transform. The F independent term in Eq. (4.28) gives the power spectrum $\Phi_0(\omega)$ in the absence of driving. It has a peak at $\omega = 0$. The term $\propto \cos\omega_F(t_1-t_2)$ gives a δ-peak and also a finite-width peak $F^2\Phi_F^{(\rm r)}(\omega)$ at frequency ω_F. The last term in Eq. (4.28) gives a driving-induced feature in the power spectrum at zero frequency $F^2\Phi^{(\rm c)}(\omega)$.

The shape of the spectra is determined by the dimensionless parameter that characterizes the ratio of the threshold to the noise amplitude $\eta(\kappa/D)^{1/2}$. For weak noise, where $\eta(\kappa/D)^{1/2} \gg 1$, the peak near ω_F has the form

$$\Phi_F^{(\rm r)}(\omega) \approx \frac{1}{D\sqrt{2\pi}}\,{\rm Re}\left(\frac{\kappa\eta^2}{4D} + i\frac{\omega-\omega_F}{\kappa}\right)^{-1/2} e^{-\kappa\eta^2/2D}. \tag{4.30}$$

Here we assumed that ω_F/κ is sufficiently large, so that the features of Φ_F centered at ω_F and $\omega = 0$ are well separated; Eq. (4.30) applies for $|\omega - \omega_F| \ll \omega_F$. The spectrum (4.30) has a characteristic non-Lorentzian form with typical width $\kappa^2\eta^2/4D$. However, its area is small.

In the opposite limit of low threshold, $\eta(\kappa/D)^{1/2} \ll 1$, to the leading order

$$\Phi_F^{(\rm r)}(\omega) \approx \frac{1}{2\sqrt{\pi}D}\,{\rm Re}\left[\Gamma\left(i\frac{\omega-\omega_F}{2\kappa}\right)/\Gamma\left(\frac{1}{2}+i\frac{\omega-\omega_F}{2\kappa}\right)\right] \tag{4.31}$$

near ω_F. This spectrum falls off slowly away from the maximum, as $|\omega-\omega_F|^{-1/2}$ for $|\omega-\omega_F| \gg \kappa$. Equation (4.31) does not contain the threshold η. The small-η correction to (4.31) for $\omega=\omega_F$ is $(1-\ln 2)\kappa\eta^2/\pi D^2$. It is positive. From the comparison of Eqs. (4.30) and (4.31), one sees that the height of the peak at ω_F first increases with the increasing $\eta(\kappa/D)^{1/2}$, but then starts decreasing.

In Fig. 4.4 we show analytical results for the power spectra obtained from Eq. (4.28) for several parameter values and compare them with the results of simulations. Immediately seen from this figure is that the driving modifies the overall spectrum most significantly near $\omega=0$ and near ω_F for large ω_F/κ. There emerges a finite-width peak at ω_F. As seen from the inset in panel (b), the width of this peak increases with decreasing noise intensity, that is, with increasing $\eta(\kappa/D)^{1/2}$. This is a counterintuitive consequence of the unusual interplay of noise and driving in a threshold detector. The height of the peak displays a nonmonotonic dependence on $\eta(\kappa/D)^{1/2}$.

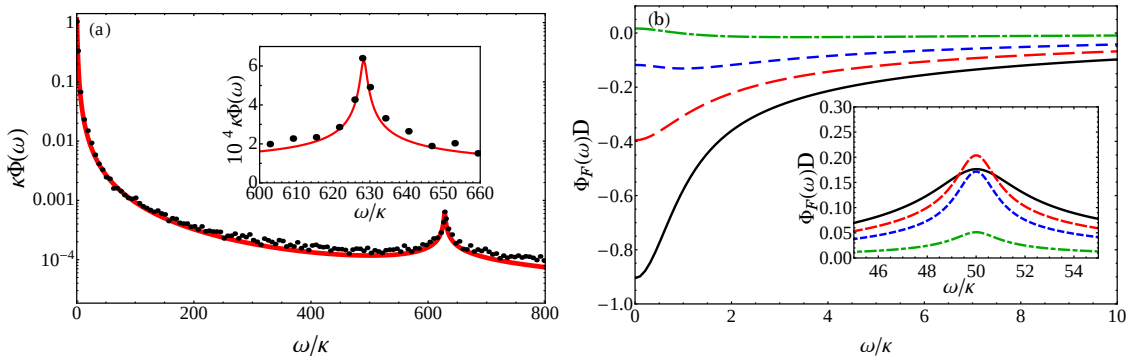

Figure 4.4 Power spectrum of the threshold detector. (a): The full power spectrum; the scaled frequency and the intensity of the driving are $\omega_F/2\pi\kappa=100$ and $F^2\kappa/D=0.0025$. The scaled threshold is $\eta(\kappa/D)^{1/2}=0.5$. Inset: the spectrum near the driving frequency. The delta peak has been subtracted. The curves and black dots refer to the theory and simulations, respectively. (b): The low-frequency part of the driving-induced term in the power spectrum for $\omega_F/\kappa=50$ as given by Eq. (4.28). The solid (black), long-dashed (red), short-dashed (blue) and dot-dashed (green) curves correspond to the scaled value of the threshold $\eta(\kappa/D)^{1/2}=0.1, 0.8, 1.2$, and 2. Inset: the spectrum near the driving frequency, $\omega_F/\kappa=50$.

The low-frequency spectrum $\Phi_F(\omega)\approx\Phi_F^{(c)}(\omega)$ also displays a pronounced feature near $\omega=0$. One can show from the analysis of the last term in Eq. (4.28) that, for small $\eta(\kappa/D)^{1/2}$, this feature is a dip, with $\Phi_F^{(c)}(0)=-1/D$ for $\eta(\kappa/D)^{1/2}\to 0$. The shape of the dip is non-Lorentzian, with

typical width κ. As $\eta(\kappa/D)^{1/2}$ increases, the depth of the dip decreases. Ultimately the shape of the spectrum changes completely. For large $\eta(\kappa/D)^{1/2}$ the spectrum $\Phi_F^{(c)}$ becomes broad and shallow. To the leading order in $[\eta(\kappa/D)^{1/2}]^{-1}$, it can be written as

$$(2/\pi D)(D/\kappa\eta^2)^{1/2}\exp(-\kappa\eta^2/2D)\tilde{\Phi}_F^{(c)}(2D\omega/\kappa^2\eta^2),$$

where the dimensionless function $\tilde{\Phi}_F^{(c)}(x)$ is zero for $x=0$, has a minimum at $x\approx 1.7$, where it is ≈ -0.6, and then approaches zero with increasing x as $x^{-1/2}$.

4.6 Formulation in terms of fluctuating susceptiblities

The change of the power spectrum induced by the driving can be analyzed in terms of the fluctuating linear and nonlinear susceptibility of the system, see Sec. (2.2.1). For nonlinear systems, the term $\Phi_F^{(2)}$ is generally nonzero, and should be kept in the power spectrum in contrast to linear systems.

A convenient way to calculate the fluctuating susceptibilities $\chi_{1,2}$ is based on solving dynamical equations of motion of the system. For example, for an overdamped Brownian particle described by the Langevin equation $\dot{q} = -U'(q) + f(t) + F\cos\omega_F t$ with nonlinear potential (4.6), one can proceed by rewriting this equation in the integral form,

$$\begin{aligned} q(t) = \quad & \int_{-\infty}^{t} dt' e^{-\kappa(t-t')} \exp\left\{ -\int_{t'}^{t} dt'' \left[\beta q(t'') + \gamma q^2(t'') \right] \right\} \\ & \times \left[F\cos\omega_F t' + f(t') \right]. \end{aligned} \tag{4.32}$$

For small f and F, one can then expand the q-dependent exponential in the right-hand side and use successive approximations in F and f. The fluctuating susceptibility χ_1 is given by linear in F terms, whereas χ_2 is given by the terms quadratic in F. The advantageous feature of this method is that it is not limited to white noise. However, the method becomes impractical if the noise intensity is not weak, and even for weak noise it becomes cumbersome if one goes to high-order terms in the noise intensity.

We have checked that the calculation based on Eq. (4.32) gives the same result for the driving-induced part of the power spectrum $\Phi_F(\omega)$ as the method of moments. We have also found that, in the second order in the noise intensity D, the term $\gamma q^4/4$ in $U(q)$ leads to the onset of a peak in $\Phi_F(\omega)$ at ω_F.

4.6.1 Fluctuating susceptibility of a threshold detector

Fluctuating linear susceptibility has a particularly simple form for a threshold detector. By linearizing in $F(t)$ expression (4.23) for the output of the detector, we obtain from the definition of the susceptibility (2.1)

$$\chi(t,t') = 2\delta(t-t'-0)\delta\big(\xi(t)-\eta\big), \tag{4.33}$$

where η is the threshold and $\xi(t)$ is the noise. Zero in $\delta(t-t'-0)$ reflects causality: the detector output $q(t)$ is determined by the value of the driving just before the observation time; the very δ-function indicates that the effect of the driving is not accumulated over time, the response is instantaneous (but causal).

The standard linear susceptibility $\chi(\omega)$ is given by expression

$$\chi(\omega) = \int_0^\infty dt e^{i\omega t}\langle\chi(t,0)\rangle.$$

From Eq. (4.33), $\chi(\omega) = 2\rho_{\rm st}^{\xi}(\eta)$. where $\rho_{\rm st}^{\xi}(\eta)$ is the stationary probability density of the noise $\xi(t)$, cf. Eq. (4.29). It applies for an arbitrary noise $\xi(t)$, not just for the exponentially correlated noise considered in Sec. 4.5.

Similarly, the fluctuating nonlinear susceptibility of the detector is

$$\chi_2(t,t',t'') = -\delta(t-t'-0)\delta(t-t''-0)\partial_\eta\delta\big(\xi(t)-\eta\big). \tag{4.34}$$

Substituting Eqs. (4.33) and (4.34) into the general expressions for the power spectrum in terms of fluctuating susceptibilities, Eqs. (2.3) and (2.4), we obtain the power spectrum in the same form as what follows from Eq. (4.28).

4.7 Conclusions

The results of this chapter demonstrate that the interplay of driving and fluctuations leads to the onset of specific spectral features in the power spectra of dynamical systems. Such features are analogs of inelastic light scattering and fluorescence in optics, where an electromagnetic field can excite radiation at a frequency shifted from its frequency and also at the characteristic system frequency. Our results show that, in classical systems and in incoherent quantum systems, the spectral features emerge as a result of the fluctuation-induced modulation of the response to the driving. Such modulation is common to nonlinear systems.

Since nonlinearity and noise are always present in real systems, the occurrence of the driving-induced spectral features in the power spectra should be also generic. However, these features are specific for particular systems, which allows using them for system characterization.

We have studied three types of systems, all of which are attracting significant interest in mesoscopic physics and in several other areas of science. The first one is an overdamped Brownian particle fluctuating in a non-parabolic potential well. This model describes, in particular, small particles and molecules optically trapped in a liquid. We find that, when the particle is periodically driven, the nonparabolicity of the potential leads to an extra spectral peak or a dip at zero frequency. For comparatively weak noise, the sign of the driving-induced term in the spectrum at small ω is determined by the competition of the cubic and quartic nonlinearity of the potential. The overall shape of the low-frequency spectrum strongly depends on the form of the confining potential as well. In addition, along with a δ-peak at the driving frequency, the driving-induced spectrum displays a peak at this frequency with a width of the order of the relaxation rate of the system.

We have also studied a two-state system that at random switches between the states. We assumed that the driving modulates the rates of interstate switching. The driving-induced spectrum has a rich form. Depending on the interrelation between the switching rates without driving and the driving-induced corrections to the rates, it can have peaks or dips both at $\omega = 0$ and at the driv-

ing frequency. The typical width of the peaks/dips is given by the sum of the interstate switching rates without driving. Interestingly, these finite-width spectral features can emerge even where the δ-peak at the driving frequency has very small (or zero) intensity.

The third system we studied is a threshold detector. Here the dynamical nature of the driving-induced spectral change is particularly pronounced, as this change does not occur if the noise in the detector is white, except for the δ-peak at the driving frequency. On the other hand, for colored noise driving does change the power spectrum nontrivially. As in other systems, we find a driving-induced spectral feature near zero frequency. It can be a peak or a dip depending on the ratio of the threshold to the appropriately scaled noise intensity. Also, the height of the finite-width peak at the driving frequency displays a non-monotonic dependence on this ratio, as does the width of the peak, too, i.e., noise can both increase or decrease the width.

In all studied systems inertial effects played no role: the peaks of the power spectra are located at zero frequency in the absence of driving. Therefore driving-induced spectral features near the driving frequency and zero frequency correspond to inelastic scattering and fluorescence, respectively. However, in contrast to the conventional fluorescence, driving can induce a dip in the spectrum at zero frequency, as we have seen in all studied systems (the total power spectrum remains positive, of course). The occurrence of the dip looks as if the driving were decreasing the noise in the system, although in fact the dip has dynamical nature.

The power spectra of weakly damped nonlinear systems should also display extra features in the presence of weak periodic driving. The effect should be most pronounced where the driving is resonant. Along with the features near the driving frequency and near $\omega = 0$, there should arise features near the eigenfrequencies of slowly decaying vibrations about the stable states. Several features of the power spectra have been studied for nonlinear oscillators in the regime of strong driving, see recent papers [101, 102] and references therein. Interestingly, the results do not immediately extend to the weak-driving regime, and the features of the interplay of nonlinearity and driving where they are of comparable strength remain to be explored. However, it is clear from the presented results that the driving-induced change of the spectra is a general effect that provides a

sensitive tool for characterizing fluctuating systems and their parameters.

CHAPTER 5

CONCLUSIONS

Fluctuations and nonlinearities are key features of mesoscopic vibrational systems. Along with the reasonably well understood thermal fluctuations of the vibration amplitude, of significant interest are fluctuations of the oscillator eigenfrequency. They lie at the root of classical and quantum coherence of mesoscopic systems. Frequency fluctuations lead to broadening of the oscillator spectra, but this broadening is hard to separate and identify, because it is mixed with other spectral broadening mechanisms such as dissipation.

In this thesis, we studied how to reveal and characterize frequency fluctuations in mesoscopic vibrational systems. We showed that the interplay of a near-resonant driving and frequency noise leads to specific features in the oscillator power spectrum. These features allow one to distinguish frequency fluctuations of different bandwidths and sources, including 1/f-type noise, broadband noise, or nonlinearity-induced frequency noise. Besides the immediate relevance to the decoherence of mesoscopic oscillators, the results bear on the general problem of resonance fluorescence and light scattering by oscillators.

The first and perhaps most generic system in which the effect of frequency fluctuations can be investigated is a harmonic oscillator. Of interest is the general case where the spectrum and statistics of the fluctuations can be arbitrary. We showed that, when the oscillator is driven by a near-resonant force, in the presence of frequency fluctuations the driving-induced part of the oscillator power spectrum contains not only a δ peak at the driving frequency, but also some extra structure away from the driving frequency. This extra structure is a result of the interplay of the driving and the frequency noise, and its shape and strength depend sensitively on the characteristics of the frequency noise. In the case where the frequency noise correlation time is much longer than the oscillator relaxation time, the extra structure looks like a “pedestal" at the bottom of the δ peak. The width of the pedestal is directly determined by the bandwidth of the frequency noise.

In the opposite case where the frequency noise correlation time is much shorter than the oscillator relaxation time, the combined effect of driving and frequency noise is to induce a broad peak near the oscillator eigenfrequency. Its shape is the same as the oscillator power spectrum in the absence of driving, and its intensity is directly proportional to the frequency noise intensity.

Our theory was applied to a carbon nanotube resonator. By comparing the experimental observations with the theory, we found that a half of the observed spectral width came from a broadband frequency noise. Also for the first time a 1/f-type frequency noise was found and its spectrum was analyzed in this system.

We studied the spectral effects of dispersive mode coupling in driven mesoscopic systems. We found that, if the driving frequency is tuned away from the resonant frequency, there emerges a characteristic double-peak structure in the power spectrum. It results from the interplay of the dispersive-coupling-induced frequency noise and the driving. The peaks enable characterization of not only the coupling strength, but also the decay rate of the mode coupled to the driven mode. This can be done even where the mode is “hidden" and is not accessible to a direct measurement. We developed a path-integral technique to average over the coupling-induced frequency noise.

We also studied the power spectrum of a driven oscillator with intrinsic nonlinearity. Because the oscillator amplitude experiences thermal fluctuations and the frequency depends on the amplitude due to the nonlinearity, the frequency is also fluctuating. We found that the driving-induced changes of the power spectrum are qualitatively different for the cases of dispersive-coupling induced frequency fluctuations and frequency fluctuations due to the intrinsic oscillator nonlinearity. This is in spite the fact that, in the absence of the driving, the nonlinearity-related changes of the spectra are not easy to distinguish between the two cases.

Our theory on harmonic oscillators with frequency noise applies to the regime where the oscillators become quantum (i.e. $k_B T \ll \hbar\omega_0$) and the frequency noise remains classical. In the case of dispersively coupled oscillators, the theory applies when the oscillator under study is quantum while the “hidden” oscillator remains classical.

We also studied the interplay of driving and fluctuations in overdamped nonlinear systems,

where inertia plays no role. We showed that this interplay also leads to characteristic features in the power spectrum. Unlike vibrational systems, these features occur at zero frequency and the driving frequency, and they can represent a dip or a peak in the spectrum depending on the parameters of the fluctuations and the mechanisms of nonlinearities.

In the course of this work we developed new and fairly sophisticated mathematical methods including a path-integral technique to average over non-Gaussian fluctuations, a method of moments to compute the correlation functions in nonlinear systems, and several asymptotic methods to analyze the spectral effects of fluctuations.

5.1 Outlook

Studies on frequency noise of mesoscopic vibrational systems are currently attracting much interests. Here I briefly mention two immediate directions to extend our theory. An important extension of our theory on driven fluctuating oscillators is a theory of the spectra in the regime of nonlinear response, i.e. comparatively strong drive. This is of particular relevance to the superconducting cavity resonators. It was found that the intensity of the frequency noise in such systems is inversely proportional to the driving amplitude. This nonlinear response is sometimes attributed to the coupling between the resonator and a bath of two level fluctuators distributed in the dielectric. However, there is no full theory that describes this effect nor is it clear how to separate it from other nonlinear effects. It would be natural to extend our formalism to such cases.

Another direction is to study not just the spectrum of the frequency noise, but also the statistics of the noise. This requires calculating higher order correlators or moments of the oscillator displacement. It is an interesting question how the statistics of the frequency noise would manifest itself in the driving induced vibrations.

BIBLIOGRAPHY

BIBLIOGRAPHY

[1] K. L. Ekinci and M. L. Roukes. Nanoelectromechanical systems. *Rev. Sci. Instrum.*, 76(6):061101, June 2005.

[2] Markus Aspelmeyer, Tobias J. Kippenberg, and Florian Marquardt. Cavity optomechanics. *Rev. Mod. Phys.*, 86(4):1391–1452, December 2014.

[3] M. H. Devoret and R. J. Schoelkopf. Superconducting circuits for quantum information: An outlook. *Science*, 339(6124):1169–1174, March 2013.

[4] M. I. Dykman, editor. *Fluctuating Nonlinear Oscillators: from Nanomechanics to Quantum Superconducting Circuits*. OUP, Oxford, Oxford, 2012.

[5] M. Sansa, E. Sage, E. C. Bullard, M. Gely, T. Alava, E. Colinet, A. K. Naik, G. L. Villanueva, L. Duraffourg, M. L. Roukes, G. Jourdan, and S. Hentz. Frequency fluctuations in silicon nanoresonators. *ArXiv e-prints*, June 2015.

[6] Arthur W. Barnard, Vera Sazonova, Arend M. van der Zande, and Paul L. McEuen. Fluctuation broadening in carbon nanotube resonators. *PNAS*, 109(47):19093, 2012.

[7] T. F. Miao, S. Yeom, P. Wang, B. Standley, and M. Bockrath. Graphene nanoelectromechanical systems as stochastic-frequency oscillators. *Nano Lett.*, 14(6):2982–2987, June 2014.

[8] J. Gao, J. Zmuidzinas, B. A. Mazin, H. G. LeDuc, and P. K. Day. Noise properties of superconducting coplanar waveguide microwave resonators. *Appl. Phys. Lett.*, 90(10):102507, 2007.

[9] C. Neill, A. Megrant, R. Barends, Y. Chen, B. Chiaro, J. Kelly, J. Y. Mutus, P. J. J. O'Malley, D. Sank, J. Wenner, T. C. White, Y. Yin, A. N. Cleland, and J. M. Martinis. Fluctuations from edge defects in superconducting resonators. *Appl. Phys. Lett.*, 103:072601, 2013.

[10] W. Heitler. *The Quantum Theory of Radiation, 3rd ed.* Dover Publications, Inc., New York, 2010.

[11] Y. Zhang, J. Moser, J. Güttinger, A. Bachtold, and M. I. Dykman. Interplay of driving and frequency noise in the spectra of vibrational systems. *Phys. Rev. Lett.*, 113:255502, 2014.

[12] D. I. Schuster, A. A. Houck, J. A. Schreier, A. Wallraff, J. M. Gambetta, A. Blais, L. Frunzio, J. Majer, B. Johnson, M. H. Devoret, S. M. Girvin, and R. J. Schoelkopf. Resolving photon number states in a superconducting circuit. *Nature*, 445(7127):515–518, February 2007.

[13] E. T. Holland, B. Vlastakis, R. W. Heeres, M. J. Reagor, U. Vool, Z. Leghtas, L. Frunzio, G. Kirchmair, M. H. Devoret, M. Mirrahimi, and R. J. Schoelkopf. Single-photon-resolved cross-kerr interaction for autonomous stabilization of photon-number states. *Phys. Rev. Lett.*, 115:180501, Oct 2015.

[14] J. D. Thompson, B. M. Zwickl, A. M. Jayich, F. Marquardt, S. M. Girvin, and J. G. E. Harris. Strong dispersive coupling of a high-finesse cavity to a micromechanical membrane. *Nature*, 452(7183):72, March 2008.

[15] Yaxing Zhang and M. I. Dykman. Spectral effects of dispersive mode coupling in driven mesoscopic systems. *Phys. Rev. B*, 92:165419, Oct 2015.

[16] Yaxing Zhang, Yukihiro Tadokoro, and M I Dykman. Fluctuation spectra of weakly driven nonlinear systems. *New Journal of Physics*, 16(11):113064–, 2014.

[17] H. A. Lorentz. *The theory of electrons and its applications to the phenomena of light and radiant heat*. Teubner, B. G., Leipzig, 1916.

[18] A. Einstein and L. Hopf. Statistical inverstigation of a resonator's motion in a radiation field. *Ann. Phys. (Leipzig)*, 33:1105–1115, 1910.

[19] A. N. Cleland and M. L. Roukes. Noise processes in nanomechanical resonators. *J. Appl. Phys.*, 92(5):2758–2769, September 2002.

[20] V. Sazonova, Y. Yaish, H. Ustunel, D. Roundy, T. A. Arias, and P. L. McEuen. A tunable carbon nanotube electromechanical oscillator. *Nature*, 431(7006):284–287, September 2004.

[21] R. Lifshitz and M. C. Cross. In H. G. Schuster, editor, *Review of Nonlinear Dynamics and Complexity*, pages 1–52. Wiley, Weinheim, 2008.

[22] G. A. Steele, A. K. Huttel, B. Witkamp, M. Poot, H. B. Meerwaldt, L. P. Kouwenhoven, and H. S. J. van der Zant. Strong coupling between single-electron tunneling and nanomechanical motion. *Science*, 325(5944):1103–1107, August 2009.

[23] B. Lassagne, Y. Tarakanov, J. Kinaret, D. Garcia-Sanchez, and A. Bachtold. Coupling mechanics to charge transport in carbon nanotube mechanical resonators. *Science*, 325(5944):1107–1110, August 2009.

[24] King Y. Fong, Wolfram H. P. Pernice, and Hong X. Tang. Frequency and phase noise of ultrahigh q silicon nitride nanomechanical resonators. *Phys. Rev. B*, 85:161410 (R), 2012.

[25] A. Siria, T. Barois, K. Vilella, S. Perisanu, A. Ayari, D. Guillot, S.T. Purcell, and P. Poncharal. Electron fluctuation induced resonance broadening in nano electromechanical systems: The origin of shear force in vacuum. *Nano Lett.*, 12(7):3551–3556, June 2012.

[26] E. Gavartin, P. Verlot, and T. J. Kippenberg. Stabilization of a linear nanomechanical oscillator to its thermodynamic limit. *Nat. Commun.*, 4:2860, 2013.

[27] J. Burnett, L. Faoro, I. Wisby, V. L. Gurtovoi, A. V. Chernykh, G. M. Mikhailov, V. A. Tulin, R. Shaikhaidarov, V. Antonov, P. J. Meeson, A. Ya. Tzalenchuk, and T. Lindstrom. Evidence for interacting two-level systems from the 1/f noise of a superconducting resonator. *Nat. Commun.*, 5:4119, 2014.

[28] L. Faoro and L. B. Ioffe. Generalized tunneling model for tls in amorphous materials and its predictions for their dephasing and the noise in superconducting microresonators.

[29] M. I. Dykman, M. Khasin, J. Portman, and S. W. Shaw. Spectrum of an oscillator with jumping frequency and the interference of partial susceptibilities. *Phys. Rev. Lett.*, 105(23):230601, December 2010.

[30] Y. T. Yang, C. Callegari, X. L. Feng, and M. L. Roukes. Surface adsorbates fluctuations and noise in nanoelectromechanical systems. *Nano Lett.*, 11:1753, 2011.

[31] A. Eichler, J. Moser, M. I. Dykman, and A. Bachtold. Symmetry breaking in a mechanical resonator made from a carbon nanotube. *Nat. Commun.*, 4:2843, 2013.

[32] S. M. Meenehan, J. D. Cohen, S. Groeblacher, J. T. Hill, A. H. Safavi-Naeini, M. Aspelmeyer, and O. Painter. Silicon optomechanical crystal resonator at millikelvin temperatures. *Phys. Rev. A*, 90:011803, March 2014.

[33] A. Einstein. Theory of opalescence of homogenous liquids and liquid mixtures near critical conditions. *Annal. Phys.*, 33(16):1275–1298, 1910.

[34] K. Lindenberg, V. Seshadri, and B. J. West. Brownian-motion of harmonic-systems with fluctuating parameters .3. scaling and moment instabilities. *Physica A*, 105(3):445–471, 1981.

[35] M. Gitterman. *The Noisy Oscillator*. World Scientific, New Jersey, 2005.

[36] Z. A. Maizelis, M. L. Roukes, and M. I. Dykman. Detecting and characterizing frequency fluctuations of vibrational modes. *Phys. Rev. B*, 84:144301, 2011.

[37] M. I. Dykman and M. A. Krivoglaz. In I. M. Khalatnikov, editor, *Sov. Phys. Reviews*, volume 5, pages 265–441, http://www.pa.msu.edu/ dykman/pub06/DKreview84.pdf. Harwood Academic, New York, 1984.

[38] R. P. Feynman and A. R. Hibbs. *Quantum Mechanics and Path Integrals*. McGraw-Hill, New-York, 1965.

[39] J. Moser, J. Güttinger, A. Eichler, M. J. Esplandiu, D. E. Liu, M. I. Dykman, and A. Bachtold. Ultrasensitive force detection with a nanotube mechanical resonator. *Nat. Nanotech.*, 8:493, 2013.

[40] M. Blencowe. Quantum electromechanical systems. *Phys. Rep.*, 395(3):159–222, 2004.

[41] K. C. Schwab and M. L. Roukes. Putting mechanics into quantum mechanics. *Phys. Today*, 58(7):36–42, July 2005.

[42] A. A. Clerk, F. Marquardt, and J. G. E. Harris. Quantum measurement of phonon shot noise. *Phys. Rev. Lett.*, 104(21):213603, May 2010.

[43] A. D. O'Connell, M. Hofheinz, M. Ansmann, R. C. Bialczak, M. Lenander, E. Lucero, M. Neeley, D. Sank, H. Wang, M. Weides, J. Wenner, J. M. Martinis, and A. N. Cleland. Quantum ground state and single-phonon control of a mechanical resonator. *Nature*, 464(7289):697–703, April 2010.

[44] A. Eichler, M. del Ålamo Ruiz, J. A. Plaza, and A. Bachtold. Strong coupling between mechanical modes in a nanotube resonator. *Phys. Rev. Lett.*, 109(2):025503–, July 2012.

[45] H. J. R. Westra, M. Poot, H. S. J. van der Zant, and W. J. Venstra. Nonlinear modal interactions in clamped-clamped mechanical resonators. *Phys. Rev. Lett.*, 105(11):117205, September 2010.

[46] Andres Castellanos-Gomez, Harold B. Meerwaldt, Warner J. Venstra, Herre S. J. van der Zant, and Gary A. Steele. Strong and tunable mode coupling in carbon nanotube resonators. *Phys. Rev. B*, 86(4):041402–, July 2012.

[47] I. Mahboob, K. Nishiguchi, H. Okamoto, and H. Yamaguchi. Phonon-cavity electromechanics. *Nature Physics*, 8(5):387–392, May 2012.

[48] I. Mahboob, K. Nishiguchi, A. Fujiwara, and H. Yamaguchi. Phonon lasing in an electromechanical resonator. *Physical Review Letters*, 110(12):127202, March 2013.

[49] M. H. Matheny, L. G. Villanueva, R. B. Karabalin, J. E. Sader, and M. L. Roukes. Nonlinear mode-coupling in nanomechanical systems. *Nano Lett.*, 13(4):1622–1626, April 2013.

[50] J. C. Sankey, C. Yang, B. M. Zwickl, A. M. Jayich, and J. G. E. Harris. Strong and tunable nonlinear optomechanical coupling in a low-loss system. *Nat Phys*, 6(9):707–712, September 2010.

[51] T. P. Purdy, D. W. C. Brooks, T. Botter, N. Brahms, Z.-Y. Ma, and D. M. Stamper-Kurn. Tunable cavity optomechanics with ultracold atoms. *Phys. Rev. Lett.*, 105:133602, Sep 2010.

[52] V. Singh, S. J. Bosman, B. H. Schneider, Y. M. Blanter, A. Castellanos-Gomez, and G. A. Steele. Optomechanical coupling between a multilayer graphene mechanical resonator and a superconducting microwave cavity. *Nat Nano*, 9(10):820–824, October 2014.

[53] P. Weber, J. Güttinger, I. Tsioutsios, D. E. Chang, and A. Bachtold. Coupling graphene mechanical resonators to superconducting microwave cavities. *Nano Lett.*, 14(5):2854–2860, May 2014.

[54] T. K. Paraïso, M. Kalaee, L. Zang, H. Pfeifer, F. Marquardt, and O. Painter. Position-squared coupling in a tunable photonic crystal optomechanical cavity. *ArXiv e-prints*, 2015.

[55] Warner J. Venstra, Ronald van Leeuwen, and Herre S. J. van der Zant. Strongly coupled modes in a weakly driven micromechanical resonator. *Appl. Phys. Lett.*, 101(24):243111, 2012.

[56] A. Vinante. Thermal frequency noise in micromechanical resonators due to nonlinear mode coupling. *Phys. Rev. B*, 90(2):024308–, July 2014.

[57] D. H. Santamore, A. C. Doherty, and M. C. Cross. Quantum nondemolition measurement of fock states of mesoscopic mechanical oscillators. *Phys. Rev. B*, 70(14):144301, October 2004.

[58] Max Ludwig, Amir H. Safavi-Naeini, Oskar Painter, and Florian Marquardt. Enhanced quantum nonlinearities in a two-mode optomechanical system. *Phys. Rev. Lett.*, 109(6):063601–, August 2012.

[59] M. I. Dykman and M. A. Krivoglaz. Classical theory of nonlinear oscillators interacting with a medium. *Phys. Stat. Sol. B*, 48(2):497–&, 1971.

[60] P. W. Anderson. Mathematical model for the narrowing of spectral lines by exchange or motion. *J. Phys. Soc. Japan*, 9:316–339, 1954.

[61] R. Kubo. Note on the stochastic theory of resonance absorption. *J. Phys. Soc. Japan*, 9(6):935–944, 1954.

[62] M. I. Dykman and M. A. Krivoglaz. Zero-phonon lineshape of impurity centers interacting with local or quasi-local vibrations. *Fiz. Tverd. Tela*, 29(2):368–376, 1987.

[63] A. A. Clerk and D. W. Utami. Using a qubit to measure photon-number statistics of a driven thermal oscillator. *Phys. Rev. A*, 75(4):042302, April 2007.

[64] I. R. Senitzky. Dissipation in quantum mechanics. the harmonic oscillator. *Phys. Rev.*, 119:670, 1960.

[65] J. Schwinger. Brownian motion of a quantum oscillator. *J. Math. Phys.*, 2(3):407, 1961.

[66] W. H. Louisell. *Quantum Statistical Properties of Radiation*. Wiley-VCH, Berlin, 1990.

[67] I. M. Gelfand and A. M. Yaglom. Integration in functional spaces and its applications in quantum physics. *J. Math. Phys.*, 1(1):48–69, 1960.

[68] R. Phythian. The functional formalism of classical statistical dynamics. *J. Phys. A*, 10(5):777–89, May 1977.

[69] R. Mannella. Integration of stochastic differential equations on a computer. *Int. J. Mod. Phys. C*, 13(9):1177–1194, November 2002.

[70] M. A. Ivanov, L. B. Kvashnina, and M. A. Krivoglaz. Spectral distribution of localized vibrations. *Sov. Phys. Solid State*, 7(7):1652–&, 1965.

[71] R. J. Elliott, W. Hayes, G. D. Jones, H. F. MacDonald, and C. T. Sennett. Localized vibrations of h- and d- ions in the alkaline earth fluorides. *Proc. Roy. Soc. London*, A289(1416):1–33, 1965.

[72] L. D. Landau and E. M. Lifshitz. *Mechanics*. Elsevier, Amsterdam, 3rd edition, 2004.

[73] M. I. Dykman and M. A. Krivoglaz. Theory of fluctuational transitions between the stable states of a non-linear oscillator. *Zh. Eksp. Teor. Fiz.*, 77(1):60–73, 1979.

[74] P. D. Drummond and D. F. Walls. Quantum-theory of optical bistability .1. non-linear polarizability model. *J. Phys. A*, 13(2):725–741, 1980.

[75] L. Mandel and E. Wolf. *Optical Coherence and Quantum Optics*. Cambirdge University Press, Camridge, 1995.

[76] A. Ashkin. Optical trapping and manipulation of neutral particles using lasers. *Proceedings Of The National Academy Of Sciences Of The United States Of America*, 94(10):4853–4860, 1997.

[77] W. J. Greenleaf, M. T. Woodside, and S. M. Block. High-resolution, single-molecule measurements of biomolecular motion. *Ann. Rev. Biophys. Biomol. Struct.*, 36:171–190, 2007.

[78] K. Berg-Sorensen and H. Flyvbjerg. Power spectrum analysis for optical tweezers. *Rev. Sci. Instr.*, 75(3):594–612, March 2004.

[79] J. Mas, A. C. Richardson, S. N. S. Reihani, L. B. Oddershede, and K. Berg-Sorensen. Quantitative determination of optical trapping strength and viscoelastic moduli inside living cells. *Physical Biology*, 10(4):046006, August 2013.

[80] G. J. Walls, D. F. & Milburn. *Quantum Optics*. Springer, Berlin, 2008.

[81] H. J. Carmichael. *Statistical Methods in Quantum Optics 2: Non-Classical Fields*. Springer-Verlag, Berlin, 2008.

[82] F. Jaramillo and K. Wiesenfeld. Mechanoelectrical transduction assisted by brownian motion: a role for noise in the auditory system. *Nat. Neurosci.*, 1(5):384–388, September 1998.

[83] W. Bialek. *Biophysics: Searching for Principles*. Princeton University Press, Princeton, 2012.

[84] O. M. Marago, P. H. Jones, P. G. Gucciardi, G. Volpe, and A. C. Ferrari. Optical trapping and manipulation of nanostructures. *Nature Nanotechnology*, 8(11):807–819, November 2013.

[85] L.D. Landau and E. M. Lifshitz. *Statistical Physics. Part 1*. Pergamon Press, New York, 3rd, revised by e. m. lifshitz and l. p. pitaevskii edition, 1980.

[86] P. Langevin. The theory of brownian movement. *Comptes Rendus Hebdomadaires Des Seances De L' Academie Des Sciences*, 146:530–533, 1908.

[87] A. J. Leggett, S. Charkavarty, A. T. Dorsey, M. P. A. Fisher, A. Garg, and W. Zwerger. Dynamics of the dissipative 2-state system (vol 59, pg 1, 1987). *Rev. Mod. Phys.*, 67(3):725–726, July 1995.

[88] P. Debye. *Polar molecules*. Dover Publications, Inc., 1929.

[89] M. I. Dykman, D. G. Luchinsky, R. Mannella, P. V. E. McClintock, N. D. Stein, and N. G. Stocks. Stochastic resonance in perspective. *Nuovo Cimento D*, 17(7-8):661–683, 1995.

[90] K. Wiesenfeld and F. Jaramillo. Minireview of stochastic resonance. *Chaos*, 8:539–548, 1998.

[91] L. Gammaitoni, P.H. Hänggi, P. Jung, and F. Marchesoni. Stochastic resonance. *Rev. Mod. Phys.*, 70:223–88, 1998.

[92] M. Thorwart, P. Reimann, P. Jung, and R.F. Fox. Quantum hysteresis and resonant tunneling in bistable systems. *Chemical Physics*, 235:61–80, September 1998.

[93] M. I. Dykman, R. Mannella, P. V. E. McClintock, and N. G. Stocks. Stochastic resonance in bistable systems. *Phys. Rev. Lett.*, 65(20):2606–2606, 1990.

[94] N. G. Van Kampen. *Stochastic Processes in Physics and Chemistry*. Elsevier, Amsterdam, 3rd edition, 2007.

[95] B. McNamara and K. Wiesenfeld. Theory of stochastic resonance. *Phys. Rev. A*, 39(9):4854–4869, May 1989.

[96] A. Nikitin, N. G. Stocks, and A. R. Bulsara. Asymmetric bistable systems subject to periodic and stochastic forcing in the strongly nonlinear regime: The power spectrum. *Phys. Rev. E*, 76(4):041138, October 2007.

[97] Kurt Wiesenfeld, David Pierson, Eleni Pantazelou, Chris Dames, and Frank Moss. Stochastic resonance on a circle. *Phys. Rev. Lett.*, 72(14):2125–2129, April 1994.

[98] Z. Gingl, L. B. Kiss, and F. Moss. Non-dynamical stochastic resonance: Theory and experiments with white and arbitrarily coloured noise. *Europhys. Lett.*, 29(3):191–196, 1995.

[99] P. Jung. Stochastic resonance and optimal design of threhold detectors. *Phys. Lett. A*, 207:93–104, 1995.

[100] H. Risken. *The Fokker-Planck Equation*. Springer, Berlin, 2nd edition, 1996.

[101] V Leyton, V Peano, and M Thorwart. Quantum noise properties of multiphoton transitions in driven nonlinear resonators. *New Journal of Physics*, 14(9):093024, 2012.

[102] M. I. Dykman, M. Marthaler, and V. Peano. Quantum heating of a parametrically modulated oscillator: Spectral signatures. *Phys. Rev. A*, 83(5):052115, 2011.